Seasonal Variation and Spatial Organization of Hydrologic Fluxes over Complex Topography

by

Eli Sava Ateljevich

Submitted to the Department of Civil and Environmental Engineering
in partial fulfillment of the requirements for the degree of

Master of Science in Civil and Environmental Engineering

at the

MASSACHUSETTS INSTITUTE OF TECHNOLOGY

September 1995

Author .....
Department of Civil and Environmental Engineering
July 21, 1995

Certified by .....
Dara Entekhabi
Associate Professor
Thesis Supervisor

Accepted by .....
Joseph M. Sussman
Chairman, Departmental Committee on Graduate Students

Seasonal Variation and Spatial Organization of Hydrologic Fluxes over Complex Topography

by

Eli Sava Ateljevich

Submitted to the Department of Civil and Environmental Engineering
on July 21, 1995, in partial fulfillment of the
requirements for the degree of
Master of Science in Civil and Environmental Engineering

Abstract

This thesis derives a seasonal derived-distribution water balance model of the unsaturated and saturated zones, and compares it to a steady state model. The seasonal model predicts the expected value of evaporation, runoff, recharge, soil moisture profile and water table location based on soil parameters and seasonal stochastic climate forcing. Two-way coupling exists between the saturated and unsaturated zones, and seasonal storage changes in the two zones are incorporated. In the Oklahoma summer rainfall climate over a planar hillslope, the model predicts abrupt transitions in the position of the water table between seasons. The high water table coincides with the rainy season; this leads to high runoff by storage excess mechanism because there is little available storage space in the unsaturated zone at the beginning of storm events. Annual mean runoff from the seasonal model is greater than annual runoff from the corresponding steady state model using annual mean climate parameters. In tests of the steady state and seasonal models using elevation data at three different resolutions (30m, 300m, 600m) on complex topography in the Little Washita river basin and a sub-basin, only the 30m resolution gives a physically realistic spatial distribution of fluxes. The results from the 30m resolution steady state model on the sub-basin agree well with topographic features and drainage patterns; zones of discharge, midline and recharge are evident. The distribution of water table depth is compared to the pre-event water table predicted by topography-based models such as TOPMODEL based on the index $\ln(a/\tan\beta)$. Although there is correlation between the results of the derived-distribution and topography-based models, the frequency distributions of water table depths given by the two types of models are different. Some of the assumptions made in the topography-based models may lead to an unrealistic distribution of expected water table depth, particularly in contributing areas.

Thesis Supervisor: Dara Entekhabi
Title: Associate Professor

Acknowledgments

I gratefully acknowledge the National Aeronautics and Space Administration (NASA) for supporting this research through subcontract NAS 5-31721.

I am particularly grateful to my advisor Dara Entekhabi for coaching me through this thesis and all of my academic career at MIT, and to Guido Salvucci for lending me his ideas and eleventh-hour debugging advice. Thanks also to Lynn Reid, resident computer genius, who announced at the beginning of my first year that she would answer no more than three computer questions from any one person; if she kept her word this thesis would still be a tree. Glenn Moglen must also be singled out for his helpfulness, particularly with the handling of elevation data and the calculation of topographical indices. Lastly, John Draves of the hydrologic sciences branch of NASA/GSFC supplied the DEM maps for the Little Washita watershed, often in tailor-made format for my applications.

Contents

List of Figures

List of Tables

Chapter 1

Introduction

The distributions of soil moisture and surface fluxes over topography are important in many areas of hydrologic investigation, including catchment response forecasting, remote sensing, climate modeling and scaling studies. One approach that has proved useful in estimating these fluxes over the climatic time scale is the derived distribution method developed by Eagleson (1978) and extended by Salvucci and Entekhabi (1995). In particular, Salvucci and Entekhabi (1995) subjects a coupled saturated saturated and groundwater system to stationary stochastic atmospheric forcing in order to approximate the mean surface fluxes and water table position over a hillslope. The model contains a two-way coupling of the saturated and unsaturated zone: recharge from the unsaturated zone provides the forcing to the saturated zone, while at the same time the position of the water table influences the dynamics of the unsaturated zone and recharge.

Chapter 2 of this thesis extends the model of Salvucci and Entekhabi (1995) to incorporate a more realistic seasonal atmospheric forcing. The inclusion of seasonality requires that the system reach a dynamic, rather than steady state, equilibrium. The hydrologic processes are modeled as periodic stochastic functions, the parameters of which vary slowly over the year. It is assumed that no mean storage accumulates from year to year, so that the ensemble mean seasonal fluxes are periodic-stationary over a time scale of many years.

This thesis will discuss results from both the steady state model and the seasonal

model. "Equilibrium model" is reserved as a general term for the derived-distribution water balance approach, and will refer collectively to both the steady state and seasonal models.

Chapter 3 applies the seasonal model (for Oklahoma climate conditions) to a synthetic planar hillslope in order to study the effects of seasonality on the equilibrium water table position and surface fluxes. The results indicate that the water table switches abruptly between low and high positions between the dry and rainy seasons. Unsaturated zone storage and storage release occurs at the transition between the seasons. Runoff is almost exclusively the product of the rainy season, and enough runoff is contributed during this period so that average annual runoff from the seasonal model is considerably higher than annual runoff from the steady state model using the mean annual climate parameters.

Chapter 4 describes the application of the model to the Little Washita river basin in Oklahoma, a flow domain with more complex topography than the synthetic hillslope. The model produces interesting seasonal patterns but is ultimately unsatisfactory because it incorporates inappropriately large horizontal cell spacing and coarse digital elevation model (DEM) resolution. The result is that seasonal variation dominates over spatial variation, reducing the model to a seasonal one-dimensional model.

The effect of DEM resolution and horizontal cell dimensions on the equilibrium water balance is discussed in Chapter 5. Here we compare the output of the steady state version of the model on a single flow domain using input elevation data at 30m, 300m, and 600m. Ultimately, only the 30m resolution produces satisfactory results. Further study is necessary to isolate the effects of resolution on local geographic features from the numerical effects of cell size on the saturated flow equations with recharge.

Chapter 6 compares the output of the steady state 30m resolution equilibrium model with complex catchment topography. This is carried out both qualitatively, by comparing maps of flux and water table output to basin elevation and drainage maps, and quantitatively by comparing the output to a topographical index, the log ratio of cumulative drainage area per contour length to slope, $\ln(a/\tan\beta)$.

As with most scientific endeavors, this thesis represents a work in progress, and each of its chapters invites further investigation. Chapter 7 discusses some of the refinements and extensions which could be made to the present research using the seasonal and steady state models.

1.1 Relevant literature

The models presented in this thesis are equilibrium (derived-distribution) models which operate at the climatic or seasonal time scale. The models incorporate two-way coupling between the saturated and unsaturated zone as well as one-way forcing from the atmosphere onto the soil system. Salvucci (1994c) reviews a number of water balance models, classifying them on the basis of time and spatial scale, type of model (running versus equilibrium), and degree of coupling between the atmosphere, unsaturated and saturated zones. The present section will not discuss these models further, except for TOPMODEL, which is relevant to the topographical analysis presented in Chapter 6.

TOPMODEL (Beven and Kirkby, 1979) is a laterally-distributed water balance model which predicts the output stream hydrograph, water table depth and runoff from storm events based on catchment topography, soil characteristics and rainfall. The model allows for two methods of flow generation, surface runoff and subsurface flow. Surface runoff is assumed to occur when rainfall falls on saturated portions of the catchment. These saturated areas expand and contract in response to watershed dynamics. Subsurface flow depends on saturated conductivity, soil depth, surface slope and "saturation deficit" (the amount of water necessary to fill the unsaturated moisture profile, which changes over an event). The model assumes that hydraulic conductivity decreases exponentially with depth and that recharge is uniform over the catchment. The governing equations are Darcy's Law and continuity.

One facet of TOPMODEL which is particularly important to this thesis is that it assumes that the initial pre-storm water table depth is related linearly to a topographical index, $\ln(a/\tan\beta)$. The equilibrium model also predicts the expected

value of water table depth and assumes that this is valid as a pre-storm condition; therefore, this aspect of the two models is directly comparable. Such a comparison is made in Chapter 6 between the equilibrium steady state model and a variant of the TOPMODEL-style topography model from Sivapalan (1987). The formulation set forth in Sivapalan (1987) assumes that mean-removed topographical index is linearly related to the mean-removed pre-storm water table position.

TOPMODEL has also been used to examine the effect of DEM resolution on water balance. Zhang and Montgomery (1994) compares the effects of grid resolution of 2m, 4m, 10m, 30m and 90m on discharge predictions for two catchments, and concluded that finer grid resolution yielded significant improvements down to about 10m. The 30m resolution models performed much better than the 90m resolution model, and Zhang and Montgomery (1994) asserts that runoff processes are governed by processes at the "intermediate" scales. As part of their analysis, Zhang and Montgomery (1994) also reports that the distribution of $\ln(a/\tan\beta)$ is most sensitive to DEM resolution in steep basins. Both drainage per contour length (a) and slope (s) were found to vary according to DEM resolution and quality.

Wolock and Price (1994) also looks at the effect of DEM resolution on the topographical index. In particular, they examine the effect of resolution and map scale on the first three moments of the distribution of $\ln(a/\tan\beta)$. Wolock and Price (1994) asserts that 30m DEMs are not necessarily a better source of topographical information than 90m DEMs for estimating depth to the water table because the water table configuration may be smoother than the surface features. In this thesis, however, the observation that the water table does not follow the land surface is presented as a shortcoming of the topography-based approach. Matching the water table by choosing among different DEMs in effect turns DEM resolution into a fitted parameter.

In the case of the equilibrium model presented in this thesis, the smooth water table argument for using coarser resolution does not apply. The water table in the equilibrium model is dynamic and is allowed to take on a smoother configuration than the surface *particularly* when a finer grid size is used. The only obstacle to a smooth

water table configuration in the equilibrium runs is the use of integer-value elevation data, which for the Little Washita basin comes in discretized intervals (90cm) almost as wide as the depth of the soil column (120cm). This makes a flat water table impossible over wide areas unless the surface is also flat.

Finally, the subject of aggregation and averaging in hydrologic modeling investigated in Wood and Price (1988), which observes that as catchment size increases, hydrologic response depends less on small-scale soil, climate and geographical features and more on larger scale characteristics of the basin. Wood and Price (1988) proposes the existence of a representative area (REA), a scale at which it is possible to represent the behavior of catchments and sub-catchments. The REA comprises an ergodic region large enough to reflect the aggregate behavior of a continuum of small scale heterogeneous properties, but not so large that it fails to capture large scale variation induced by major geographical features. The existence of the REA is supported in Wood and Price (1988) by numerical experiments using TOPMODEL.

This thesis makes some attempt to study aggregation, but is hampered by improper choice of resolution. The author nonetheless proposes that the equilibrium model will prove to be a valuable tool in scaling studies of hydrologic fluxes.

Chapter 2

Seasonal Derived-Distribution Water Balance Model

2.1 Introduction

This chapter describes the formulation of the seasonal derived-distribution water balance model. The governing equations of the model are water balances in the saturated and unsaturated zones. These water balances are, in turn, constructed from mean point flux and storage terms (e.g., infiltration) which are calculated using derived distributions of point soil processes. Closure is achieved by expressing the mean flux and storage terms as functions of two model state variables: expected water table position and recharge.

The present work incorporates many aspects of the steady-state Salvucci and Entekhabi (1995) model, and thus the first section of this chapter summarizes some of the techniques, assumptions and results associated with the steady state model. The second section fully develops the seasonal model and discusses modifications and extensions to the steady state model which are necessary in order to accommodate seasonally-varying forcing. The third section addresses solution and computation issues. Finally, the last section compares the results of the steady state and seasonal models on a simple one dimensional problem using a planar hillslope.

2.2 Steady State Model

2.2.1 Governing Water Balance

The equations governing the water balance for the saturated and unsaturated zone in steady state are:

1. Unsaturated:

$$E[P(\sigma)] - E[R_{ie}(q_v, Z_{wt}, \sigma)] - E[R_{se}(q_v, Z_{wt}, \sigma)] - E[E_s(q_v, Z_{wt}, \sigma)] - q_v = 0 \tag{2.1}$$

where P denotes precipitation, R_{ie} is infiltration excess ("Horton") runoff , R_{se} is storage excess ("Dunne") runoff, E_S is bare soil evaporation and q_v is equivalent steady recharge to the saturated zone (positive down, towards the saturated zone). The surface fluxes are expressed in terms of an equivalent water table position Z_{wt}, equivalent steady recharge q_v and a vector of soil and climate parameters σ. Equivalent recharge q_v, is assumed to approximate mean recharge, an assumption which is discussed in Salvucci and Entekhabi (1994b,c). Appendix A contains the relevant expressions for the expected values of fluxes in Equation (2.1), as given by Salvucci and Entekhabi (1995)

2. Saturated:

$$\nabla \cdot \mathbf{Q_g} + q_v = 0 \tag{2.2}$$

where $\mathbf{Q_g}$ represents the lateral flow in the unconfined saturated zone, given by Darcy's Law:

$$\mathbf{Q_g} = -K_{sat} H \nabla H \tag{2.3}$$

in which K_{sat} denotes the saturated hydraulic conductivity and $H = Z_{wt} + \Psi_{sat}$ is the height of the water table (phreatic surface) plus the thickness of the tension saturated zone, which is assumed to conduct horizontal flow. The thickness of the tension saturated zone Ψ_{sat} is taken as positive.

2.2.2 Groundwater flow

The steady state model assumes that flow in the unsaturated zone is vertical and one dimensional. At the event time scale, (unsaturated) vertical flow is assumed to dominate over (saturated) horizontal flow. Thus, during a storm event, the water table will not reorganize itself due to lateral saturated flow, although the soil column is allowed to fill vertically through the unsaturated zone as part of the calculation of storage excess runoff.

In the test case summarized in Chapter 3, the saturated flow is assumed to be one-dimensional Dupuit flow, although the model is applied to more complicated types of saturated flow in later chapters. The tension saturated zone, in which hydraulic conductivity is approximately at its saturated level, is included as part of the saturated zone.

2.2.3 Derived mean fluxes

The steady state model follows Eagleson (1978b) in adopting a statistical-dynamical approach, in which the input to the model is a distribution of storm sequences and the output is the expected value of vertical fluxes and a groundwater system in equilibrium with these fluxes.

In the steady state model, the climatic forcing is modeled as a stationary Poisson arrival process of independent rectangular storm pulses of exponentially distributed duration (t_r) and intensity (i), between which are interstorm periods (t_b) of fixed potential evaporation (e_p).

The annual expected values of surface fluxes are determined by time-averaging the response of the unsaturated zone over the distribution of year-long storm sequences. This task may be immediately simplified by making two assumptions, viz.:

1. that the number of of storms and storm depth are independent. This simplification is justified because we assume $t_r \ll t_b$, so that the number of storms per

year, the mean of which is given by:

$$m_\nu = \frac{1\text{year}}{t_b + t_r}$$

is nearly independent of t_r, and thus also of storm depth, the mean of which is given by:

$$h = i \cdot t_r$$

2. that a single surrogate initial condition may be found for all storm and interstorm events so that the responses to individual storms may be calculated without having to account for past events in the storm sequence. This is a major assumption which is discussed in Section 2.2.4 under "equivalent steady state moisture profile".

After making the two above assumptions, the annual expected value of a surface flux $\langle F_a \rangle$ such as infiltration may be expressed as:

$$\langle F_a \rangle = m_\nu \int_0^\infty \int_0^\infty F(\xi, \tau) f_{t_r}(\tau) f_i(\xi) d\tau d\xi \tag{2.4}$$

where F is the cumulative flux corresponding to a storm of intensity i and duration t_r, and f_i and f_{t_r} are the probability densities of storm intensity and storm duration. Notice that the mean number of storms per year, m_ν, has been removed from the integral in Equation (2.4), which is a consequence of the independence assumption (1) above.

The soil processes themselves are modeled using modifications of well-known approximate analytical solutions to the Richard's equation. The selection of their analytical approximations and the solution of the resultant integrals in Equation (2.4) constitute a major portion of Eagleson (1978a-g) and Salvucci and Entekhabi (1995). The derivations of these solutions are not repeated here; however the final equations for the expected values of fluxes are included in Appendix A .

2.2.4 Model assumptions

The solution of Equations (2.1), (2.2), and (2.4) requires a number of simplifying assumptions beyond those discussed above. Appendix B contains a list of model assumptions made by Eagleson (1978a-g) and Salvucci and Entekhabi (1995), including Brooks-Corey soils, time compression and the neglect of vegetation. The assumptions discussed below are relevant to the present work because they will be extended or modified in the formulation of the seasonal model.

Equivalent steady state moisture profile

Perhaps the strongest assumption made in the steady state model is that the soil moisture conditions preceding every storm and interstorm event in a storm sequence may be characterized by a single initial moisture profile. Without this simplification, the moisture condition following each storm or interstorm event is the initial condition for the next event, and thus the output from a year-long storm sequence cannot be obtained simply by summing the output from its constituent storms. In order to resolve this difficulty, the steady state model includes a single surrogate storm and interstorm initial condition called the "equivalent steady state moisture profile". This is the profile that transmits the steady state mean recharge rate uniformly through a unsaturated Brooks-Corey soil column bounded by a water table. The steady state moisture profile is determined completely by the position of the water table and the recharge percolating through it. Salvucci and Entekhabi (1995) tested this profile in numerical simulations using a fixed water table position and found that it could be substituted as an initial moisture condition without seriously affecting mean surface fluxes. The steady state moisture profile is given in Appendix A.

Equivalent steady state water table

The steady state model assumes that the water table that is in equilibrium with the mean recharge rate, called the "equivalent steady state water table", is a close approximation to the mean water table. The need for this approximation is apparent

if we examine the the saturated zone water balance in isolation, ignoring for the moment the feedback between head and recharge and considering only one direction of flow. Substituting Equation (2.3) into Equation (2.2), expanding $H = Z_{wt} + \Psi_{sat}$ as the sum of its mean ($\bar{H}$) and a fluctuation(H'), and taking expected values, we obtain:

$$\frac{d}{dx}\bar{H}\frac{d\bar{H}}{dx} + \frac{d}{dx}\overline{H'\frac{dH'}{dx}} + \bar{q}_v = 0 \tag{2.5}$$

Due to the nonlinearity of the governing equation, the covariance term $\frac{d}{dx}\overline{H'\frac{dH'}{dx}} = \frac{d}{dx}\overline{H'^2}$ appears, and because of this term using the mean recharge rate in Equation (2.1) does not necessarily return the mean water table profile. Of course, the dependence of recharge on water table (and thus H) will add even more complicated cross-covariance terms. Furthermore, any error that occurs in calculating the mean water table will propagate into the unsaturated system because recharge and soil moisture are functions of water table height. However, tests conducted by Kim, Entekhabi and Salvucci (1994) demonstrate that this effect is small. They compared results from the steady state model to those from long term simulations using an event-based model and found that the water table position and fluxes from the two models (equilibrium and statistical mean) are in close agreement.

2.3 Seasonal model

2.3.1 Seasonal climate

The seasonal water balance model is different from the steady state model in that it subjects the hillslope hydrologic system to a seasonally varying climatic forcing. The output from the model are the mean surface fluxes and equilibrium water table position at different times during the year.

The climate is modeled as a periodic, inhomogeneous Poisson arrival process which is the time-varying analog of the climate forcing to the steady state model: independent rectangular storm pulses of exponentially distributed duration (t_r) and intensity (i), between which are interstorm periods (t_b) of fixed potential evaporation (e_p).

The parameters of the probability distribution for storm properties and the mean interstorm potential evaporation vary periodically in time.

The seasonal time scale over which the climate variables vary is very long compared to the the time scale of individual storms, so that storm duration, interstorm duration and intensity may be considered to be exponentially distributed with parameters which do not change over the period surrounding an event.

2.3.2 Governing equations

The governing equations for the seasonal unsaturated and saturated water balances are:

unsaturated:

$$E[P(\sigma(t))] - E[R_{ie}(Z_{wt}(t), q_v(t), \sigma(t))] - E[R_{se}(Z_{wt}(t), q_v(t), \sigma(t))] - E[E_s(Z_{wt}(t), q_v(t), \sigma(t))] - q_v(t) = E[\Delta V_{unsat}] \quad (2.6)$$

and saturated:

$$\nabla \cdot \mathbf{Q_g} + q_v = \Delta V_{sat} = S_y \frac{dZ_{wt}}{dt} \quad (2.7)$$

where Z_{wt} is the water table height,

Q_g represents the lateral flow in the saturated zone,

q_v is the recharge flux (positive down) to the saturated zone,

S_y is the specific yield, and

V_{unsat} and V_{sat} are the volumes of water stored in the unsaturated and saturated regions of the water column. These volumes are expressed through:

$$V_{unsat} = \int_{Z_{wt}+\Psi_{sat}}^{Z_s} n_e \cdot s(Z_{wt}, q_v, zl) dzl \quad (2.8)$$

and

$$V_{sat} = n_e \cdot (Z_{wt} + \Psi_{sat} - Z_0) \quad (2.9)$$

where $s(Z_{wt}, q, z)$ is the steady state relative soil saturation at a height z in the soil

column (the prime symbol indicates that z is an integration variable),

n_e is effective porosity,

Z_s is the elevation of the top of the soil column, and

Z_0 is the elevation at bedrock.

In this formulation, the time derivative of saturated storage (V_{sat} in Equation (2.7)) is expressed linearly as a constant specific yield (S_y) times the time derivative of head (or Z_{wt}). Specific yield (available pore space) is typically less than porosity because the soil immediately above the tension saturated zone is partially saturated, so that a head change may be achieved with less water than would be necessary to saturate total pore space. In Figure 2-1, which depicts a changing water table, only the area (D) need be filled with water in order to achieve the given change in water table, because area (C) already contains water.

The available pore space ΔV that fills or drains during a shift in water table Z_{wt} is:

$$\Delta V = n_e - \int_{Z_{wt}(t)+\Psi_{sat}}^{Z_{wt}(t+\Delta t)+\Psi_{sat}} n_e s(Z_{wt}(t), q_v, z')dz' \tag{2.10}$$

for a rising water table or

$$\Delta V = n_e - \int_{Z_{wt}(t)+\Psi_{sat}}^{Z_{wt}(t+\Delta t)+\Psi_{sat}} n_e s(Z_{wt}(t+\Delta t), q_v, z')dz' \tag{2.11}$$

for a falling water table.

The change in saturated storage resulting from a change in water table may then be expressed as:

$$\begin{aligned} \frac{dV_{sat}}{dt} &= S_y \frac{dZ_{wt}}{dt} \\ &= n_e \frac{dZ_{wt}}{dt} - \frac{n_e}{\Delta t} \int_{Z_{wt}(t)+\Psi_{sat}}^{Z_{wt}(t+\Delta t)+\Psi_{sat}} \min[s(Z_{wt}(t), q_v, z'), s(Z_{wt}(t+\Delta t), q_v, z')]dz' \end{aligned} \tag{2.12}$$

The last term in this expression is area (C)the in Figure 2-1 and it represents the exchange between the saturated or unsaturated storages due to a shift in the water table position. Additionally, net recharge q_v is taking place. If we define an apparent

recharge q_a as

$$q_a \equiv q_v + \frac{n_e}{\Delta t}\int_{Z_{wt}(t)+\Psi_{sat}}^{Z_{wt}(t+\Delta t)+\Psi_{sat}} \min[s(Z_{wt}(t), q_v, z'), s(Z_{wt}(t+\Delta t), q_v, z')]dz' \quad (2.13)$$

then Equation (2.7) may be written as:

$$\nabla \cdot Q_g + q_a = n_e \frac{dZ_{wt}}{dt} \quad (2.14)$$

By substituting q_a for q_v and n_e for S_y in Equation (2.7), the model may be reconciled to the usual form for unconfined saturated flow. The saturated flow portion of the model may then be solved by using a standard groundwater simulation package (the author selected MODFLOW, McDonald and Harbaugh, 1988).

The resulting coupled saturated-unsaturated water balance is clearly illustrated using Figure 2-1 for the case of a rising water table. At time t, the saturated zone is defined by area (F) and the unsaturated zone by area (A+C). At time $t + \Delta t$, the saturated zone is defined by area (C+D+F) and the unsaturated zone by area (A+B). The net transfer of water from the unsaturated zone to the saturated zone is area (C+D+G), which represents growth in the defined volume of the saturated zone (C+D) plus the net lateral flux into the control volume (G). Area (C+D+G), then, divided by the time increment, is the apparent flux to the saturated zone, q_a in Equation (2.14). On the other hand, the actual equivalent recharge flux q_v (upon which the surface fluxes are calculated) is best approximated by region (D+G). The difference between q_a and q_v is water that does not "move" (area (C) in Figure 2-1, or the volume expressed in Equation 2.10); ie., it changes in definition between unsaturated and saturated but is not part of the actual recharge flux. The model computes both the actual vertical flux (q_v) at the water table and the corresponding apparent recharge (q_a).

On the other hand, the mean surface fluxes are expressed as functions not of the net definitional transfer of water from unsaturated zone to the saturated zone, but of the actual vertical flux of moisture at the interface between the two zones, which is

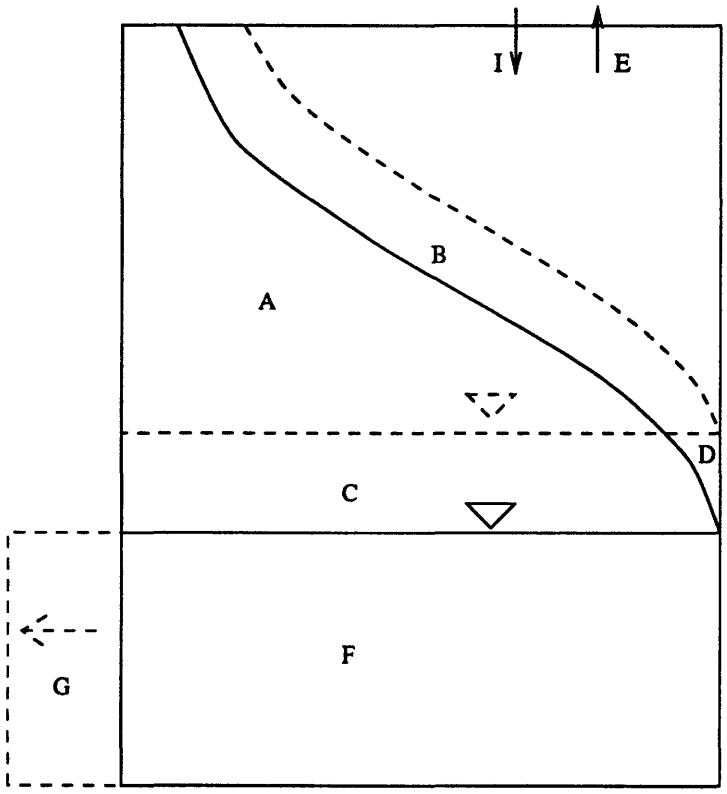

Figure 2-1: Incremental change in water balance due to a shift in water table position. Solid lines depict conditions at time t; dashed lines correspond to time $t+\Delta t$. During the time increment, recharge to the saturated zone results in a rising water table position.

best approximated by region (D+G). Area (D+G), then, is the q_v which appears as the argument in the flux functions of Equation (2.6).

2.3.3 Derived mean fluxes

The seasonal water balance model retains the expected flux equations described by Eagleson (1978a-g) as modified by Salvucci and Entekhabi (1995), which are given in Appendix A. These expected fluxes now vary seasonally, however, since they depend on climate, expected water table position and recharge, which are periodic functions of time. The expected value of a surface process is given by the ensemble average:

$$\langle F_{\Delta t}(t) \rangle = m_\nu(t)\Delta t \int_0^\infty \int_0^\infty f(\xi,\tau,t) f_{t_r}(\tau,t) f_i(\xi,t) d\tau d\xi \qquad (2.15)$$

where m_ν in Equation (2.4) has been replaced by $m_\nu(t)\Delta t$, in which $m_\nu(t)$ represents the current number of storms expected per unit time and Δt is the length of the period over which the expected value is being taken. Because the probability distributions of m_ν, t_r and i are assumed not to vary over the event time scale, Δt must be reasonably short.

2.3.4 Modified assumptions

Soil moisture profile constraints

In order to close the governing Equations (2.7) and (2.6) with time-varying fluxes and storage terms, the seasonal model incorporates additional assumptions concerning the shape of the unsaturated moisture profile and the link between recharge and storage.

In the seasonal model, the equivalent unsaturated moisture profile is allowed to change in time, but is constrained to maintain similarity within a family of equivalent steady state moisture profiles. This method is analogous to the method of "successive steady states" described in Bear (1988). A direct result of this assumption is that changes in mean recharge propagate instantly throughout the vertical extent of the soil column, consistent with the uniform vertical flux given by the steady state moisture

profile. The constraint on the shape of the soil moisture profile also leads to a modest dependence of the results on time step length, a matter which will be discussed in Section 2.4.1.

In addition, the integral of the equivalent unsaturated moisture profile at a given time is assumed to represent the expected value of current unsaturated storage. This assumption is slightly weaker than an assumption that the equivalent unsaturated moisture profile is actually the expected value of the current soil moisture profile. The purpose of this assumption is to render the storage term in Equation (2.6) a function of the two state variables.

Lastly, the equivalent soil moisture profile in the seasonal model is still assumed to be the initial condition for storm and interstorm events for purposes of calculating the current expected value of surface fluxes. The assumptions of no lateral unsaturated flow and no horizontal reorganization of the water table on the event time scale are also retained.

Equivalent equilibrium water table

The principle of the equivalent steady state water table can also be extended for use in the seasonal model. Here we simply assume that the (periodic) water table $Z_{wt}(t)$ that is in equilibrium with equivalent recharge $q_v(t)$ is actually equal to the current expected water table position $E[Z_{wt}(t)]$.

2.4 Solution algorithm

The coupled Equations (2.6) and (2.7) can be solved using an iterative procedure. The solutions presented in this thesis come from simulations using a modification of MODFLOW, McDonald and Harbaugh (1988). MODFLOW is a finite-difference three dimensional groundwater flow model developed by the United States Geological Survey. The program is modular in format, allowing the unsaturated water balance to be introduced as an interactive recharge module.

When used to model an unconfined aquifer, MODFLOW conducts two levels of

iterations, "outer iterations" and "inner iterations". During outer iterations, MODFLOW reformulates the equations for the current time step based on the latest values of head. Inner iterations are then used by the solver to refine solutions to the current matrix formulation of the problem. The interactive recharge module presented in this thesis recalculates recharge at every outer iteration.

Figure 2-2 gives a flow chart outlining the solution algorithm. The algorithm proceeds as follows:

1. the water table height and apparent recharge q_a from at the last time step are known from the model results or initial conditions.

2. a guess for the water table height at the new time step is obtained by recycling the apparent recharge rate q_a from the last iteration or time step into the saturated flow equations.

3. the unsaturated zone water balance is solved iteratively (by bisection) to find a q_v for the new time step that corresponds to the water table height from step (2). A new value of q_a corresponding to this value of q_v and the latest guess at Z_{wt} is also calculated.

4. the saturated flow equations are reformulated using the revised q_a and solved for water table height. The procedure is repeated until a new water table position and recharge rate are found that satisfy both water balances.

The model is integrated through many seasons until a dynamic equilibrium is reached in which the fluxes repeat themselves from year to year. This equilibrium occurs in fewer than six9 years for the cases studied in this thesis.

The initial condition for the model for most of the simulations described in this thesis was obtained by applying the steady state model on the mean climate and gradually introducing seasonality by increasing the amplitude of the periodic components of the climate parameters. The principal reason for initializing the model in this way is that it avoids guessing at an initial value of q_a. In steady state, q_a=q_v because storage and water table position are not changing. Under seasonal conditions, it is

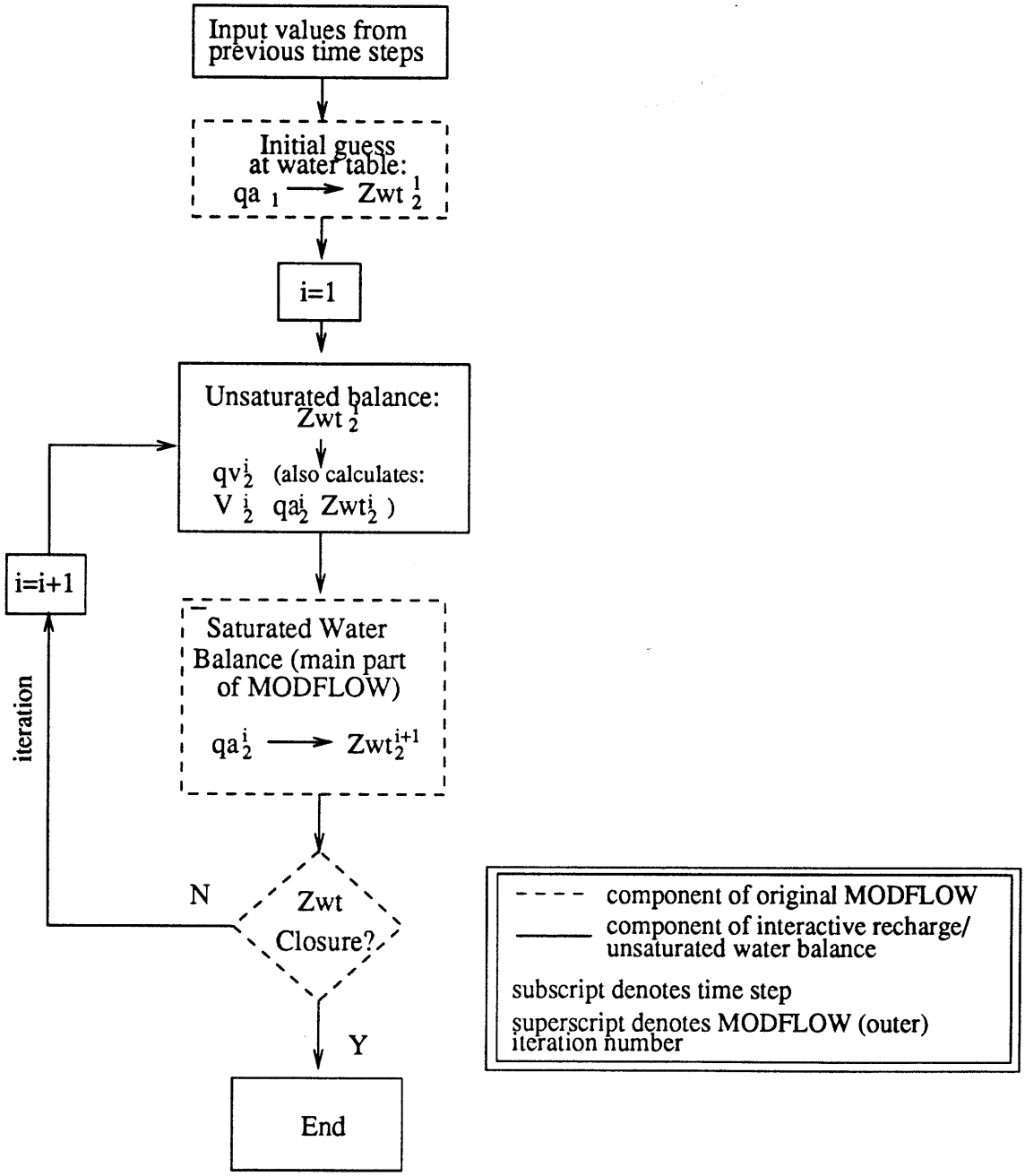

Figure 2-2: Solution algorithm (left) and variables known after each solution step(right). The system is solving for the states at time step two, based on information from the two previous time steps.

difficult to estimate an initial q_a accurately enough for the model to be stable. The model is more robust towards inaccurate choices of q_v and Z_{wt}.

2.4.1 Time step dependence

The assumption that the soil moisture profile in the unsaturated zone instantaneously adjusts itself to changes in head and recharge introduces a model dependence on time step length. As an illustration, compare Figures 2-3(a) and 2-3(b) . In Figure 2-3(a) the time step is large. Recharge must fill up region (D) in order to effect a head change of ΔZ_{wta}. In Figure 2-3(b), the initial recharge rate is the same, but the time step length is half as long. After the first time step, only region (D') is filled, but then the unsaturated zone automatically adjusts itself into equilibrium with the water table at position ΔZ_{wtb}. After another time step (at an incrementally smaller recharge rate), the water table rises again by ΔZ_{wtc}. The total increase in water table height is greater when the change is made over two time steps instead of one, because area (J) is filled "automatically". Thus time step length affects apportionment of water between unsaturated storage and recharge.

For discrete problems using time steps on the event time scale (0.5–1.0 days), the solution was found to be fairly insensitive to the choice of time step length. This scale was selected because it is seems like a reasonable period (within an order of magnitude) for the moisture in a soil column to reorganize itself vertically.

2.4.2 Solution difficulties due to soil and climate types

In some cases, soil and climate parameters combine in ways that render the equilibrium solution difficult to find or nonexistent.

One such case occurs when dry climate coincides with low infiltration, causing negative net recharge all the way from surface to bedrock (negative recharge indicating away from the water table). In this case, some model cells may dry out completely. The drying of cells creates two difficulties. First, a mechanism must be developed in order to account for unsaturated zone dynamics during the drying season. The

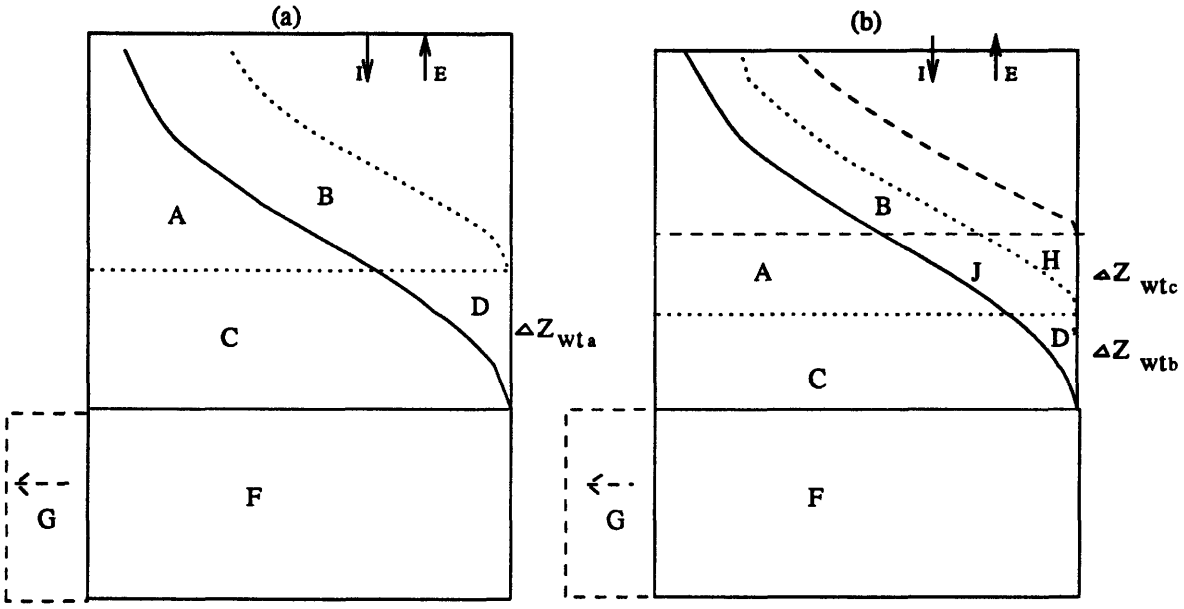

Figure 2-3: Effect of long (a) and short (b) time step length on the incremental water balance.

volume of water stored in the unsaturated zone would have to decrease, although the water table is at bedrock or does not exist. Second, a method must be developed to account for rewetting during the wet season. The rewetting module in MODFLOW is not useful for this purpose because it depends on comparing the bottom elevation of the dry cell to the head in neighboring wet cells. Using hillslopes with thin soil layers and coarse elevation resolution, the head in neighboring cells may not reach the threshold necessary to wet the dry cell.

A second pathological case occurs when the equilibrium solution requires that negative recharge occur that is greater than the maximum capillary rise. Maximum capillary rise is the maximum negative recharge which can occur in a Brooks-Corey soil without forcing the surface soil moisture to become negative. The magnitude of maximum capillary rise (w) is given by:

$$w = \frac{K_{sat}(\frac{(Z_s - Z_{wt})}{\Psi_{sat}})^{-mc}}{1 - (\frac{(Z_s - Z_{wt})}{\Psi_{sat}})^{-mc}} \tag{2.16}$$

for $Z_{wt} < Z_s - \Psi_{sat}$, Eagleson (1978c).

Here m is the Brooks-Corey size distribution index and c is the pore disconnectedness index. Maximum capillary rise does not depend on climate or season, and decreases with soil depth.

When mc is large or Ψ_{sat} is small, w becomes small in magnitude, particularly at deeper soil depths. If the water balance calls for negative recharge in excess of w, then no solution exists. This situation is most likely to occur during the dry season, when the water table falls.

Chapter 3

Comparing seasonal and steady state models: application to a planar hillslope

3.1 Description of simulation

This section compares the seasonal model to the steady state model by applying it to a planar hillslope under Oklahoma climate conditions. The comparison is made using seasonally-varying climate parameters in the seasonal model and the mean of these parameters on the steady state model.

The hillslope used in the present simulation is 75 meters long (measured horizontally, not along the slope), with a ten percent gradient and a uniform soil layer two meters in depth above impermeable bedrock. The top and bottom of the hill were specified as no flow boundaries in order to mimic the effects of a hillslope divide and a symmetrical valley. A seepage face was allowed to develop at the bottom of the hill, and water exiting the soil through the seepage face or in the form of runoff was removed immediately from the system. These conditions are similar to to those used by Salvucci and Entekhabi (1995) and the results may be compared.

The soil was assumed to be a homogeneous Brooks-Corey silt-loam soil, the hydro-

Table 3.1: Brooks-Corey soil parameters for two sample soils.

parameter	silt-loam	sand-loam
K_{sat} (cm/d)	29.3	293.8
Ψ_{sat} (cm)	45	25
n_e	0.35	0.25
m	1.2	3.3

Source: Bras (1990)

Table 3.2: Oklahoma climate parameters.

month	ep(cm/d)	i(cm/d)	t_r(days)	t_b(days)
Jan	0.03	1.75	0.13	7.83
Feb	-	2.03	0.17	5.38
Mar	-	3.40	0.21	5.38
Apr	0.2	4.70	0.25	4.62
May	-	6.28	0.33	3.46
Jun	-	7.73	0.29	3.83
Jul	0.34	5.43	0.21	5.71
Aug	-	5.70	0.25	4.83
Sep	-	5.21	0.21	5.13
Oct	0.21	4.00	0.21	5.67
Nov	-	2.12	0.13	8.29
Dec	-	2.16	0.17	6.79
annual mean	0.20	4.21	0.21	5.58

Sources: Hawk and Eagleson (1992), Mintz and Sarafini (1981)

logic properties of which are given in Table 3.1. This soil type was selected because of its intermediate hydraulic properties, not because its prevalence in the Oklahoma region.

In keeping with both the seasonal and steady state models, flow in the unsaturated zone was assumed to be vertical. Flow in the saturated zone was assumed to be horizontal Dupuit flow, although MODFLOW is not constrained to such simplified flows.

Storm data was obtained for Oklahoma from Hawk and Eagleson (1992), and is shown in Figure 3-1 and Table 3.2. Quarterly potential evaporation estimates for

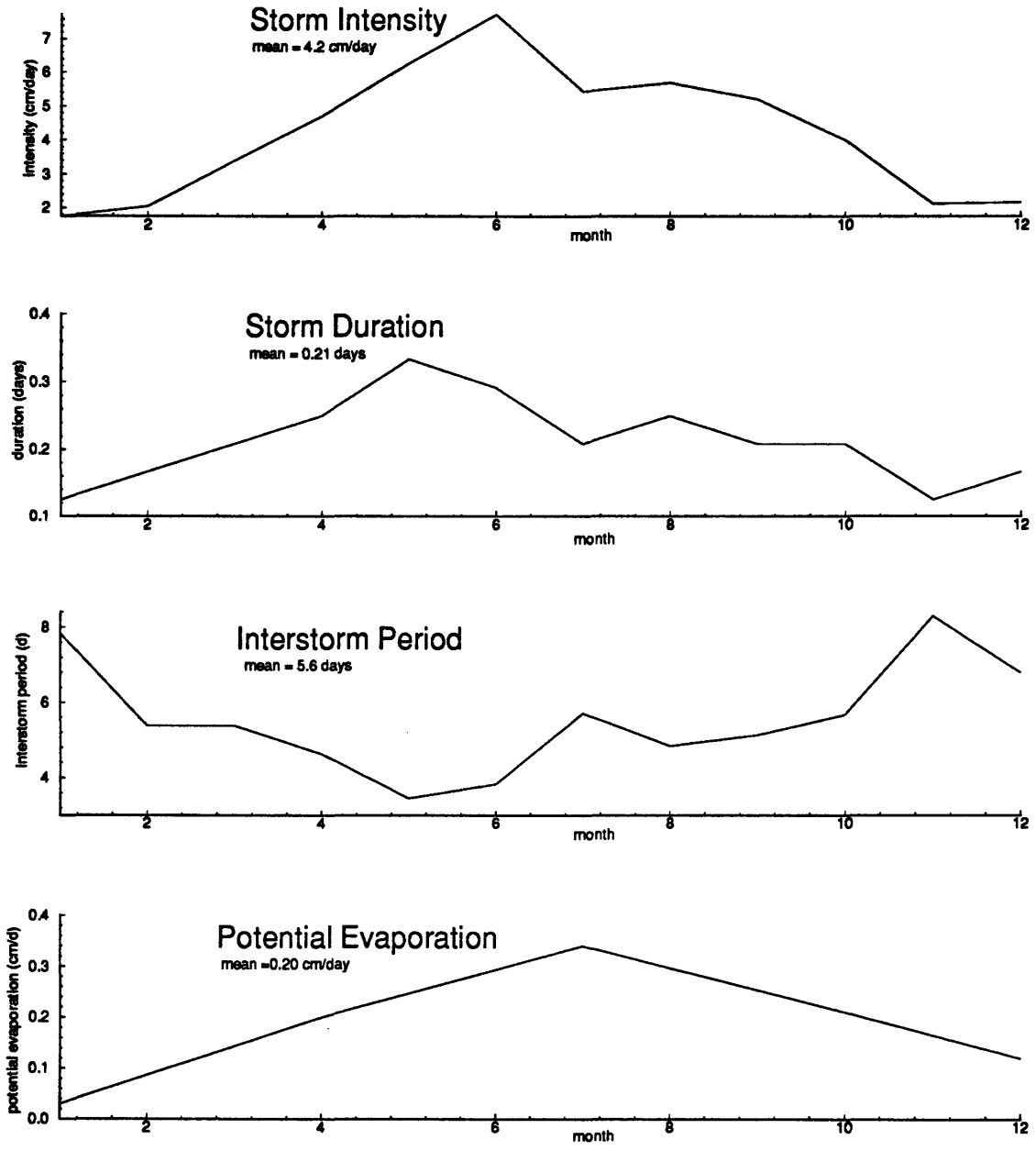

Figure 3-1: Oklahoma climate parameters.

Oklahoma were obtained from Mintz and Sarafini (1981) and are also shown in Figure 3-1 and Table 3.2. These estimates agree well with pan evaporation data for the Little Washita area from Allen and Naney (1991). In the model, all of the monthly and quarterly data are fit to a smooth curve (using Fourier series in six terms) in order that the system not be jarred by large monthly jumps.

These climate parameters indicate a strong seasonal cycle in both precipitation and potential evaporation. The potential evaporation rate follows closely the seasonal cycle of radiative forcing. The precipitation seasonal cycle is characterized by more frequent and longer duration storms in the May to August period. The intensity of storms also peaks in summer. This is essentially a summer rainfall climatic region.

3.2 Simulation results

Figures 3-2, 3-3 and 3-4 show the water table, spatially-averaged fluxes and normalized fluxes resulting from the seasonal simulation. Figure 3-5 shows the results of a similar run using the steady state model using the temporal mean climate parameters (note that as a group the mean climate parameters do not necessarily characterize the climate at any one time).

One of the most distinct results of the seasonal simulation is the abrupt transition between periods of high and low water table positions. Figure 3-6 shows the evolution of the water table height at a point halfway up the hillslope, which approximates a square wave. This switching phenomenon is characteristic of all points on the hillslope, and the division between the high and low water table positions is demonstrated in Figure 3-2, which shows the water table along the entire hill at four points during the season. The magnitude of the seasonal shift is greater at the middle of the hill than at the bottom or top, where the seepage face and bedrock provide a sort of hinge to limit head fluctuations. The seasonal switching illustrates the role of unsaturated storage, which absorbs much of the initial increase in precipitation during Spring.

The magnitude of the seasonal shift in water table position determines the influence of the water table on the control of surface processes. For example, the base of

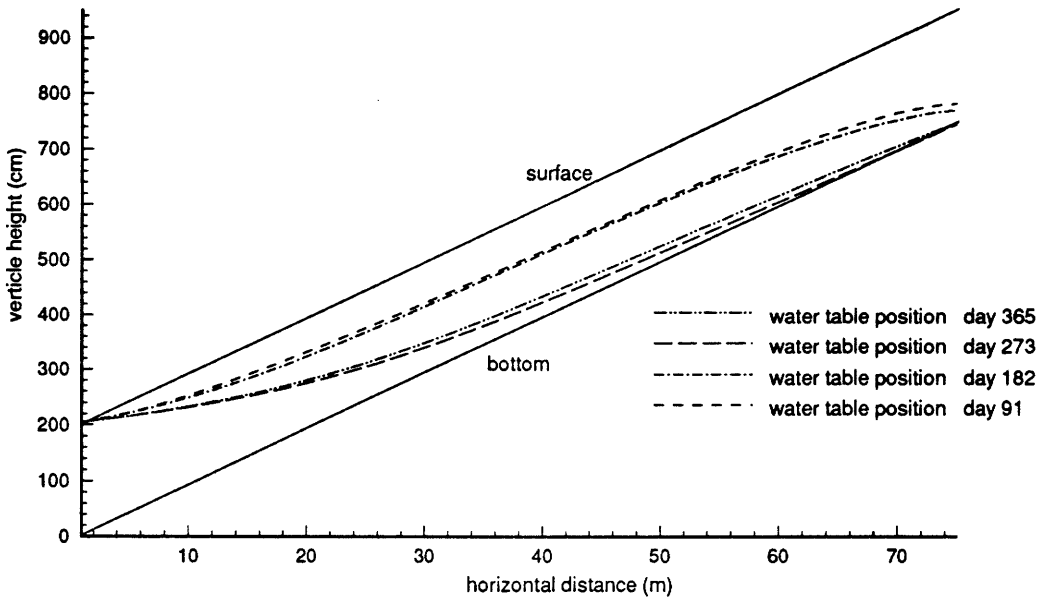

Figure 3-2: Water table profile over a seasonal cycle.

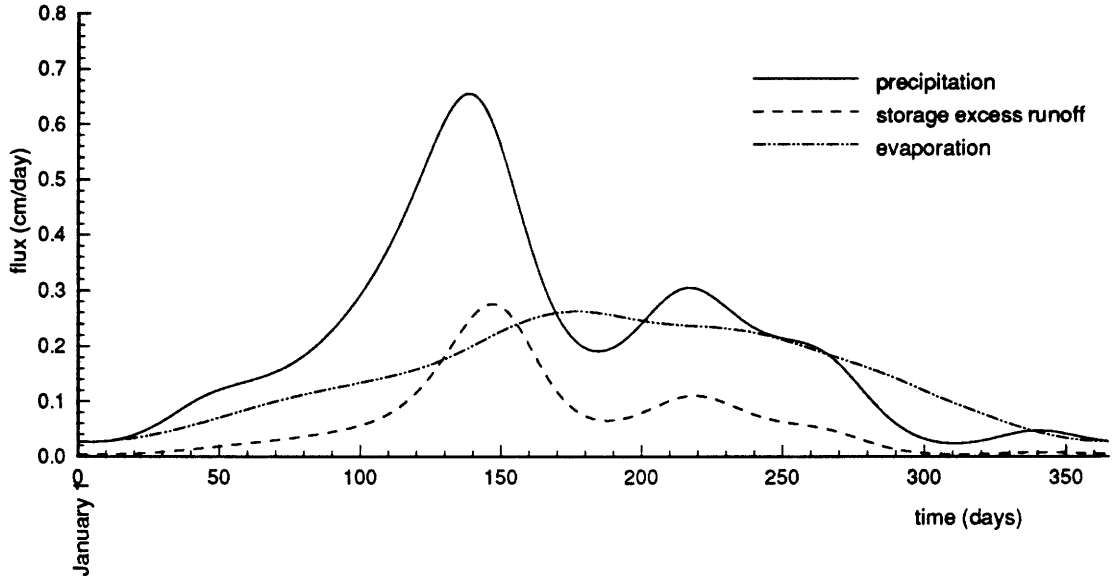

Figure 3-3: Spatially-averaged precipitation, evaporation and storage excess runoff (averaged over the entire hillslope) over a seasonal cycle.

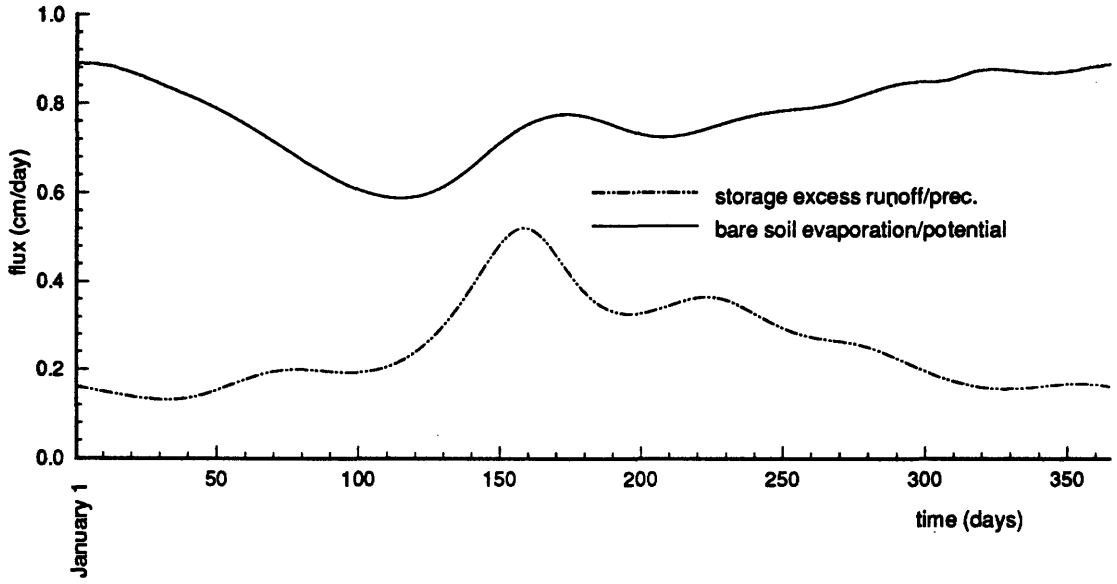

Figure 3-4: Spatially-averaged evaporation normalized by potential evaporation and storage excess runoff normalized by precipitation over a seasonal cycle.

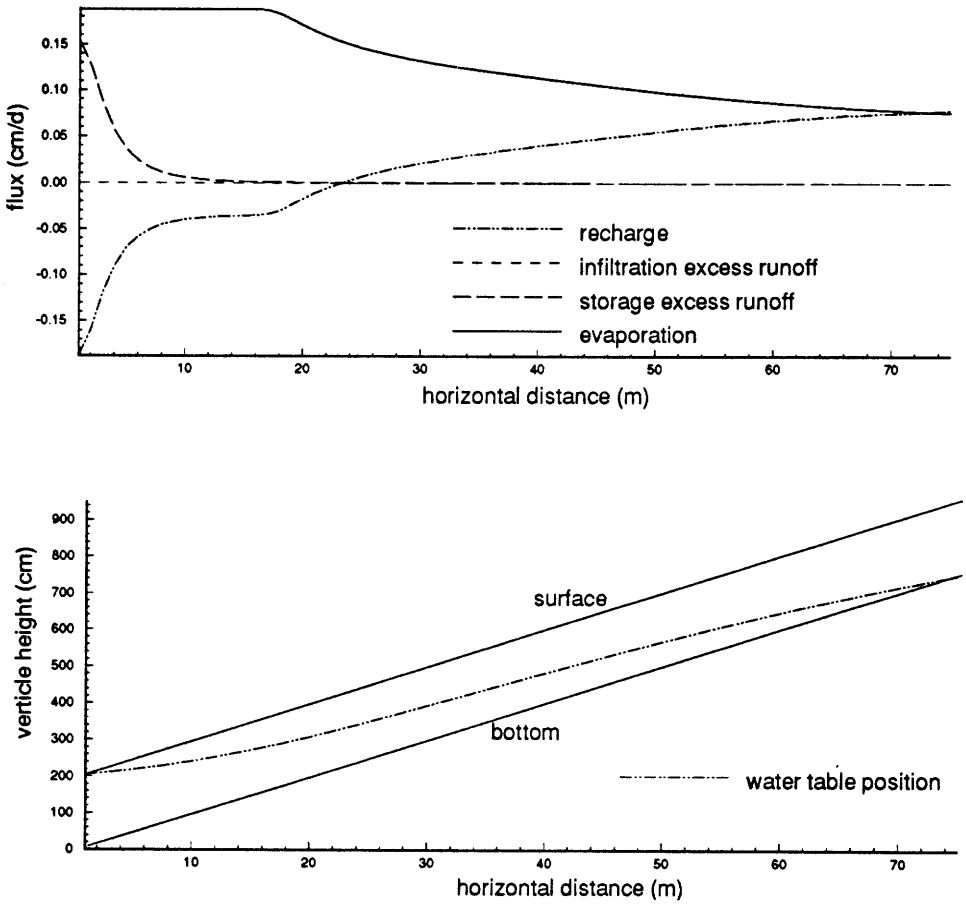

Figure 3-5: Fluxes (top) and water table profile (bottom) from the steady state model using the mean climatic parameters.

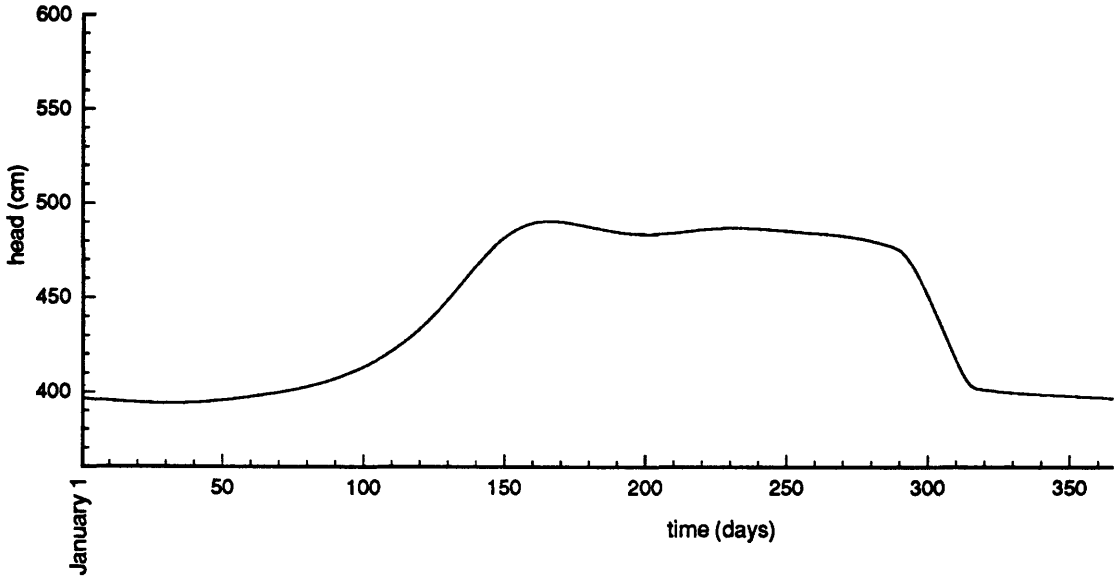

Figure 3-6: Water table position at a point halfway up the hillslope over a seasonal cycle.

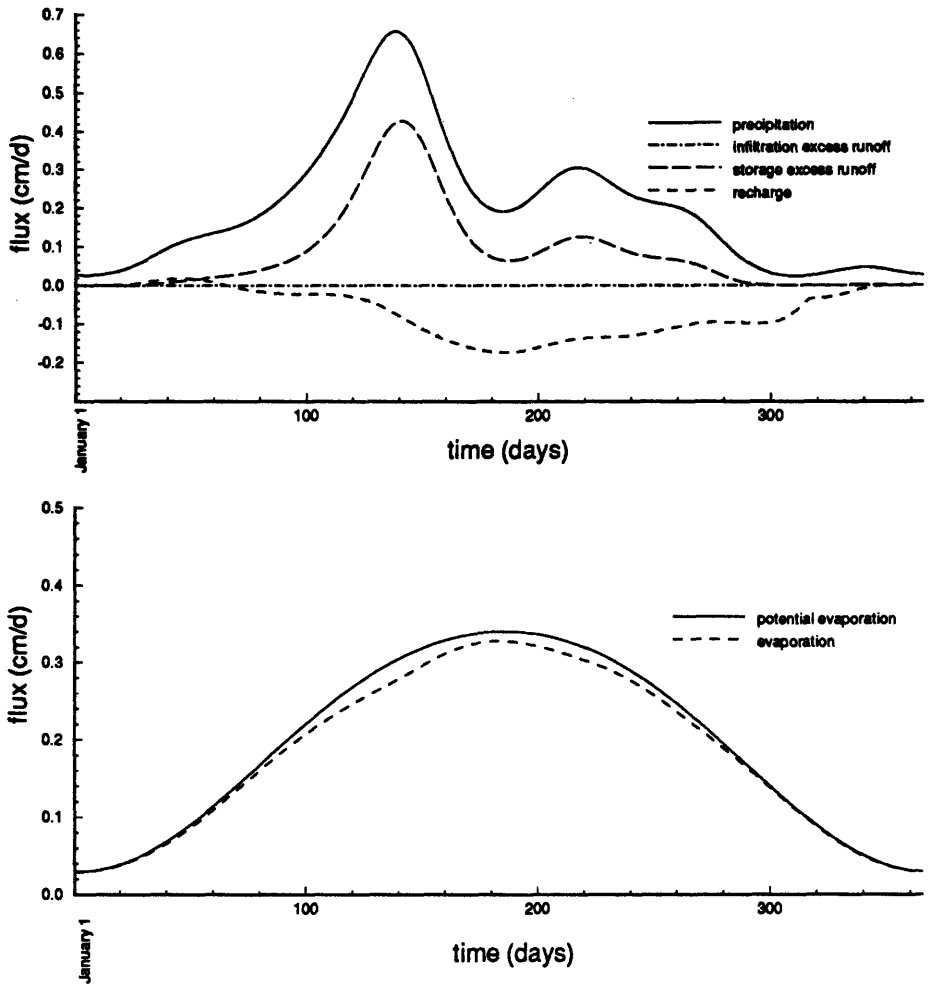

Figure 3-7: Fluxes at a point 5 meters from the base of the hill.

the hill is characterized by a shallow water table that moves relatively little over a seasonal cycle. Since the water table is close to the surface, we would expect runoff and evaporation to be important fluxes in this region. Indeed, Figure 3-7 shows that these fluxes occur at almost their respective potential levels, runoff being limited by precipitation and evaporation being limited by potential evaporation. The recharge is large and positive at this point on the hillslope indicating a large net positive supply from upslope areas. At this point on the hillslope the water table varies little, so that its influence on the surface process is minimal compared to that of climate. This riparian region is effectively atmosphere-controlled.

In contrast, the water table appears to have a much greater influence on evaporation at the middle and top of the hill. Figures 3-8 and 3-9 show that evaporation in these two regions rises and falls between a high and low level, in much the same way

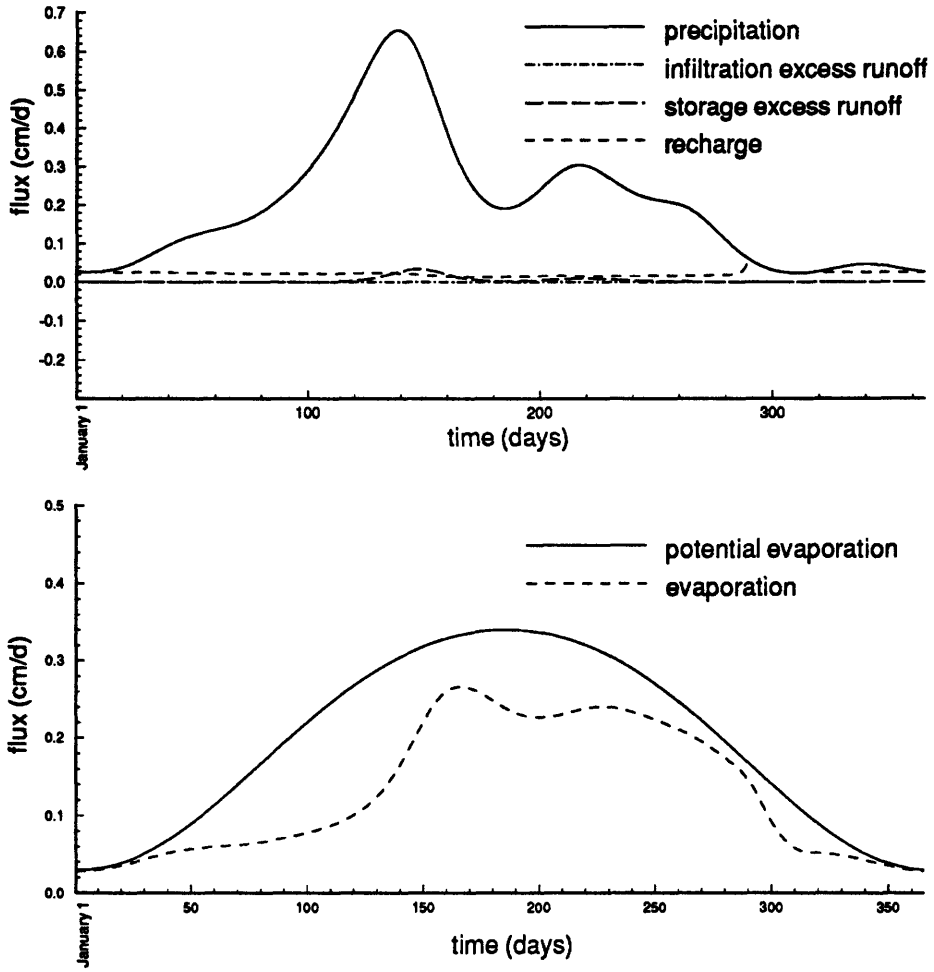

Figure 3-8: Fluxes at a point 37.5 meters from the base of the hill.

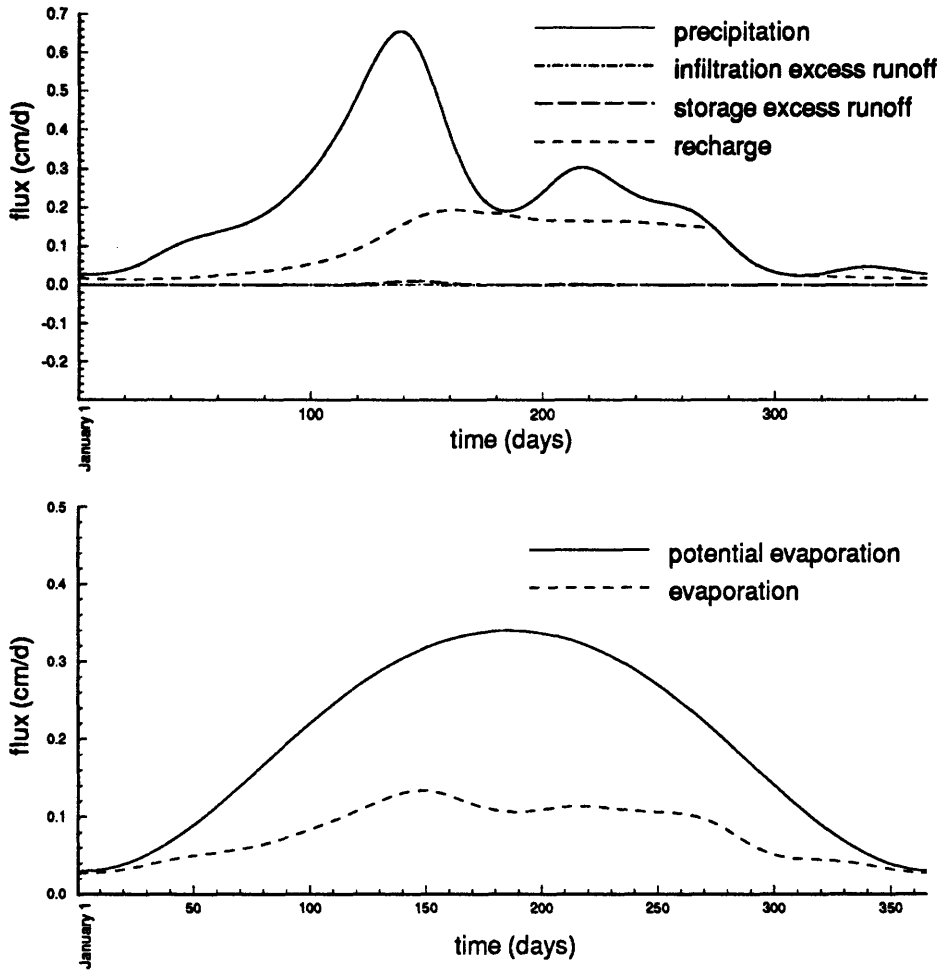

Figure 3-9: Fluxes at a point 71 meters from the base of the hill.

that the water table does. This suggests that evaporation in this region is limited by the availability of water from below (ie., the position of the water table), and not by potential evaporation. In the middle of the hillslope (37.5 meters from the base of the hill), for instance, the summer increase in evaporation is delayed until the water table reaches its high level (see also the rise in normalized evaporation during the summer in Figure 3-4). This effect is less pronounced at the top of the hill (71 meters), where the perennially deep water table allows evaporation to increase only a little in Summer. Evaporation proceeds at the potential rate over the entire hillslope in Winter, largely because the potential rate is so low that the water table would have to be deeper than two meters in order to force evaporation below potential.

One possible analysis that may be carried out using the steady state model, discussed in Salvucci and Entekhabi (1995), is the division of the hillslope into three regions. The lower region is an area of negative net recharge, characterized by high evaporation and runoff. The upper region is an area of lower evaporation and positive recharge. The middle region or "midline" region is an area of zero net recharge which acts as a channel with resistance between the two regions. The water table in the midline is parallel to the bedrock. In the seasonal model, the point halfway up the hillslope clearly approximates the conditions in a midline region; recharge and runoff are both almost exactly zero year around. The horizontal extent of the midline region appears to vary seasonally. No quantitative measure is made here of the size of this region, but the area in which the water table is approximately parallel to the bedrock is more pronounced during the high water table season.

The seasonal patterns of fluxes at the bottom, middle and top of the hill help to explain the variation of the hillslope-averaged fluxes over time, which are shown in Figure 3-3. The spatially averaged runoff signal follows closely the runoff signal at the bottom of the hill, which is not surprising since Figures 3-8 and 3-9 show that almost no storage excess runoff is expected even at the middle of the hillslope (Horton runoff is not significant anywhere on the hill). The spatially averaged evaporation graph shows the influence of both the climate and water table. From Figures 3-7, 3-8 and 3-9 it is clear that significant contributions to evaporation come from all over the

hillslope, though they are stronger towards the bottom of the hill.

In Figure 3-4 runoff has been normalized by precipitation and evaporation has been normalized by potential evaporation. The figure shows that runoff is closest to its potential in Spring as the water table reaches its high position. The response of runoff to precipitation increases during Spring; not only does runoff rise with precipitation, the percentage of precipitation that becomes runoff also increases. This phenomenon can be attributed to the rise in the water table which follows the Spring rains. The higher water table and concomitant higher soil moisture levels in the unsaturated zone increase the fraction of precipitation that becomes storage excess runoff and the size of the region that contributes to runoff. Storage excess runoff is particularly sensitive to the storage capacity of the unsaturated zone because it represents a storm depth threshold below which no runoff occurs and above which all precipitation is converted into runoff.

Evaporation is closest to its potential in the winter. The bottom of the hill is always evaporating at its potential rate, whereas the top of the hill comes closest to potential during the Winter when potential evaporation is low. Overall, the response of evaporation to changes in potential evaporation is less nonlinear than that of runoff to changes in precipitation.

The average annual evaporation and storage excess runoff averaged over the whole hillslope are 46.6cm and 2.7cm using the steady state model and the annual average values of the climate parameters. Using the seasonally-varying parameters and the seasonal model, the hillslope average annual evaporation and storage excess runoff become 52.6cm and 23.1cm. This dramatic difference illustrates the nonlinear response of the hillslope to time-varying climate forcing. In particular, runoff production is much higher in the seasonal model. This occurs because the peak rainy season coincides with the time when the water table is in its high position. When the water table is high, there is little unsaturated storage space available before an event, so storage excess runoff occurs early. In contrast, the steady state model produces a water table at intermediate depth which, when used as a pre-storm initial condition, requires a large volume of rainfall to fall before saturation (and thus runoff) can occur.

Chapter 4

Application of the Equilibrium Model to the Little Washita basin

4.1 Introduction

This chapter describes the application of the seasonal model to a real watershed – the Little Washita river basin in Oklahoma. This watershed encompasses complex topographical features, unlike the planar hillslope example of Chapter 3. Due to the computational burden of the seasonal model, application to the entire Little Washita basin required the use of coarser elevation data than the 30m resolution Digital Elevation Model maps which are available for the basin. The 30m data was resampled at a rate of one in twenty, resulting in a 600m DEM characterization of the basin. An elevation map for the basin is given for this resolution in Figure 4-1.

The seasonal model failed in this case because of scaling difficulties which form the motivation for Chapter 5. This chapter serves primarily as an introduction to the Little Washita watershed and to document the negative affect of large cell size and coarse DEM resolution on both the steady state and seasonal models.

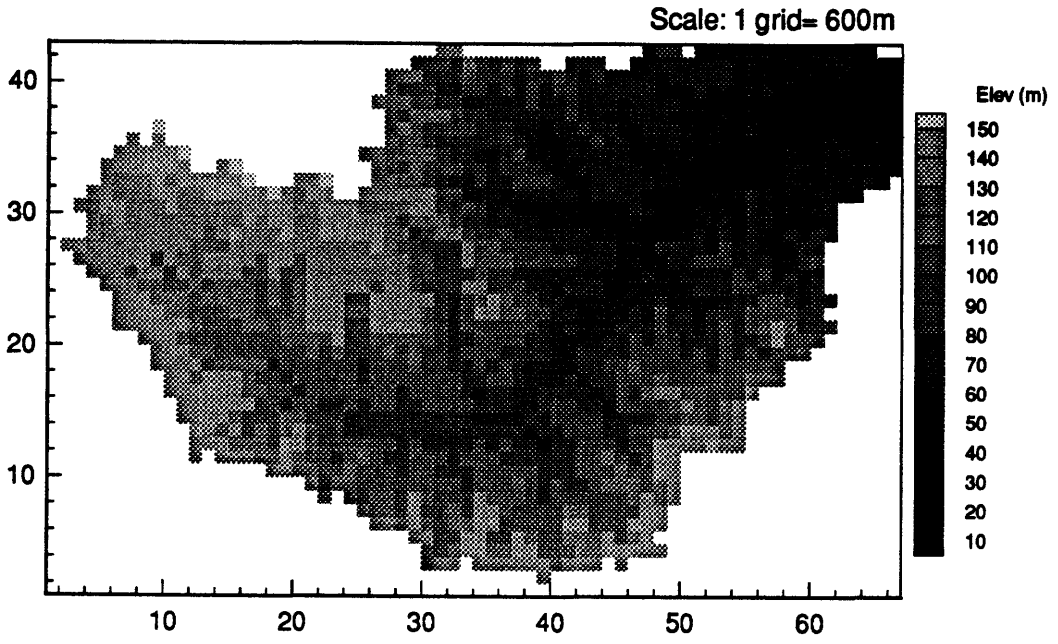

Figure 4-1: Little Washita basin at 600m resolution.

Table 4.1: Brooks-Corey soil parameters for a 2:1 mix of sand loam to silt loam.

K_{sat} (cm/d)	203.6
Ψ_{sat} (cm)	31.4
n_e	0.31
m	2.6

Source: Bras (1990)

4.2 Characterization of watershed

The Little Washita River watershed drains from the southwest into the study reach of the Washita River in Oklahoma. The drainage of the basin is approximately 655 square kilometers. With the exception of a few rocky, steep hills the topography of the basin consists of gently to mildly rolling hills. Maximum relief in the watershed is only about 200m, and slopes are typically less than ten percent. In the alluvial areas, the slopes are often one percent or less.

Topographical information for the simulation was obtained using 30m DEM data prepared by the Agricultural Research Service. For computational purposes, it was necessary to resample this data at the much lower resolution of 600m, or 1:20 of the original data. Resampling is preferred over averaging since the topographic peaks and valleys are better preserved in the reduced data set. The effects of changing the resolution of elevation data are investigated in Chapter 5.

A number of soil types are represented in the basin. Based on soil information from the Agricultural Research Service, the basin mostly comprises a 2:1 mix of sand-loam to silt-loam. The Brooks-Corey parameters for sand-loam were calculated by weighted interpolation of values from Bras (1990), which are reproduced in Table 3.1. This approach was adopted, despite the availability of quantitative soil data for the Little Washita, in order to achieve consistency with other model runs in this thesis and in Salvucci and Entekhabi (1995). The interpolated parameters are summarized in Table 4.2.

Allen and Naney (1991) contains of map of soil depth throughout the basin. In

the northeast, where alluvial soils predominate, in the south, where slopes are less steep and more erosion resistant and in the upstream western section, where soils formed from the Cloud Chief formation, the soil is deepest, typically over five feet. In contrast, the scarps around the Cloud Chief formation outliners in the west have soil depths as shallow as 50cm. A depth of 127cm appears to best characterize the basin as a whole, and was used in the model applications.

A land-use survey of the basin was made by the Agricultural Research Service (ARS) in 1974. According to this survey, approximately 66% of the area is used as rangeland, 18% is cultivated and 16% is used for miscellaneous purposes. Dense timberland covers only 5% of the land area, and is calculated as part of the miscellaneous group. The effects of land use and vegetation are neglected in the model.

Runoff from approximately 19.5% of the drainage area of the basin is controlled by farm ponds in the west part of the watershed; as a result these areas do not contribute directly to runoff. In addition, the Soil Conservation Service (SCS) has installed at least 45 flood-retarding reservoirs throughout the basin. These structures will also attenuate the effect of runoff.

The climate on the Little Washita is the same as the Oklahoma climate described in Chapter 3. Figure 3-1 and Table 3.2 show the relevant climate parameters.

4.3 Seasonal model results

The cell size and coarseness of DEM data used in the seasonal model turned the basin into almost a one-dimensional model. The seasonal variations in water table position and vertical fluxes were much greater than the spatial variations. To illustrate this, Figures 4-2 and 4-3 show depth to volumetric saturation for January (the dry season) and May (the wet season). The January plot is repeated in Figure 4-4 with a narrower contour range. During January, the mean depth to volumetric saturation is 46.9cm, and the standard deviation is 1.5cm. During May, the mean depth to volumetric saturation is 7.4cm, and the standard deviation is only 0.4cm. The spatial range of variation is thus on the order of a few centimeters, whereas the seasonal variation is

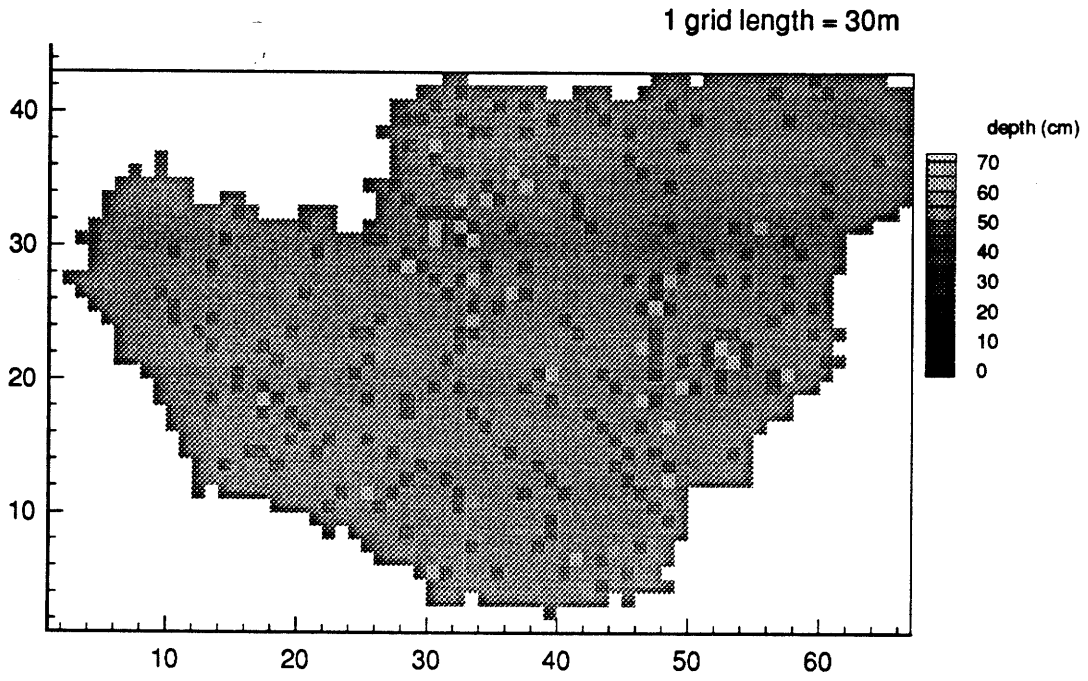

Figure 4-2: Distribution of depth to volumetric saturation in January over the Little Washita basin. The mean is 46.9cm and the standard deviation is 1.5cm.

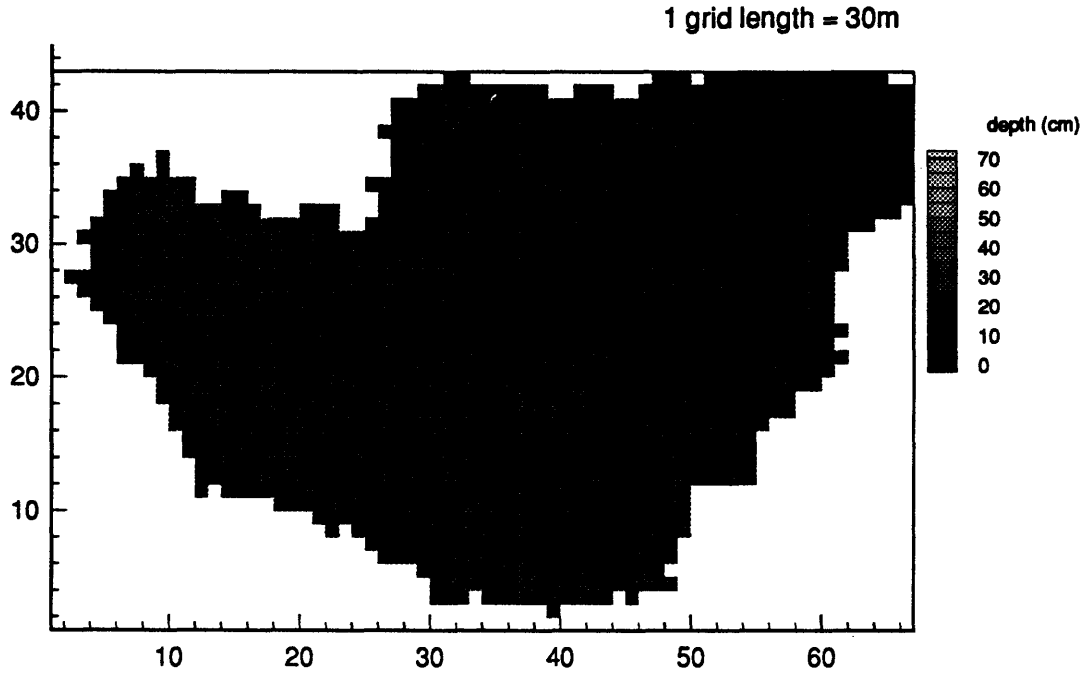

Figure 4-3: Distribution of depth to volumetric saturation in May over the Little Washita basin. The mean is 7.4cm and the standard deviation is 0.4cm.

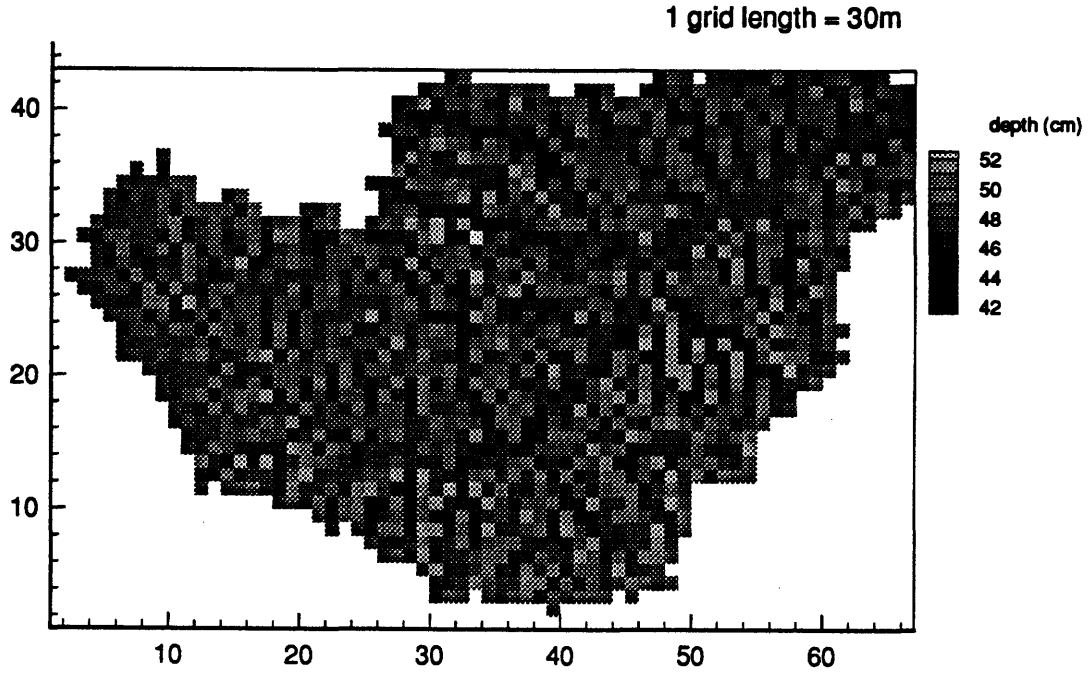

Figure 4-4: Distribution of depth to volumetric saturation in January over the Little Washita basin using a narrow contour range in order to highlight spatial variations.

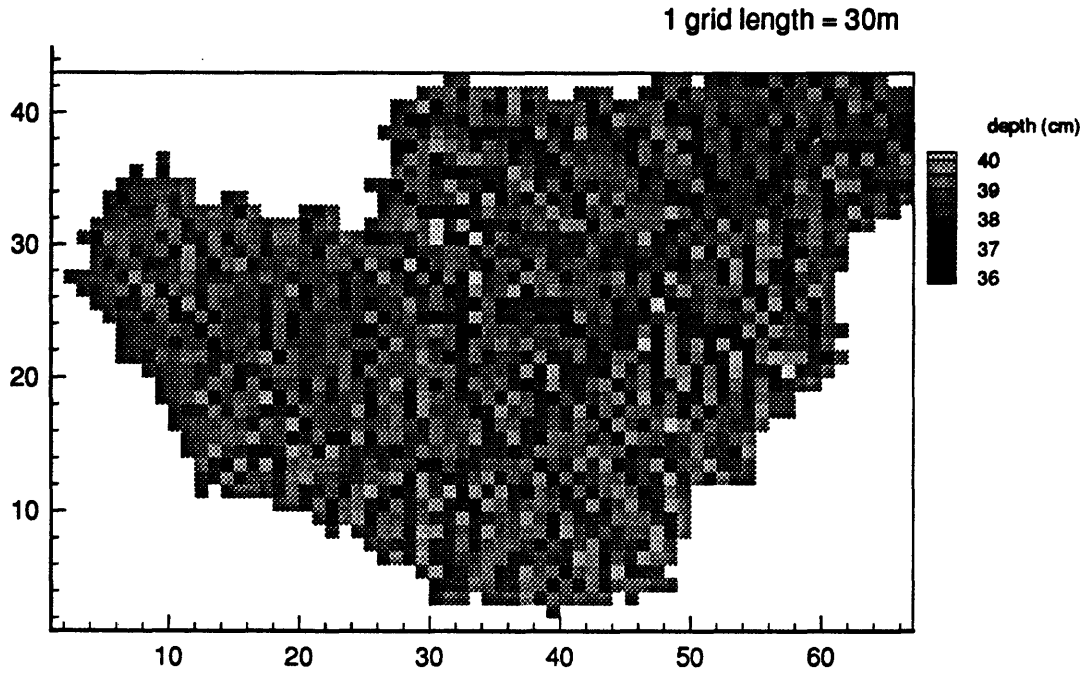

Figure 4-5: Distribution of depth to volumetric saturation over the Little Washita basin for the steady state model.

approximately forty centimeters.

These results do not tally with the results from the planar hillslope case, which suggest that regions of high and low water tables exist throughout the seasonal cycle, although the distribution between the two levels shifts dramatically between the rainy and dry seasons.

Depth to the water table from the steady state model also shows little spatial variation for this flow domain and DEM resolution. Figure 4-5 shows the depth to volumetric saturation for the steady state case, which is confined to a range of just a few centimeters. This magnitude of variation differs greatly from that obtained from a 30m resolution steady state run on a Little Washita sub-basin which will be summarized in Chapter 5. The distribution of water table depths in the present case centers around the equilibrium depth which yields zero recharge, a phenomenon which will also be analyzed further in Chapter 5.

The large seasonal variations in water table depth and fluxes resulting from the seasonal model are further demonstrated in Figure 4-6, which shows the seasonal cycle at cell [42,9] on the 600m resolution map (which lies within the sub-basin examined in Chapter 5). This cell exhibits a low water table position ten months of the year, along with low runoff. Immediately following the beginning of the rainy season in May, the water table jumps and expected runoff increases to 0.9 cm per day. After June, the water table subsides, coinciding with peak evaporation and the end of the brief summer rainy season. Like in the planar hillslope model, storage occurs in the spring before the runoff season begins. Water is released from storage several months later, in the beginning of the hydrologic dry season.

Because of the lack of spatial variation, all cells in the basin exhibit seasonal patterns similar to those of cell [42,9]. Thus it must be emphasized again that even though the results shown in Figure 4-6 capture the dynamics of a seasonal cycle, they are essentially the results of a one-dimensional model.

The homogeneous spatial pattern of depth to volumetric saturation for the seasonal model of the Little Washita basin at coarse (600m) resolution is also reflected on components of the surface water balance. The partitioning of precipitation into

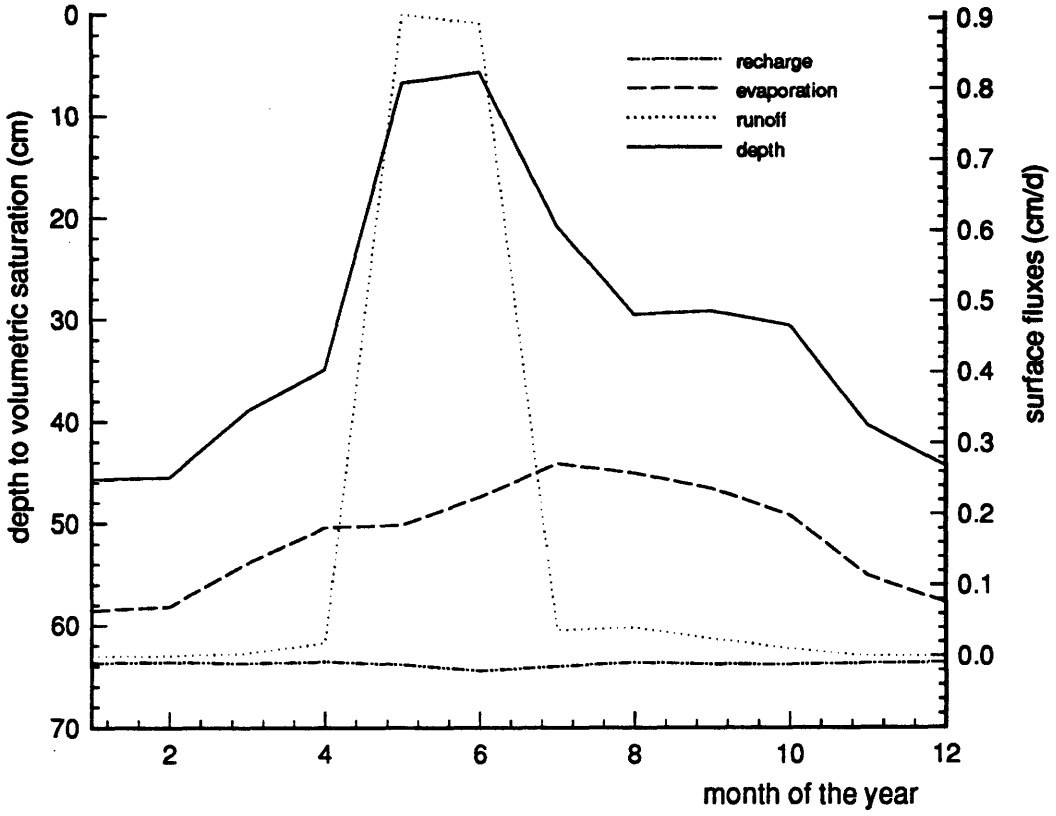

Figure 4-6: Seasonal cycle of fluxes for a location within the Little Washita basin.

surface fluxes is closely related to the position of the water table in the derived-distribution seasonal model.

Clearly none of the topographic features (drainage network, convergent and divergent zones) are reflected in Figures 4-2 through 4-5, except when the scale is blown up to exaggerate minute variations in depth to the water table. The position of the water table adjusts itself in response to the seasonal forcing to maintain low net exchange between the saturated and unsaturated zones, which is reflected in the near-zero recharge values throughout the year in Figure 4-6. A conceptual-physical explanation for this behavior is presented in the next chapter. It will also be shown that this problem is associated with the coarse resolution of the DEM (600m). When the elevation is characterized at higher resolution and smaller cell size is used, the tendency for the equilibrium solution to seek zero-recharge is eliminated.

Chapter 5

Effects of DEM resolution and aggregation

5.1 Introduction

This chapter investigates how DEM resolution and aggregation affect the steady-state water balance model. The goal of this investigation is twofold: to determine a discretization length for which the equilibrium water balance model functions effectively, and to study the effects of spatially aggregating and averaging model processes.

The results presented in this chapter come from the steady state model using elevation data at 30m, 300m and 600m. The 30m DEM represents the finest resolution elevation data available for the Little Washita basin. The two coarser resolution resolution DEMs were created by resampling the 30m data. A resolution of 300m was the finest at which the author was able to integrate the steady state model over the whole basin given computing constraints. Chapter 4 outlines the results from integrating the seasonal and steady state models over the full basin at 600m resolution.

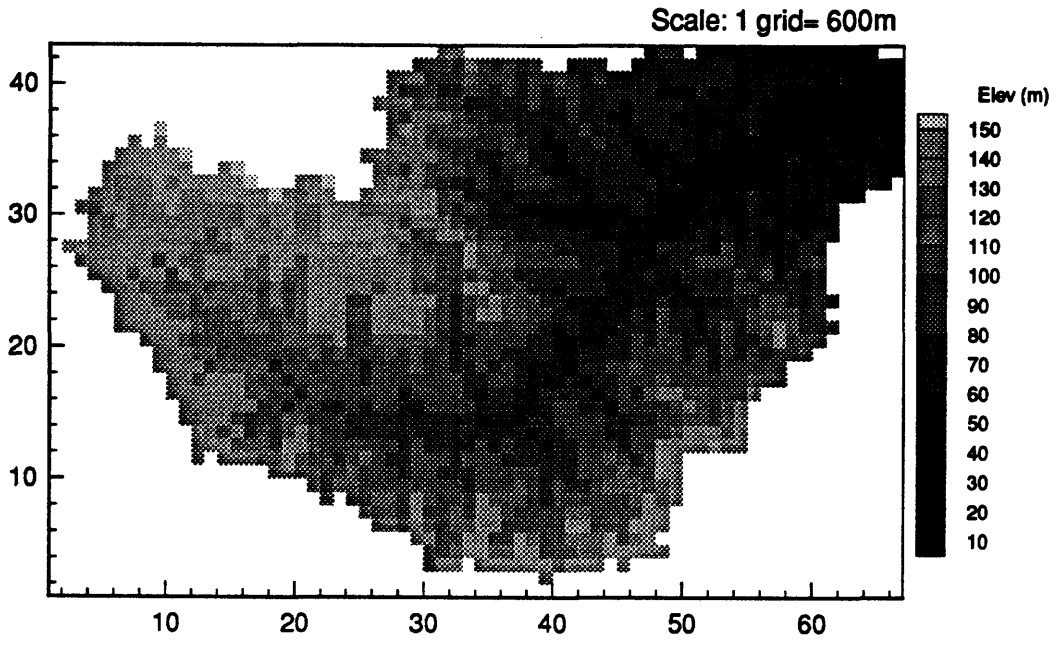

Figure 5-1: Little Washita basin at 600m resolution.

5.2 Study areas

The present investigation focuses on two areas. The first is the entire Little Washita watershed, for which we compare aggregate results of the steady state model (no seasonal cycle) on grids of 300m and 600m. Figures 5-1 and 5-2 are elevation maps of the Little Washita basin at these two resolutions.

The second study area is part of a sub-basin in the southern portion of the Little Washita watershed. The location of this sub-basin is shown in Figure 5-2. The study area comprises a rectangular portion of the sub-basin, which is depicted at 30m, 300m and 600m resolution in Figure 5-3. The column and row coordinates given in this

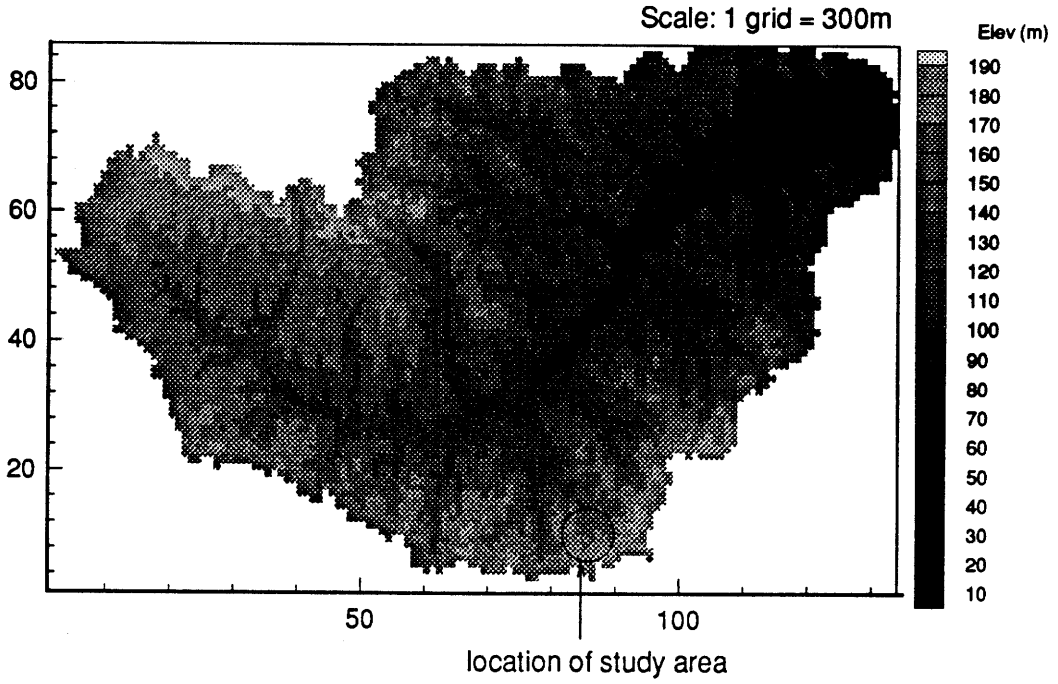

Figure 5-2: Little Washita basin at 300m resolution, with the location of the study sub-basin.

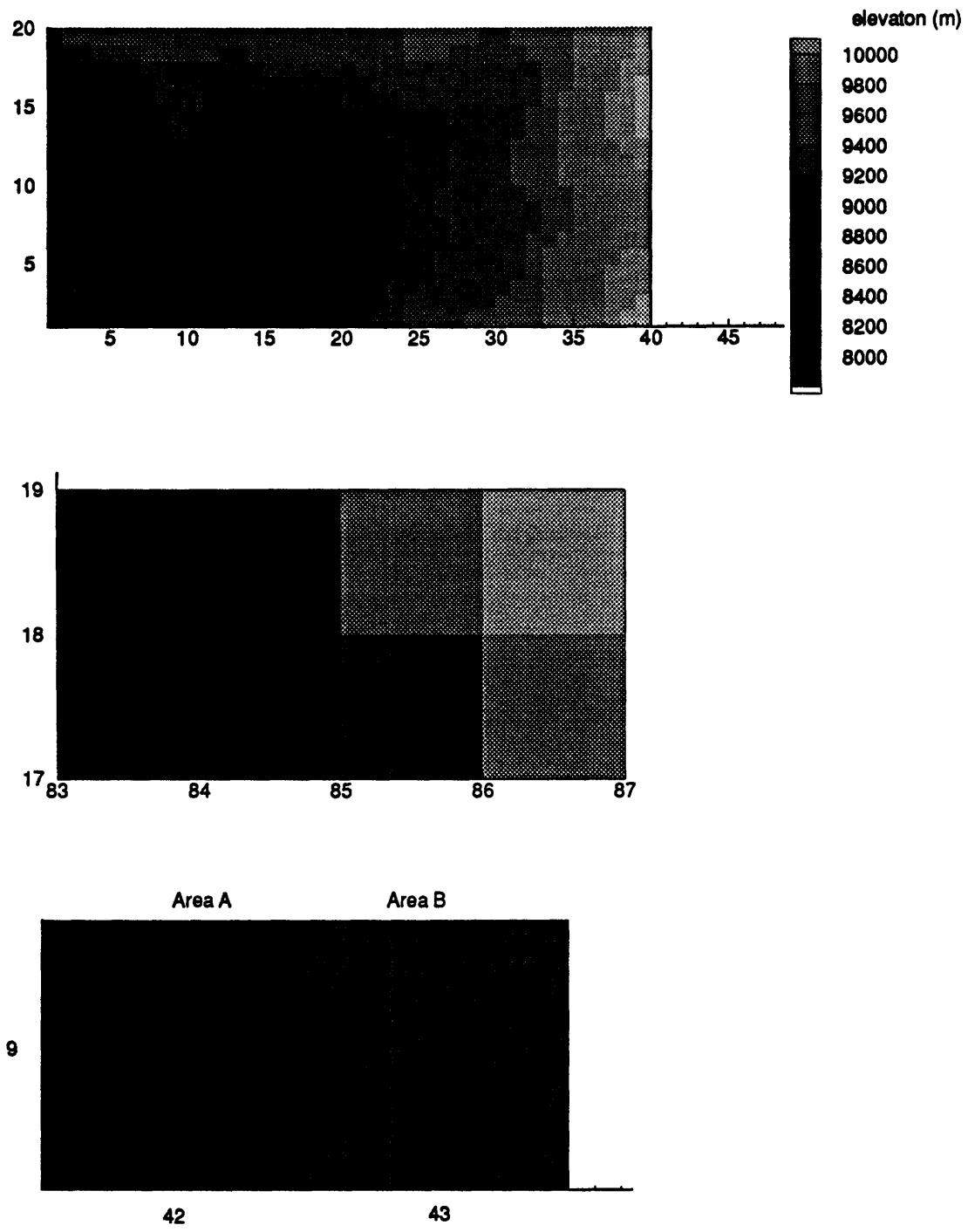

Figure 5-3: Rectangular study area at 600m, 300m and 30m resolution. Area A and Area B refer to the areas encompassed by the two 600m resolution pixels.

figure indicate the position of cells within the 300m and 600m resolution maps of the Little Washita basin. Note that at 600m resolution the study area comprises just two cells, and that these are referred to as Area A and Area B respectively. In this case, the decrease in resolution causes a significant reduction in the topographical gradient.

In order to compare results at 30m resolution, it was necessary to carry out a new steady state model simulation on the sub-basin. The sub-basin simulation was conducted using the same climate and soil parameters that were used in the full basin simulations discussed in Chapter 4. An elevation map of the full sub-basin is given in Figure 6-1 in the following chapter.

5.3 Flux partitioning

Figure 5-4 shows the partitioning of rainfall into recharge, evaporation and storage excess runoff for the full Little Washita basin at 300m and 600m resolution. All runoff is storage excess runoff; infiltration excess runoff in the present case is negligible. Figures 5-5 and 5-6 show the same partitioning in the sub-basin for Area A and Area B respectively. From these three figures, it is apparent that there is little difference between the flux partitioning at 300m and 600m resolution. Moreover, Figure 5-4, as well as Figures 4-2 through 4-6 from the last chapter, suggest that the models at coarse resolutions (300m or 600m) seek a solution of zero recharge. At 30m resolution, the model is better able to capture local areas of convergence and diverge which produce shallow and deep water tables.

At least in part, the pathological zero recharge solution is due to large cell size and not to the actual sampling of the DEM. The saturated flow equations used in MODFLOW for steady unconfined saturated flow in homogeneous media resemble the following:

$$\Delta y K_{sat} H \frac{(H(i+1,j) - H(i,j))}{\Delta x} + \Delta y K_{sat} H \frac{(H(i-1,j) - H(i,j))}{\Delta x}$$
$$+ \Delta x K_{sat} H \frac{(H(i,j+1) - H(i,j))}{\Delta y} + \Delta x K_{sat} H \frac{(H(i,j-1) - H(i,j))}{\Delta y}$$
$$+ \Delta x \Delta y q_v = 0$$

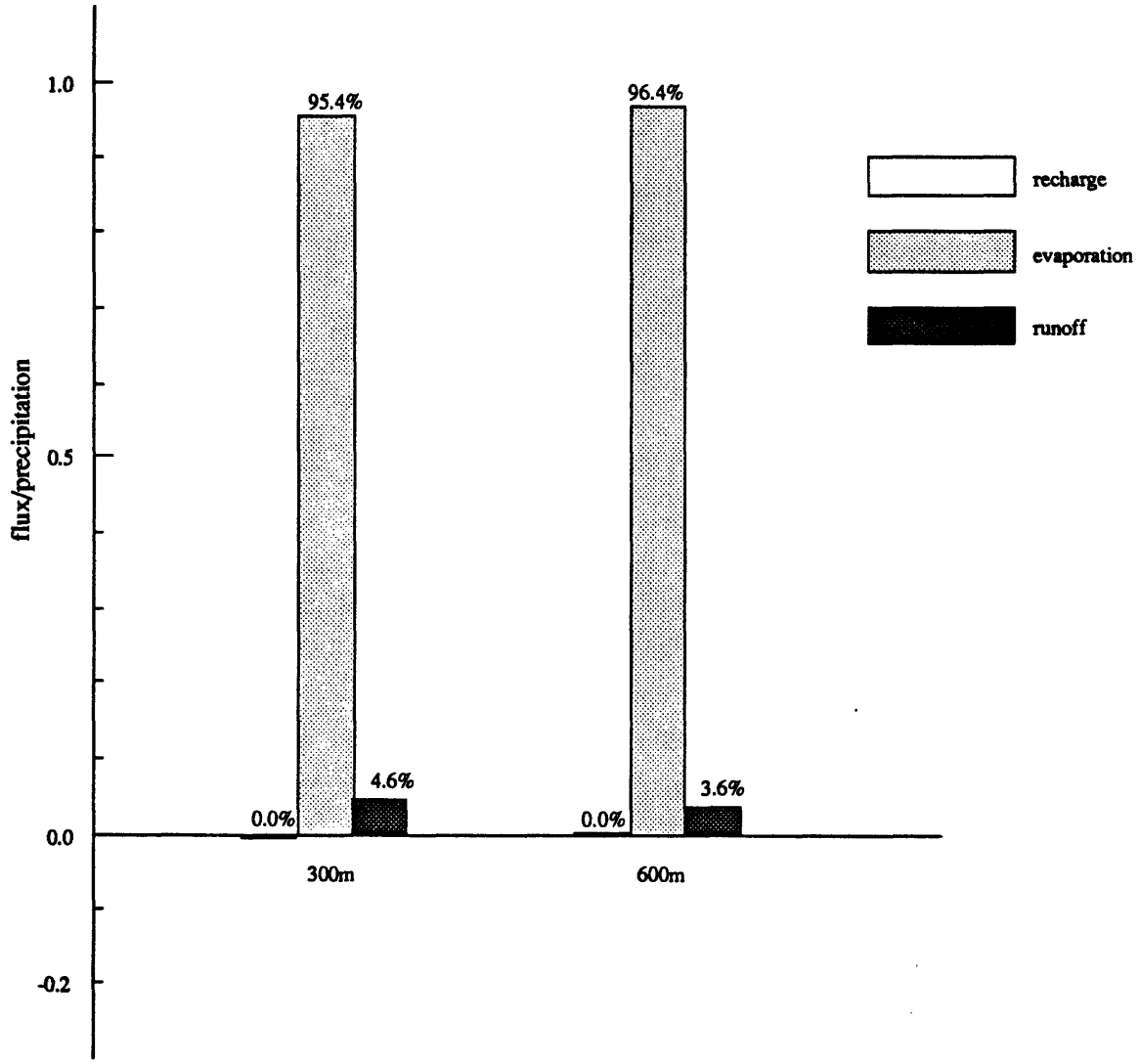

Figure 5-4: Partitioning of rainfall between surface fluxes for the full Little Washita basin.

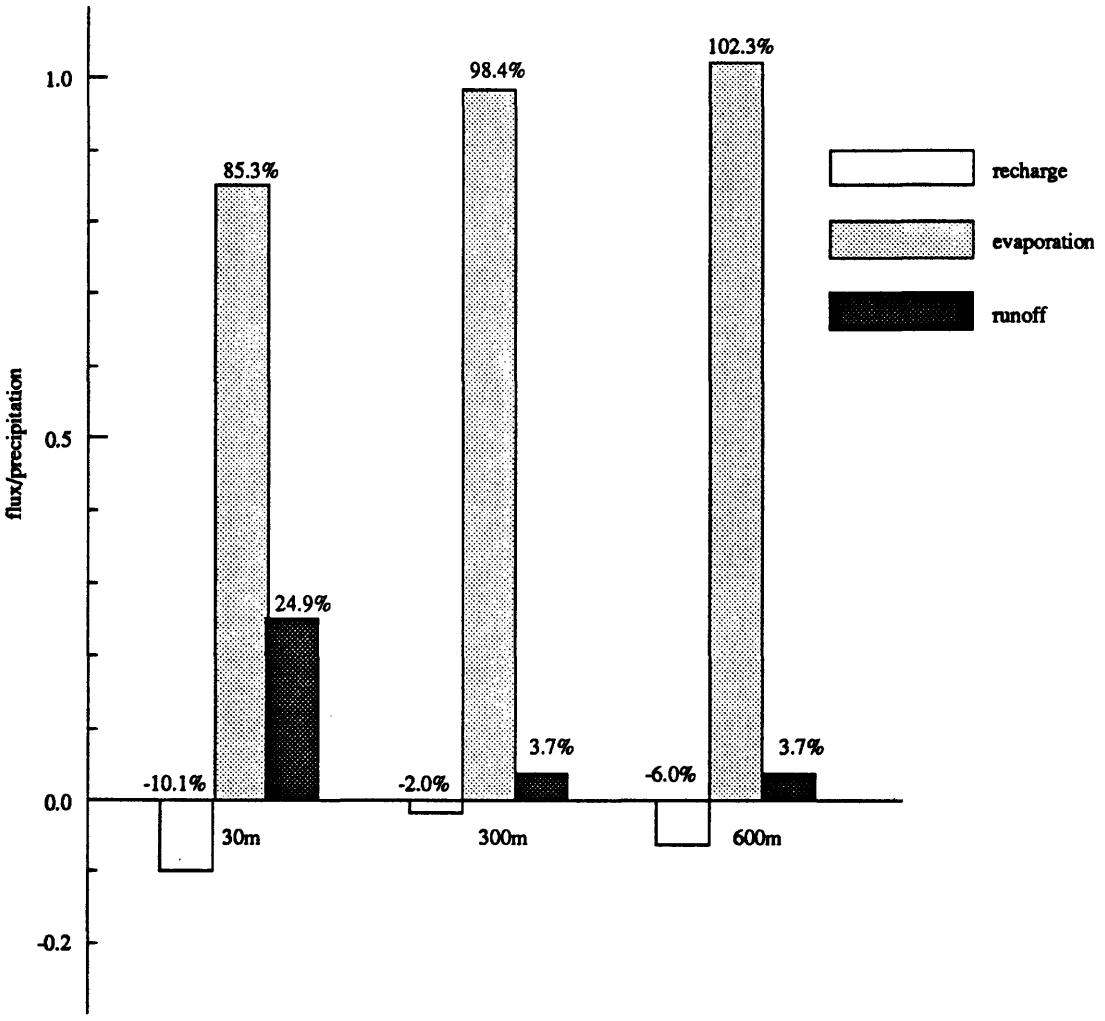

Figure 5-5: Partitioning of rainfall between surface fluxes for Area A.

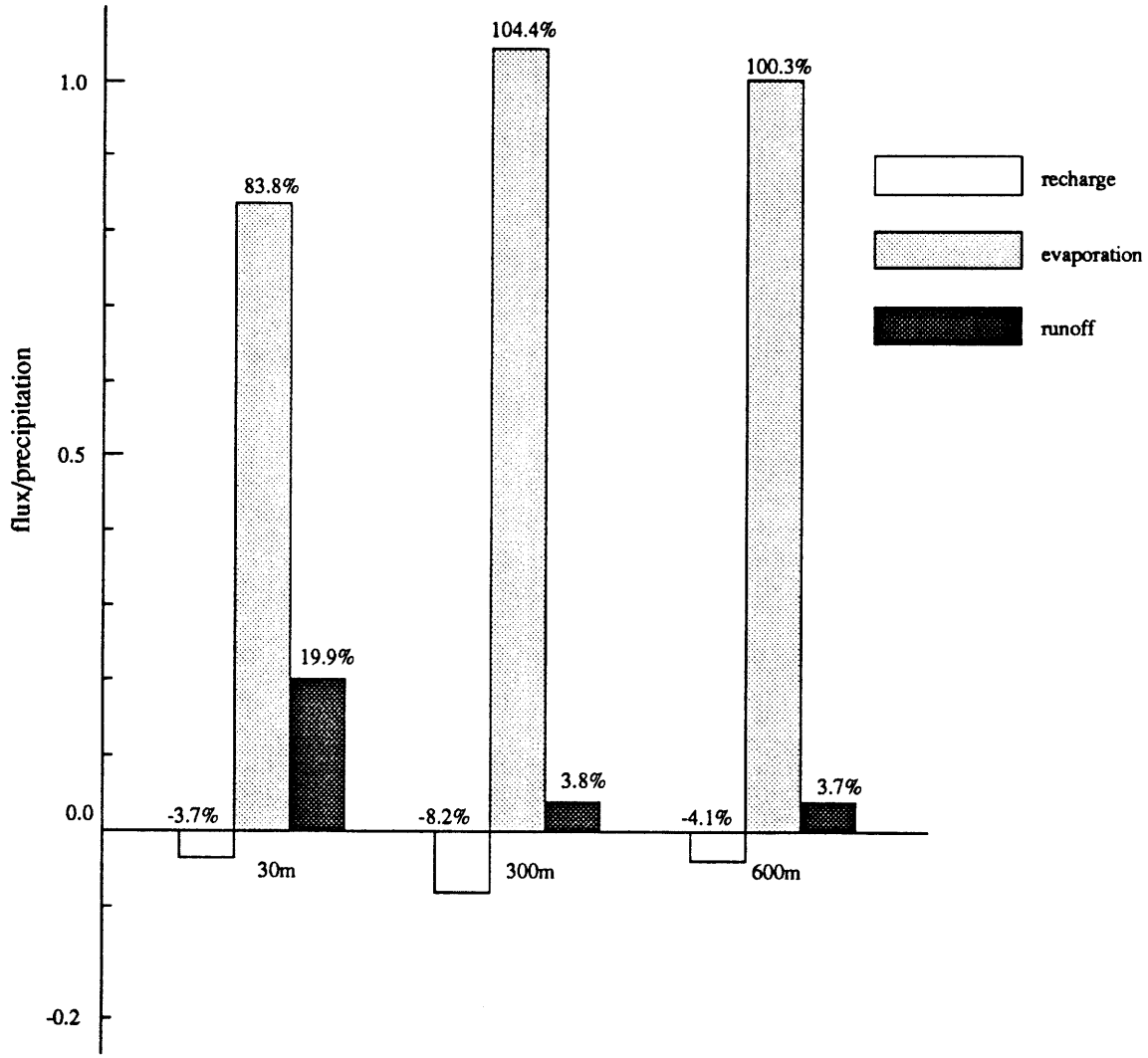

Figure 5-6: Partitioning of rainfall between surface fluxes for Area B.

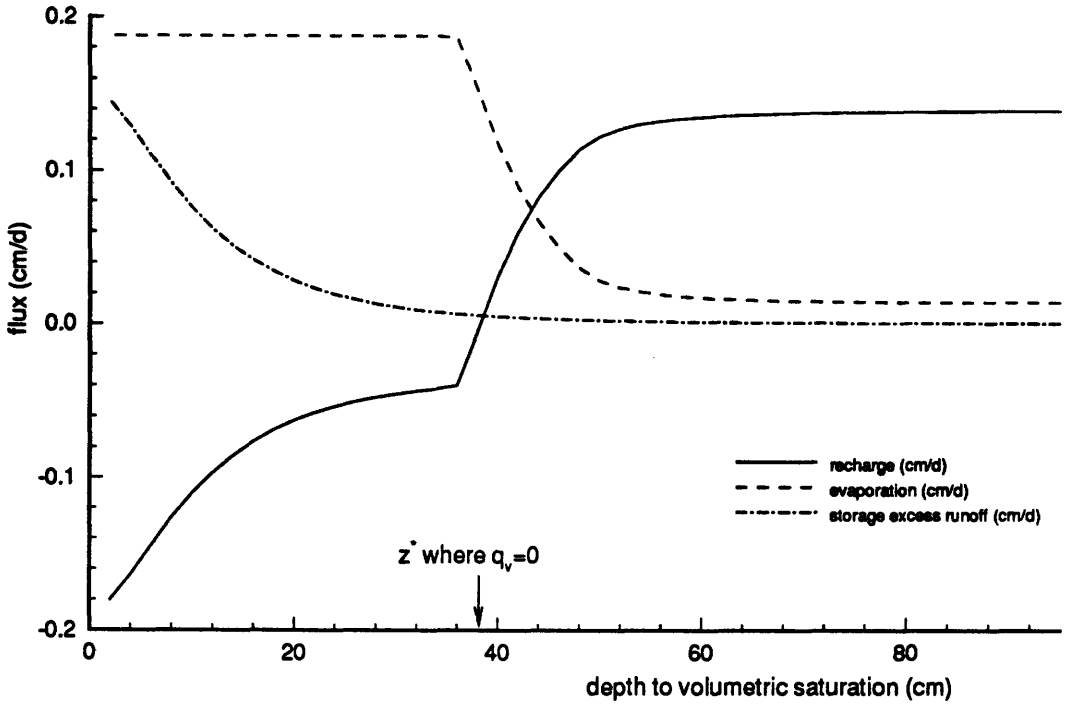

Figure 5-7: Variation of surface fluxes with depth to volumetric saturation for the steady state model using soil and climate parameters from the Little Washita.

where the notation of this thesis has been adopted and single layer flow in the vertical direction has been assumed.

As Δx and Δy become large, the recharge term (the last term on the left hand side) dominates. Recharge q_v grows as $\Delta x \Delta y$, whereas the lateral flow terms grow only as Δx or Δy. For large Δx and Δy, it is possible that the water balance is satisfied by $q_v = 0$ and no longer maintains head gradients to create convergent and divergent groundwater flow. Because in our model recharge is a function of head, the two are able to equilibrate when the depth to the saturated zone in every cell is close to Z^* (38.3cm), the depth for which the equivalent steady flux is zero (see Figure 5-7).

The work done here suggests that large horizontal pixel lengths of 300m and 600m are inadequate to characterize the distributed water balance over complex topography,

in part these resolutions are larger than the scale of local convergence and divergence, and in part because large cell size leads to a poor approximation of the saturated flow. Further work is necessary to isolate these two causes of inaccuracies.

5.4 Flux frequency distribution

The properties of the model solutions at various resolutions are further demonstrated by the frequency distribution of fluxes and water table depth over the basin. Figures 5-8 through 5-11 show estimated frequency densities of surface fluxes and of depth to saturation for the full Little Washita basin at different resolutions. The distribution denoted "300m resolution aggregated to 600m" was constructed by averaging the resulting 300m resolution fluxes in four-pixel square blocks, yielding the same number of data points as in the 600m resolution case.

All of the frequency distributions in Figures 5-8 through 5-11 are unimodal and Gaussian in shape. The 300m resolution results have a considerably larger spread around their mean than do the 600m resolution results. The aggregated (600m to 300m) fluxes have distributions very similar to those of the 600m fluxes, although the distributions in both cases are too poor to draw any conclusions about aggregation. The tendency of net recharge to approach zero is evident in Figure 5-8. This is consistent with Figure 5-11, which shows a strong preference for the depth Z^* to the top of the saturated zone (the depth which gives $q_v = 0$, see Figure 5-7). The symmetric spread in all the figures is indicative of the role of various factors such as divergence, convergence, slope and cumulative drainage area, none of which is strong enough to serve as more than noise around a dominant solution.

Figures 5-12 through 5-15 show the distribution of fluxes for the steady state model over the entire sub-basin (including regions outside of the rectangular study area) at 30m resolution. These distributions are similar to those expected based on past model results from synthetic hillslopes, and may be divided into the three zones identified in Salvucci and Entekhabi (1995): 1) relatively isolated regions of net recharge near the topographic divide, 2) similarly narrow regions of net discharge over

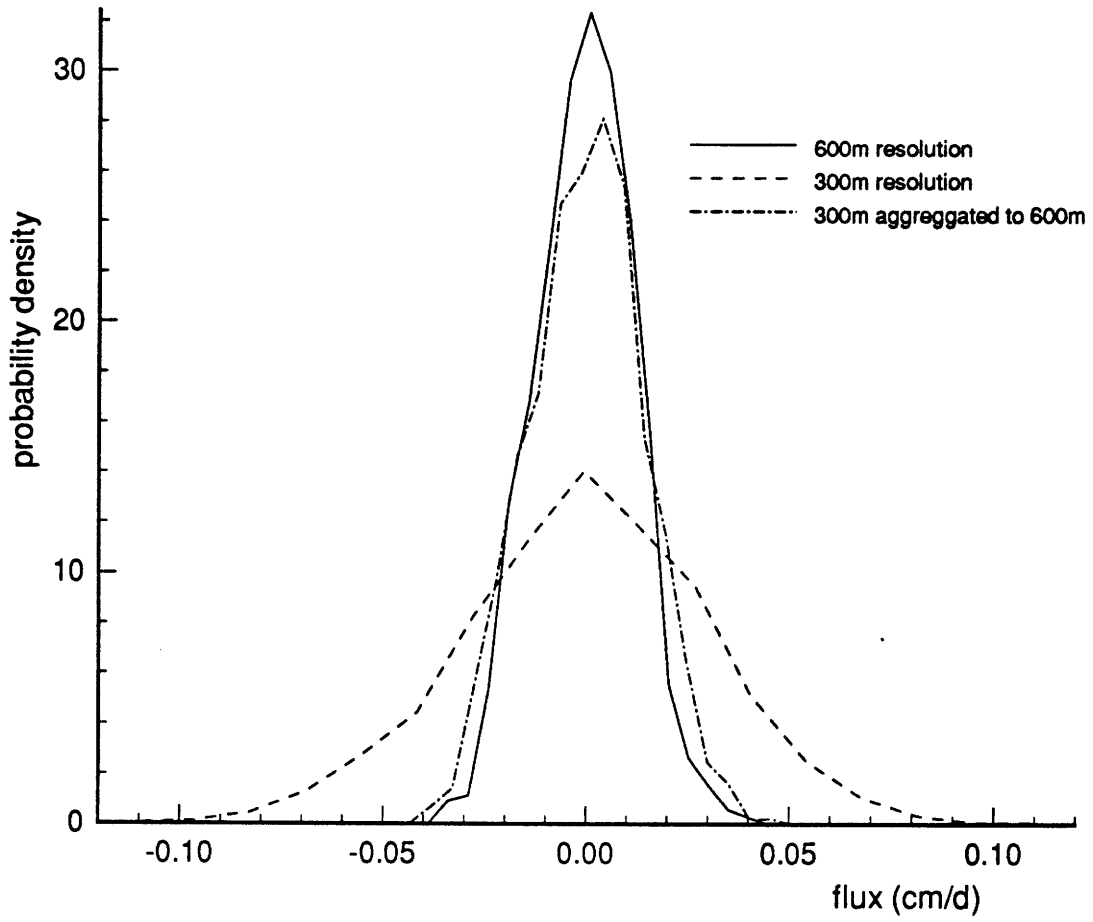

Figure 5-8: Frequency distribution of recharge for the Little Washita basin at three resolutions.

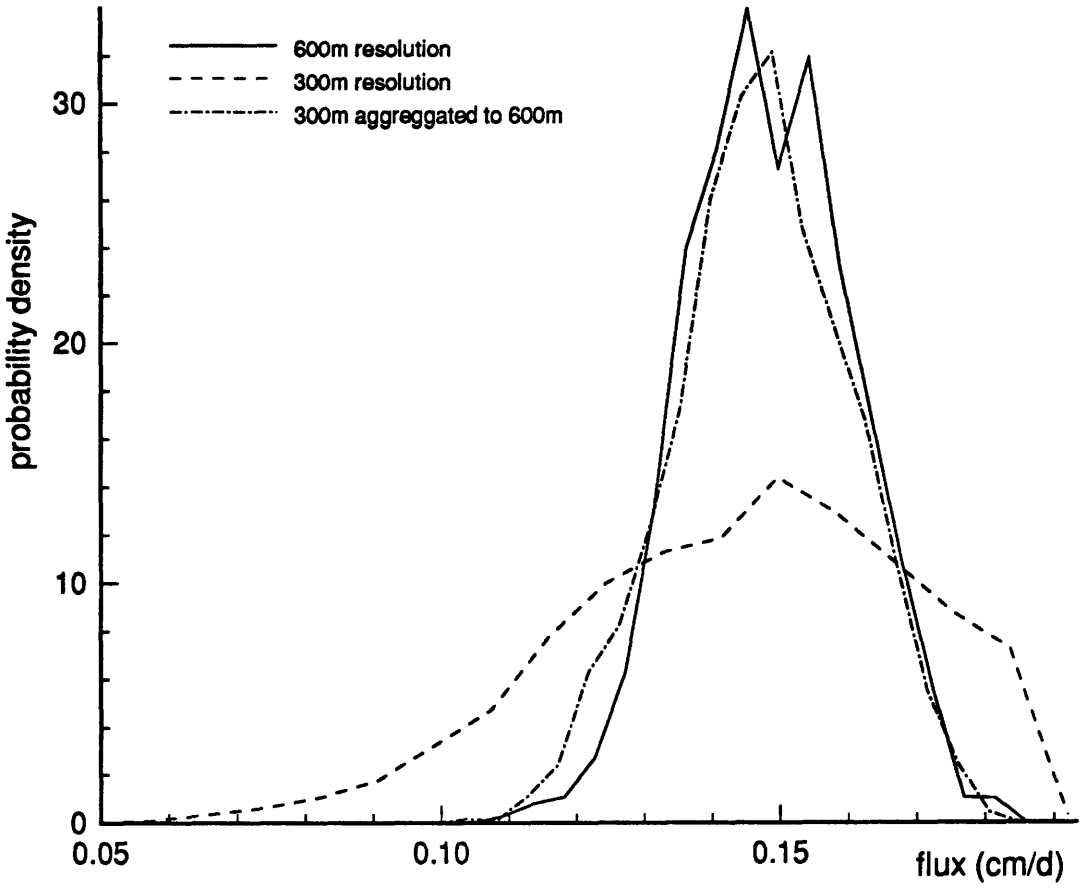

Figure 5-9: Frequency distribution of evaporation for the Little Washita basin at three resolutions.

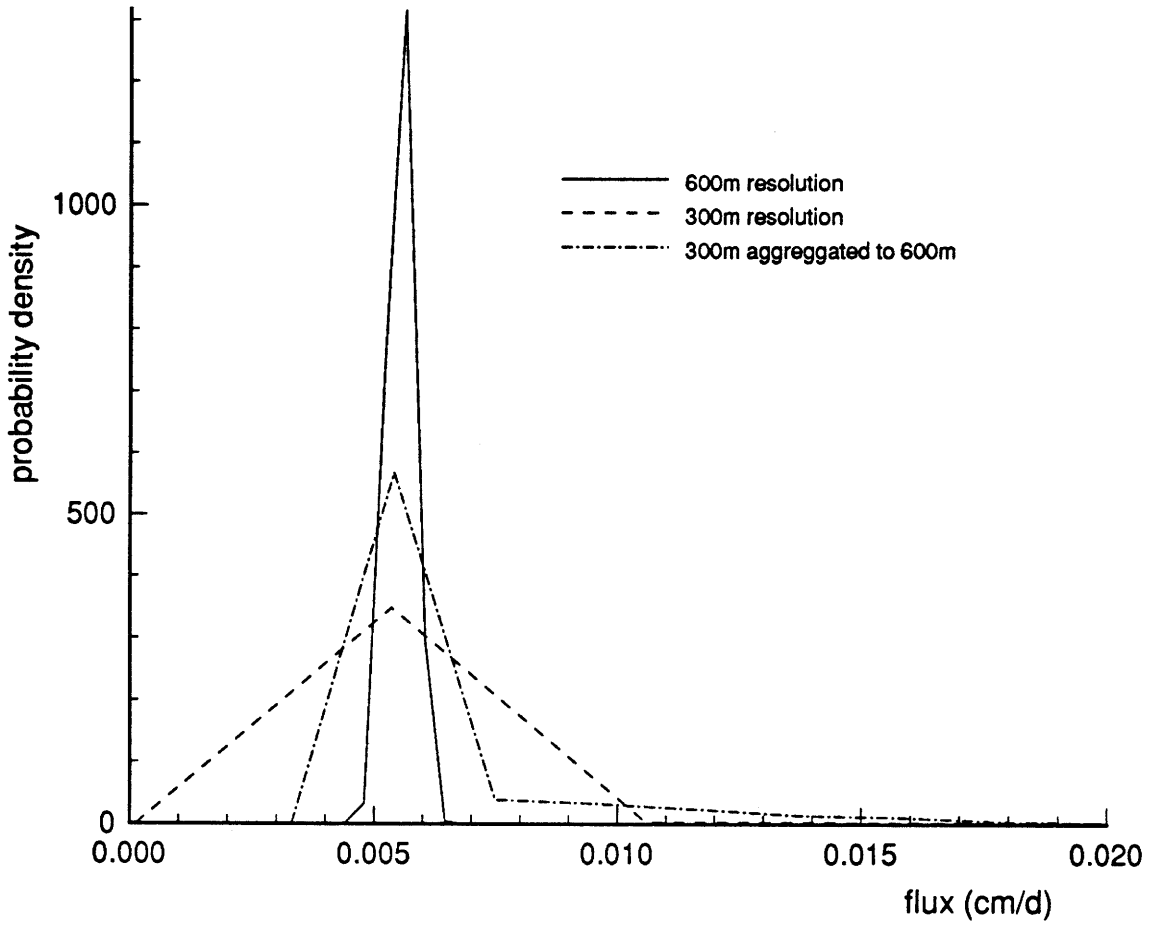

Figure 5-10: Frequency distribution of runoff for the Little Washita basin at three resolutions.

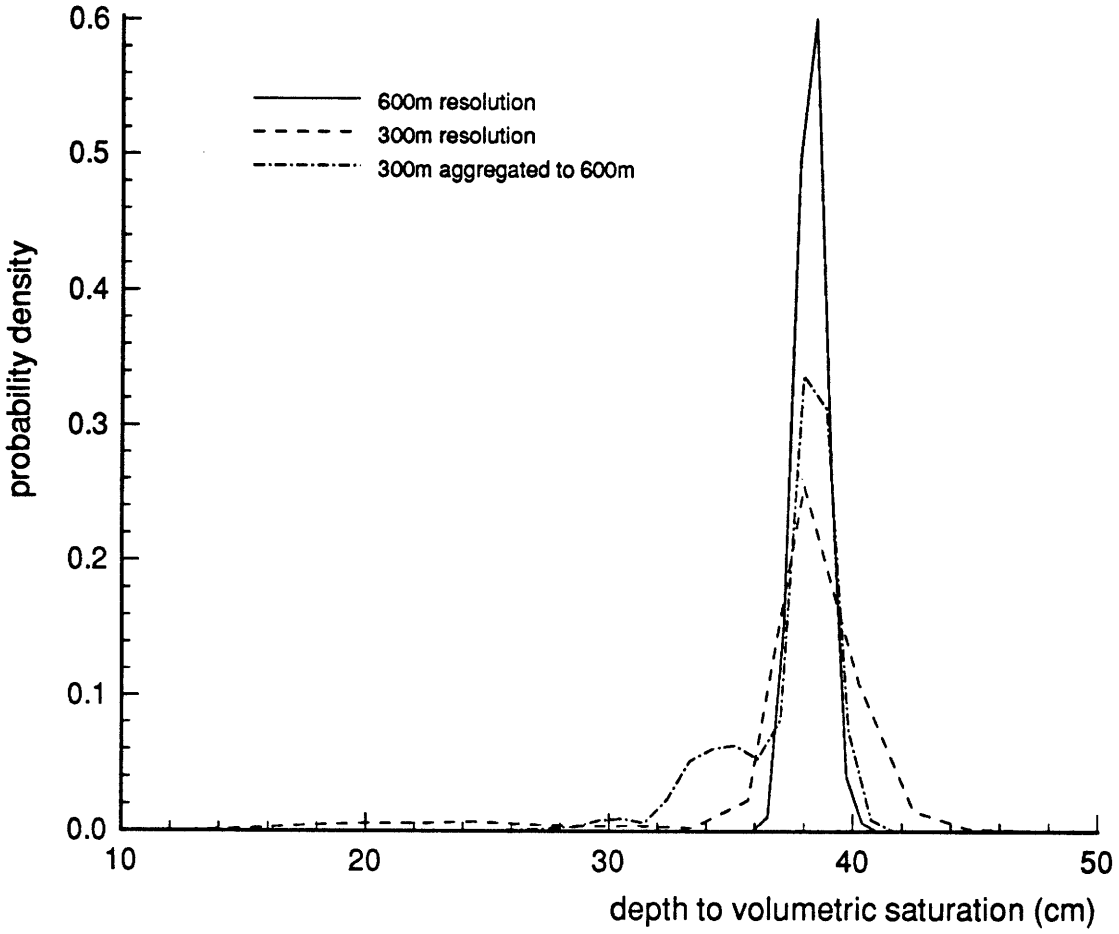

Figure 5-11: Frequency distribution of depth to volumetric saturation for the Little Washita basin at three resolutions.

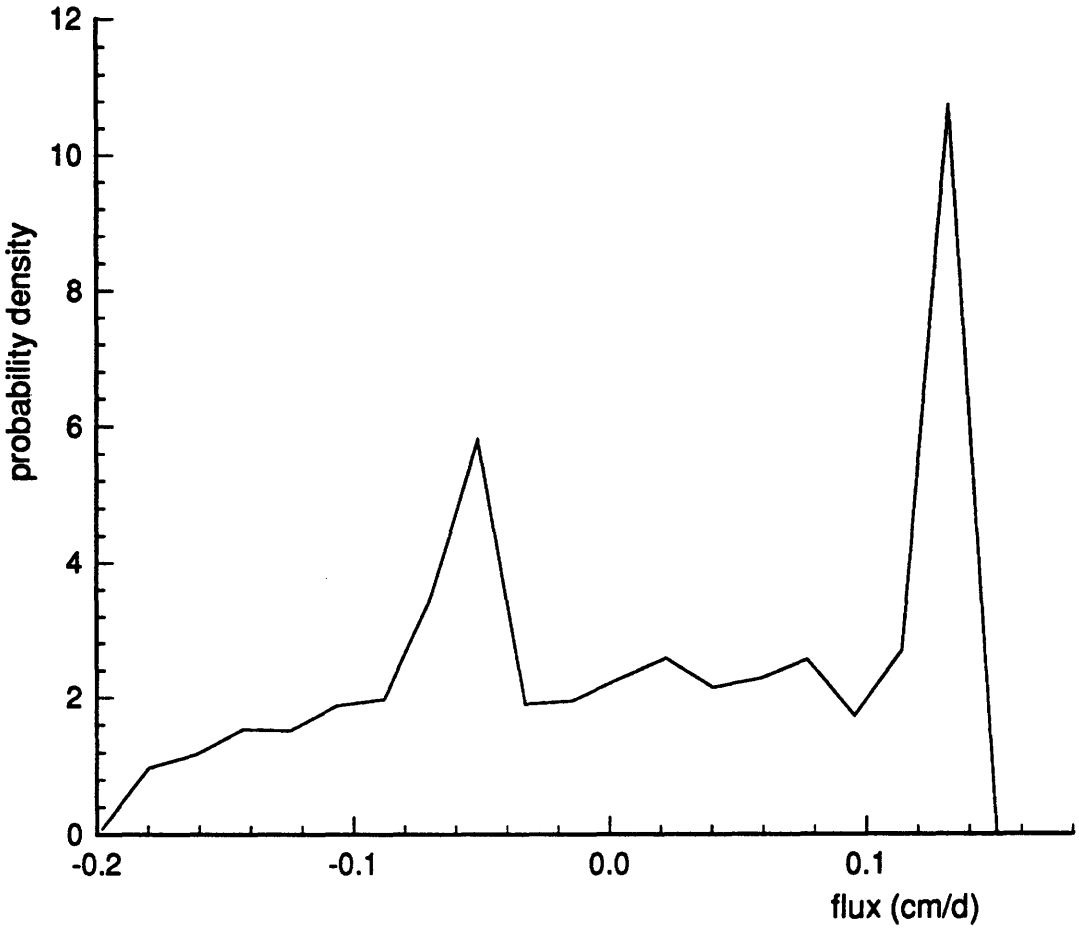

Figure 5-12: Frequency distribution of recharge for the study sub-basin at 30m resolution.

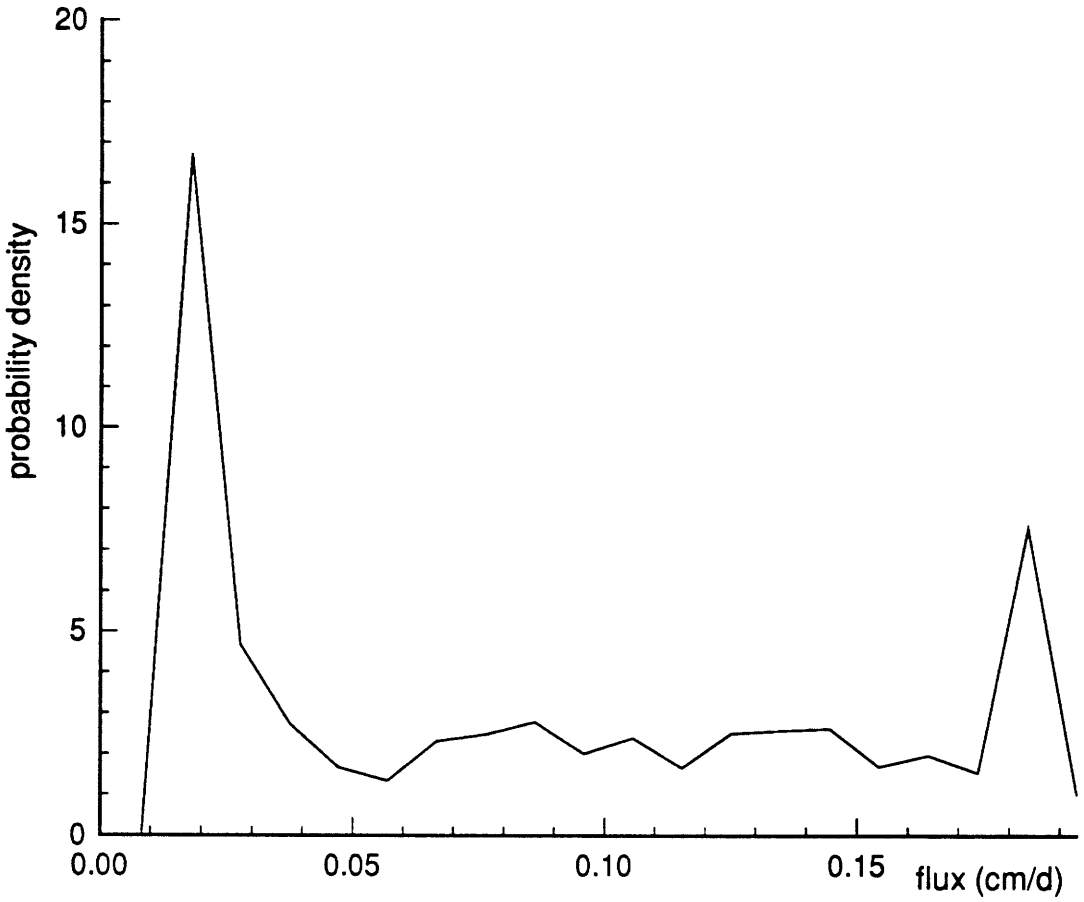

Figure 5-13: Frequency distribution of evaporation for the study sub-basin at 30m resolution

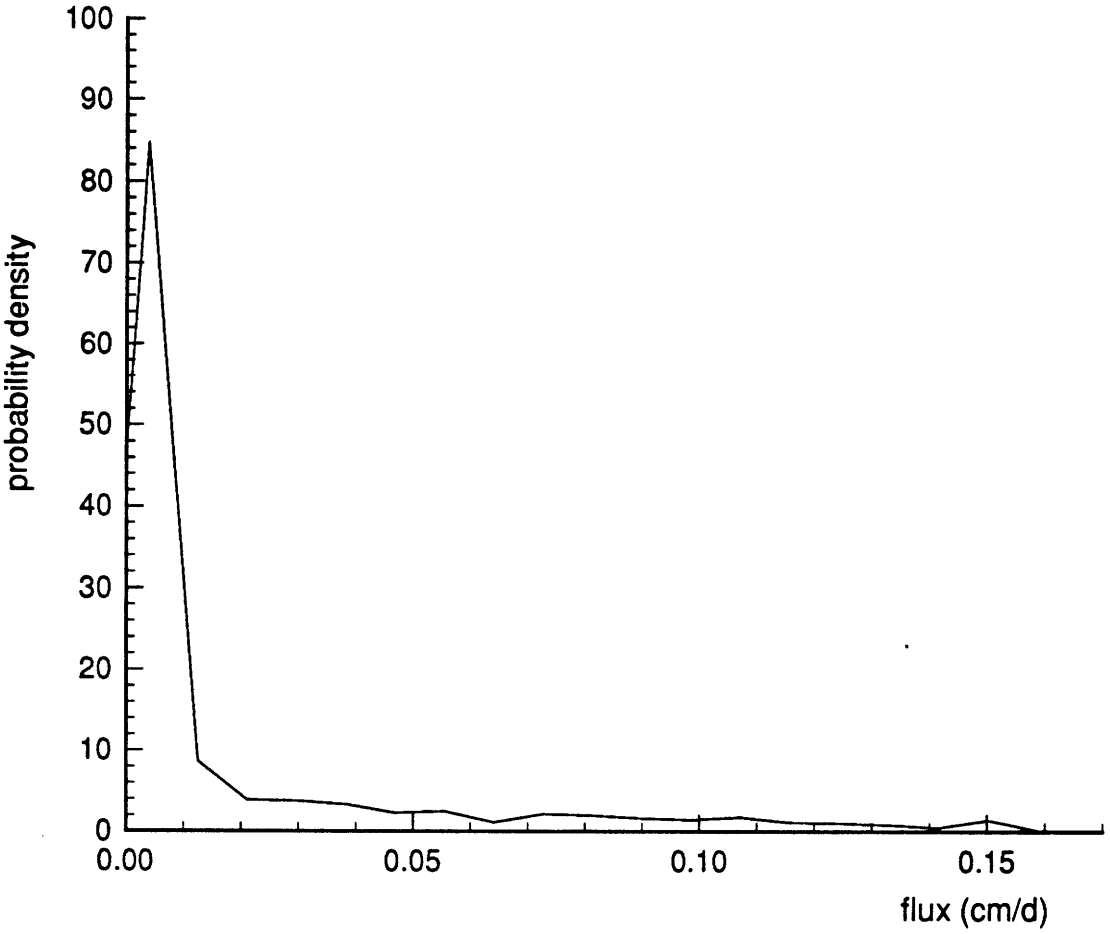

Figure 5-14: Frequency distribution of runoff for the study sub-basin at 30m resolution.

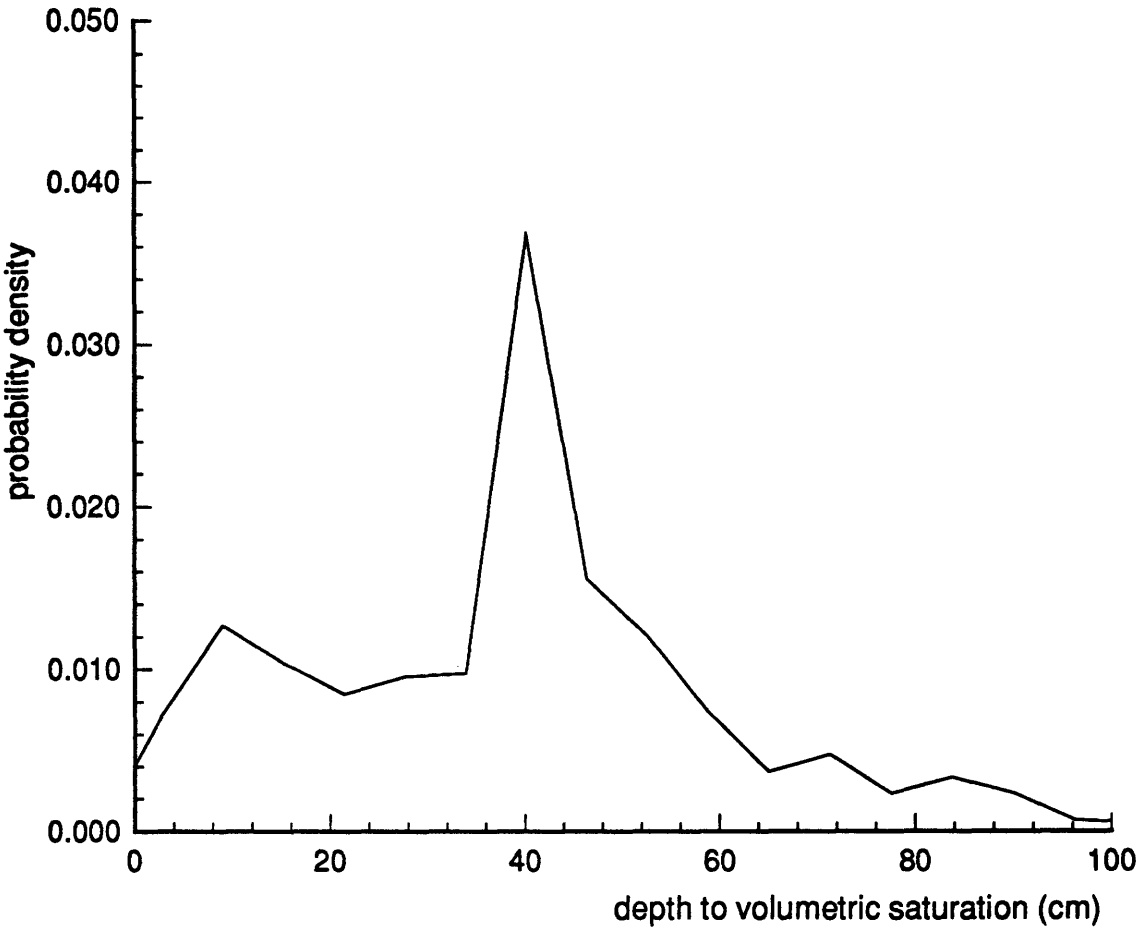

Figure 5-15: Frequency distribution of depth to volumetric saturation for the study sub-basin at 30m resolution.

the riparian areas along the drainage network, and 3) extended midline regions where the water table follows surface topography and net groundwater flux divergence is small, indicating that the net exchange with the unsaturated zone is zero. The depth to saturation over the midline is Z^*, the depth which yields a net recharge of zero (see Figure 5-7).

The distribution of depth to volumetric saturation is depicted in Figure 5-15. The peak in the middle represents the extensive midline region where there is little net exchange between the saturated and unsaturated zones. There are also significant, nearly uniform tails on either side of the peak representing shallow and deep water tables which correspond to areas of discharge and recharge.

Given the distribution of depth to saturation, the distributions of surface hydrologic fluxes such as recharge, evaporation and storage excess runoff are transformations of the distribution of depth according to the functional dependence of the fluxes on the position of the water table. These dependencies are shown in Figure 5-7.

Recharge in the present case varies nearly linearly with depth to saturation up until a threshold at which it asymptotes to a maximum value. Since capillary rise (Equation (2.16)) is zero for large depths to the water table, beyond a certain depth recharge is essentially unit gradient (gravity) flow for a uniform soil moisture profile. This value for recharge is constant for depths below the threshold. Given the organization of the phreatic surface over the basin into a large midline region and small net recharge and discharge zones (Figure 5-15), the recharge frequency distribution has a large concentration at the asymptotic value (the peak at about +1.2cm/d in Figure 5-12) corresponding to the areas above the threshold depth to the saturated zone. A secondary peak at small recharge rates indicates the dominance of the midline and discharge regions over the small catchment.

Similar to recharge, bare soil evaporation response to the position of the water table is also characterized by a threshold behavior. Up to a critical position of the water table, the near-surface soil is adequately moistened by capillary rise such that evaporation is limited by available energy, which manifests itself in the potential evaporation rate. As the depth to saturation increases, the soil control on evaporation

also increases due to a drying of the soil moisture profile. The reduction is rapid enough to resemble a step function (see Figure 5-7). Given the organization of the water table over the study basin, the frequency distribution of evaporation has two modes, one at the potential rate and one at the maximum soil-limited rate (Figure 5-13). Thus over complex topography, a small portion of the basin contributes a large portion of regional evaporation. In particular, in high drainage riparian zones and regions of groundwater convergence, evaporation proceeds at its potential rate.

Storage excess runoff is generated only where the water table is positioned near the surface and the soil moisture profile is almost saturated. Under these conditions the available storage is small and precipitation events will saturate the soil column and contribute to storm runoff. These shallow water table regions appear near the high drainage and convergence zones. The frequency distribution of runoff rates over the basin reflects the extent of the shallow water table regions in the basin; Figure 5-14 shows that runoff is significant only in a small number of pixels.

The frequency distributions of recharge, bare soil evaporation, and storage excess runoff indicate that there is considerable spatial organization of fluxes within the basin. There is evidence of a division in the basin between regions of midline, discharge and recharge. The ordering of these regions over topography and drainage patterns has important implications for the aggregation of hydrologic fluxes across scales. In the next chapter, the link will be examined between spatial patterns of topographical features and the frequency distributions of fluxes introduced in this chapter.

Chapter 6

Comparison of equilibrium model with topographic features

6.1 Introduction

This chapter explores the connection between the output of the steady state model and basin topography. Two approaches are taken in this comparison. The first is to make a qualitative comparison between the flux and water table depth output and a map of basin features. The second is to compare water table depth to $\ln(a/\tan\beta)$, a commonly-used index of hydrologic response based on the cumulative drainage area per contour length (a), and local surface slope ($\tan\beta$).

Any analysis using the index $\ln(a/\tan\beta)$ invites comparison to TOPMODEL, summarized in Beven and Kirkby (1979). TOPMODEL is a variable source area model of hydrologic response, which predicts surface runoff in terms of saturated area and precipitation intensity, and predicts subsurface runoff in terms of "saturation deficit". One important assumption in TOPMODEL is that the initial pre-storm water table depth is a function of $\ln(a/\tan\beta)$ and upstream recharge. This chapter will compare this assumption to results from the equilibrium model and attempt to explain discrepancies that exist between the two.

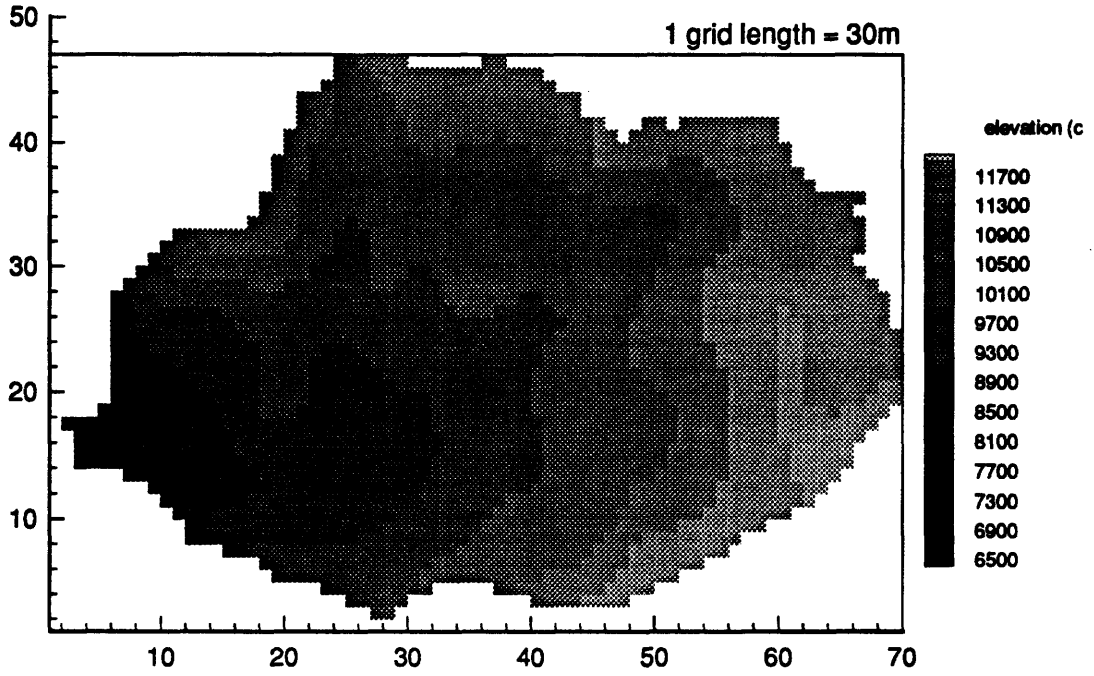

Figure 6-1: Sub-basin used in resolution and topographical studies.

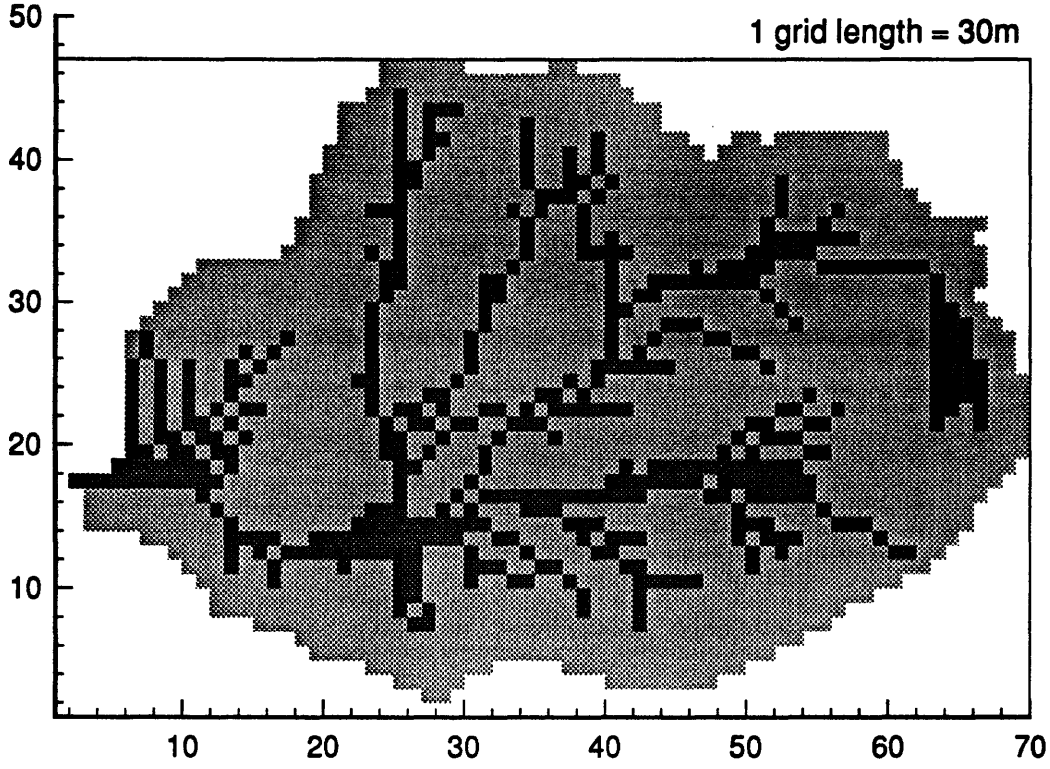

Figure 6-2: Regions (dark) with cumulative drainage of more than 11 pixels.

6.2 Study area description

The present study focuses on the sub-basin of the Little Washita introduced in the previous chapter. The study considers only the steady-state model using 30m resolution DEM elevation data because this was the resolution found in the last chapter to give a physically reasonable spatial distribution of fluxes. An elevation map of the study sub-basin is presented in Figure 6-1.

The sub-basin is characterized by a main channel system originating in the east (right center) and winding in a gentle "s" shape towards the basin outlet in the west at coordinate [2,17]. This channel system appears more obviously in Figure 6-2, which isolates points in the basin with cumulative drainage areas of eleven or more pixels. Slopes for the basin are gentle, rarely exceeding 6–10%.

The drainage area and slopes for the basin were determined using methods from Tarboton et al. (1989). This approach involves the filling of topographical pits, and therefore there may be some discrepancies between the drainage system depicted in Figure 6-2 and the actual drainage pattern of the sub-basin used as input to the model runs.

6.3 Comparison of the model with topographical features

The link between topography and hydrology may be observed by comparing the model output for the sub-basin with the drainage pattern suggested by Figure 6-2. Figures 6-3 through 6-6 represent the water table depth and flux patterns of the study sub-basin under the steady state equilibrium model.

Depth to the water table displays three characteristic regions, viz. the regions of recharge, discharge and midline. Recharge occurs at local high elevations and areas of topographical divergence, where the water table is deep. Three such regions are particularly obvious in Figure 6-3 where the depth to volumetric saturation is great (two near the outlet and one at the opposite end of the basin, corresponding

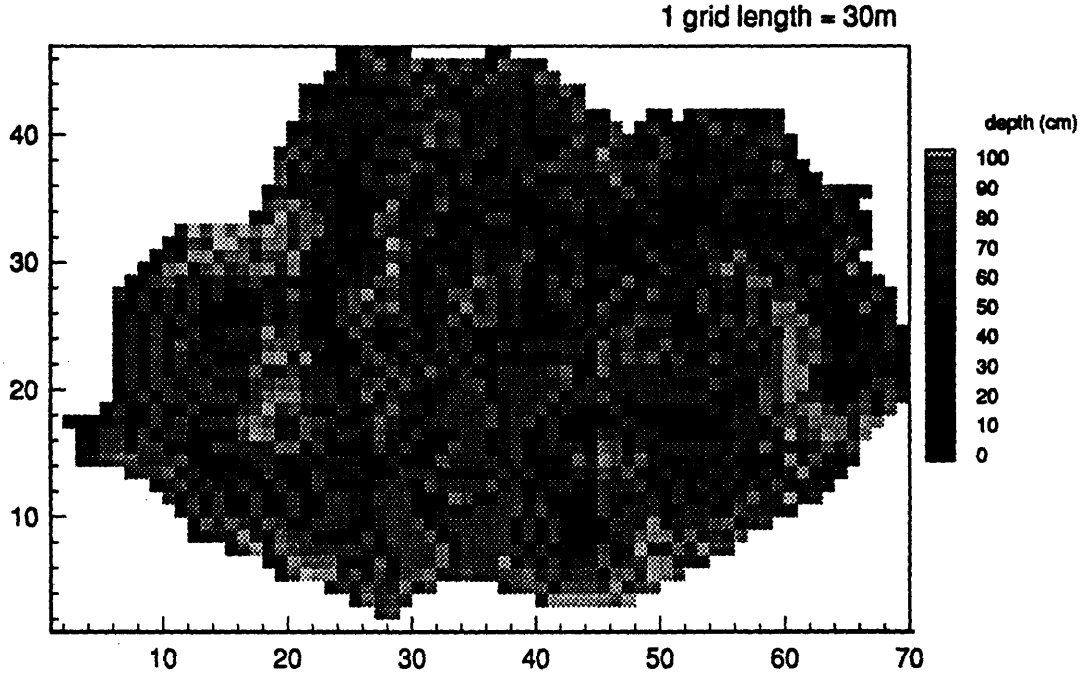

Figure 6-3: Depth to volumetric saturation from the steady state equilibrium model.

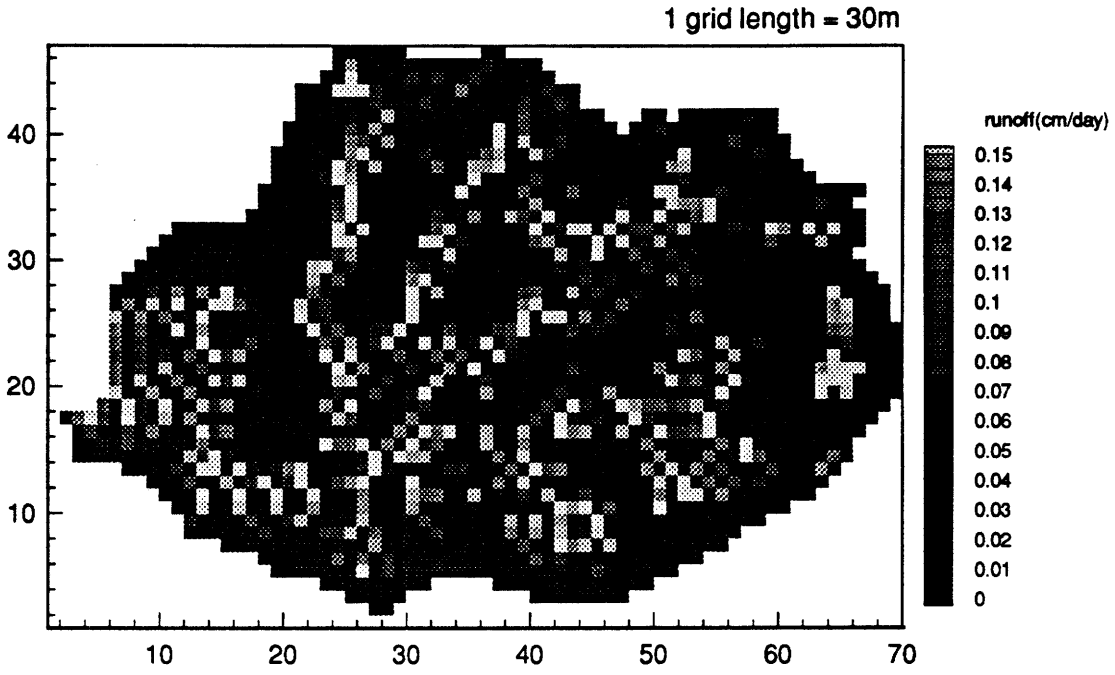

Figure 6-4: Storage excess runoff given by the steady state equilibrium model.

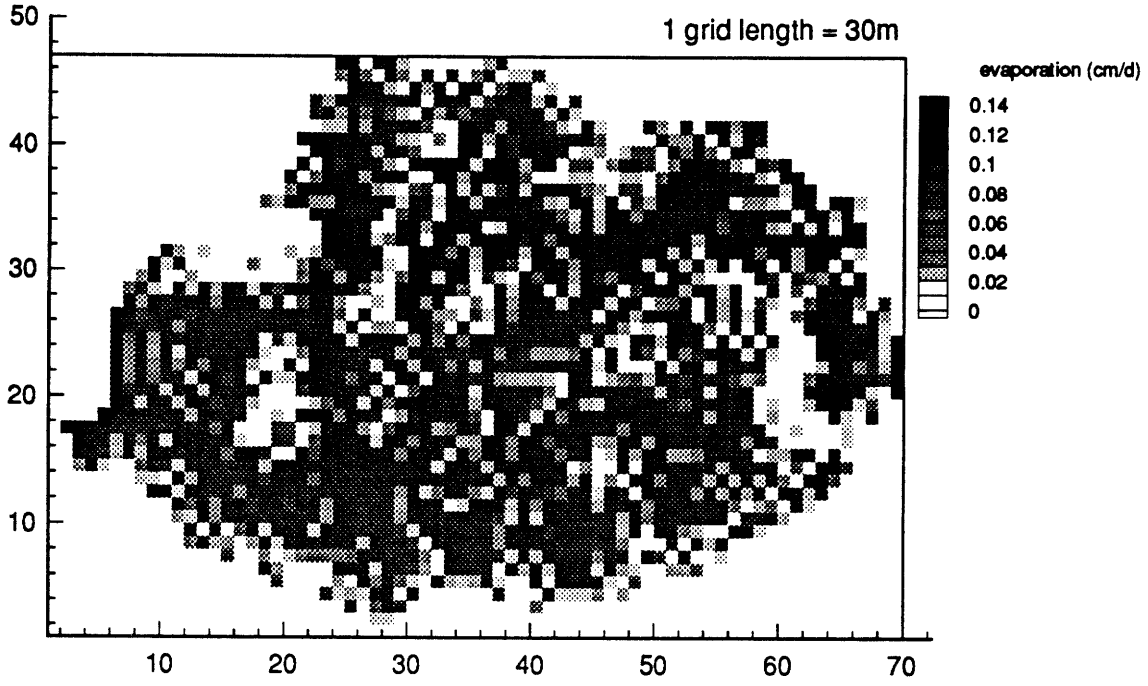

Figure 6-5: Evaporation given by the steady state equilibrium model.

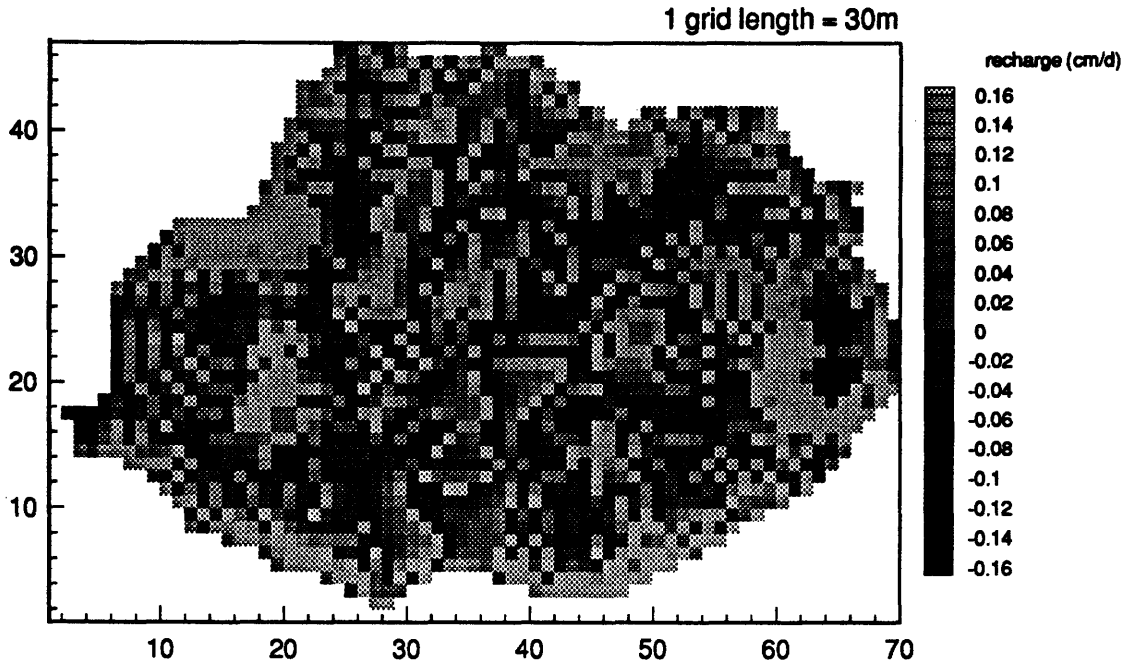

Figure 6-6: Net recharge given by the steady state equilibrium model.

to topographic highs in Figure 6-1). Discharge occurs in lower elevation areas with greater cumulative drainage and local convergence, where the water table is close to the surface. The drainage network from Figure 6-2 manifests itself as areas of shallow water table positions in Figure fig:equidepthh.

Runoff, evaporation and recharge for the basin are the equilibrium values corresponding to water table depth, which were given in Figure 5-7. Runoff, which in this case is entirely storage excess runoff, only occurs substantially in areas with a very shallow water table. For this reason there is no distinction in terms of runoff between the medium-depth midline region and the deep water table region; both have close to zero runoff. Runoff, as depicted in Figure 6-4, therefore follows the drainage pattern (Figure 6-2) very closely.

The variation of evaporation with depth in the water table also behaves very much like a step function. Above a certain threshold of depth to the water table, evaporation carries on at nearly the potential rate. Below this threshold, evaporation drops off sharply down to a semi-infinite evaporation rate near zero (see Figure 5-7. The only reason why intermediate shades exist at all in the evaporation map for this basin (Figure 6-6) is that the drop from potential evaporation to semi-infinite evaporation occurs at a depth which is very common. This depth is Z^*, or the depth at which the net exchange between the saturated and unsaturated zones is zero. Over the extensive midline, $Z_{wt} = Z^*$ dominates. The regions of peaks and ridges are reflected in the evaporation map as areas of near-zero evaporation.

Recharge, shown in Figure 6-6, behaves much like evaporation, becoming negative and large near shallow water tables and positive and large near deep water tables. The variation of recharge with water table depth is more gradual than that of evaporation, resulting in a larger number of intermediate recharge values. In particular, a midline region of zero recharge occurs uphill of alluvial areas (zero recharge is, in fact, one of the defining characteristics of the midline region). The existence of a midline notwithstanding, the drainage pattern is evident in the recharge map.

6.4 Topographical indices

Before we can compare water table depth to topographical indices based on $\ln(a/\tan\beta)$, we must define an appropriate form for this index, which is written differently in different applications. Some researchers include hydraulic conductivities and transmissivities inside of the natural logarithm; we will be dealing mostly with mean-removed indices using uniform contour lengths hydraulic conductivities and transmissivities, so these parameters eventually drop out.

The models of Beven and Kirkby (1978) (TOPMODEL) and Sivapalan et al. (1987) both assume a dependence of water table depth on this topographical index. These models rely on two additional assumptions. The first is spatially uniform recharge, ie.:

$$q_v(x,y) = q_v = R \tag{6.1}$$

and the second is exponential decline of hydraulic conductivity with depth:

$$K_{sat}(z) = K_0 \exp(-fz) \tag{6.2}$$

where z is the (positive) depth from the surface.

Using a constant recharge rate R, TOPMODEL assumes that local saturated flow per unit contour is given by:

$$q = aR \tag{6.3}$$

where a is again the cumulative contributing area per unit contour. TOPMODEL additionally assumes that the hydraulic gradient equals the topographic gradient $\tan\beta$. Thus another expression for q is:

$$q = \int_{z_i}^{\infty} K_{sat}(z') \tan\beta dz' \tag{6.4}$$

where z_i is the depth to the saturated zone. Substitution of Equation (6.2) into Equation (6.4) and equating the resulting expression to Equation (6.3) results in the

following expression for local depth to the saturated zone:

$$z_i = -\frac{1}{f}\ln(\frac{aR}{T_0 \tan\beta}) \tag{6.5}$$

where $T_0 = K_0/f$. Sivapalan et al. (1987) then subtracts the areal mean values of this index to define:

$$z_i - \bar{z} = -\frac{1}{f}\left[\ln\left(\frac{aT_e}{T_0 \tan\beta}\right) - \lambda\right] \tag{6.6}$$

in which $\frac{aT_e}{T_0 \tan\beta}$ is defined as a combined topography-soil index and λ and T_e are given by:

$$\lambda = \frac{1}{A_{tot}}\int_{A_{tot}} \ln\left(\frac{a}{\tan\beta}\right) d\alpha \tag{6.7}$$

and

$$T_e = \frac{1}{A_{tot}}\int_{A_{tot}} \ln(T_0) d\alpha \tag{6.8}$$

where A_{tot} is the total area of the basin.

In comparing topography-based models to the results of the steady state equilibrium model, some simplifications must be made. Transmissivity under the Sivapalan et al. (1987) model is given by integrating Equation (6.2) over the saturated portion of the soil column:

$$T(z_i) = \int_{Z_0}^{Z_i} K_{sat} dz = \frac{K_0}{f}\{\exp(-fz_i) - \exp(-fZ)\} \tag{6.9}$$

where Z is the depth of the soil column.

It is common to assume that f is large enough that the exponent terms in Equation (6.9) reduce to one and zero. If we further assume that the surface saturated conductivity (K_0) is the same as the uniform saturated conductivity used in the equilibrium model (K_{sat}) and that transmissivity in the equilibrium model may be based on the full depth of the soil column, we may set the right hand side of Equation (6.9) equal

to $K_{sat}Z$, and simplify to obtain a new extinction rate for hydraulic conductivity:

$$\frac{1}{f} = Z \tag{6.10}$$

Physically, this approach assumes that that the transmissivity of the soil column is the same in both models and that the hydraulic conductivity in both models is the same at the surface. The equilibrium model has a constant hydraulic conductivity down to bedrock, whereas the topography-based model declines exponentially with depth. Equal transmissivity implies greater (infinite) soil depth in the topography-based model. This assumption is not fully satisfying, and it may be possible to find combinations of K_0 and f which give better agreement with soil depth and with the equilibrium model results. However, transmissivity is spatially uniform and drops out of Equation (6.6); f appears in this equation only as a scaling factor. A meaningful comparison between the models can therefore still be made even if the selection of f is inappropriate.

Taking advantage of the uniformity of transmissivity and contour length, Equation (6.6) simplifies to the following simple linear relationship between the mean-removed depth to the water table and mean-removed $\ln(a/\tan\beta)$:

$$z_i - \bar{z} = -\frac{1}{f}\left[\ln\left(\frac{a}{\tan\beta}\right) - \lambda\right] \tag{6.11}$$

Figure 6-7 shows the cumulative drainage area using the drainage direction approach of Tarboton et al. (1989). For the basin under consideration, the distribution of the cumulative drainage area per unit contour length (a) is the principal contributor to the spatial patterns formed by the topographic index, $\ln(a/\tan\beta)$. Figure 6-8 represents the values of this index and the strong influence of cumulative drainage on the index is evident.

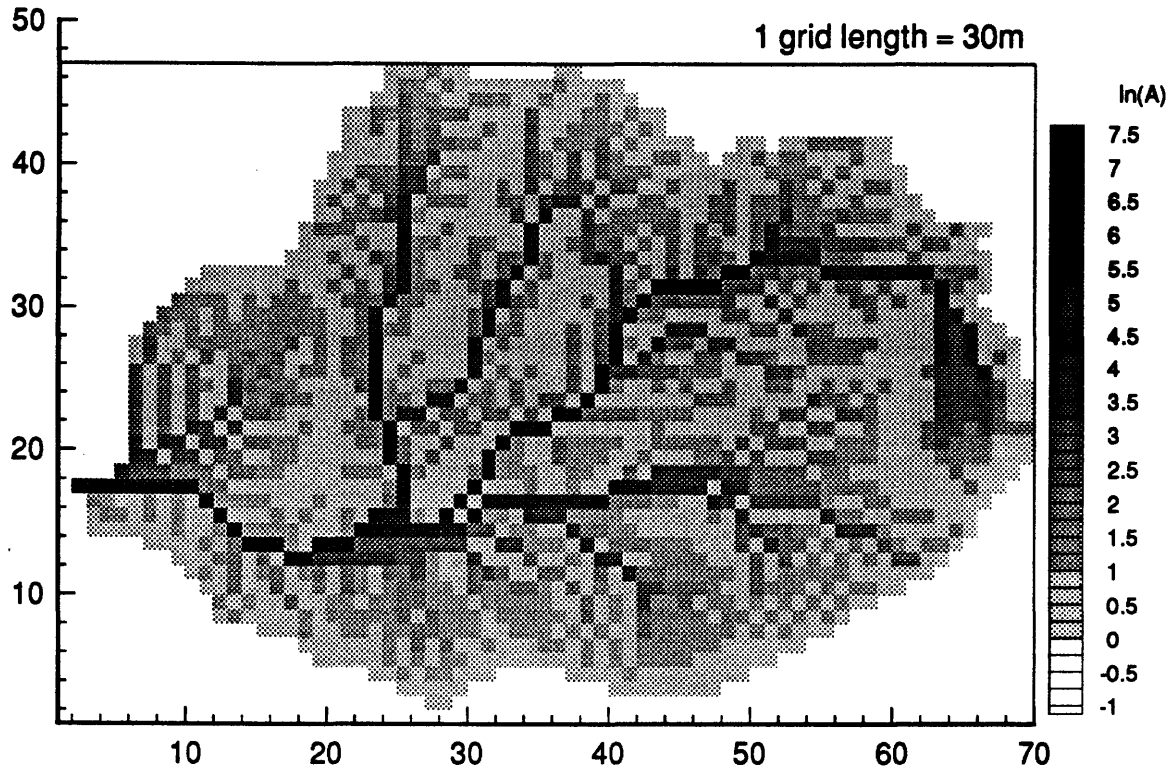

Figure 6-7: Log cumulative drainage area for the study sub-basin.

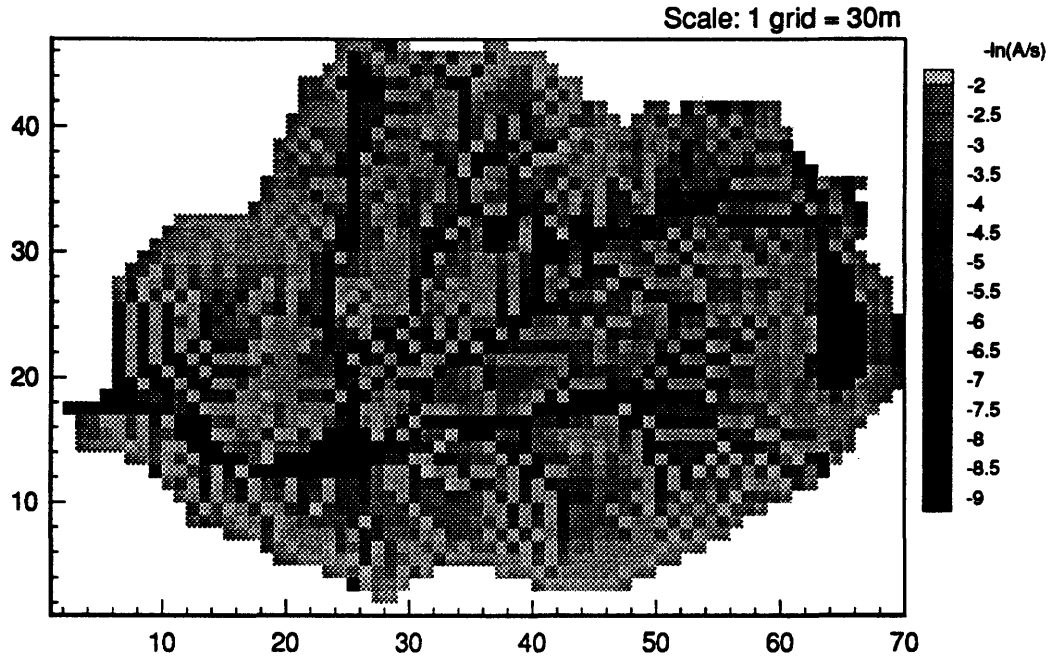

Figure 6-8: Spatial distribution of the index: $-\ln(a/\tan\beta)$.

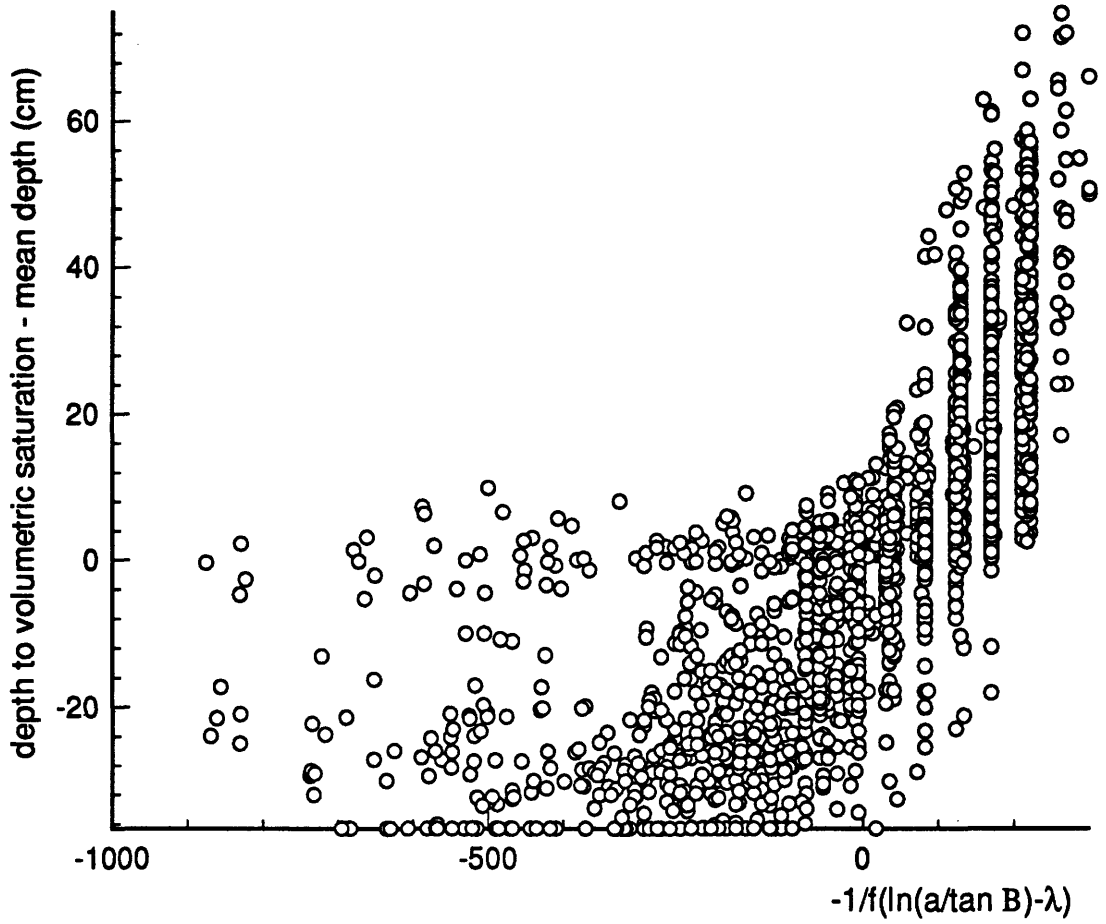

Figure 6-9: Mean-removed depth to volumetric saturation versus mean-removed $-\frac{1}{f}\ln(a/\tan\beta)$.

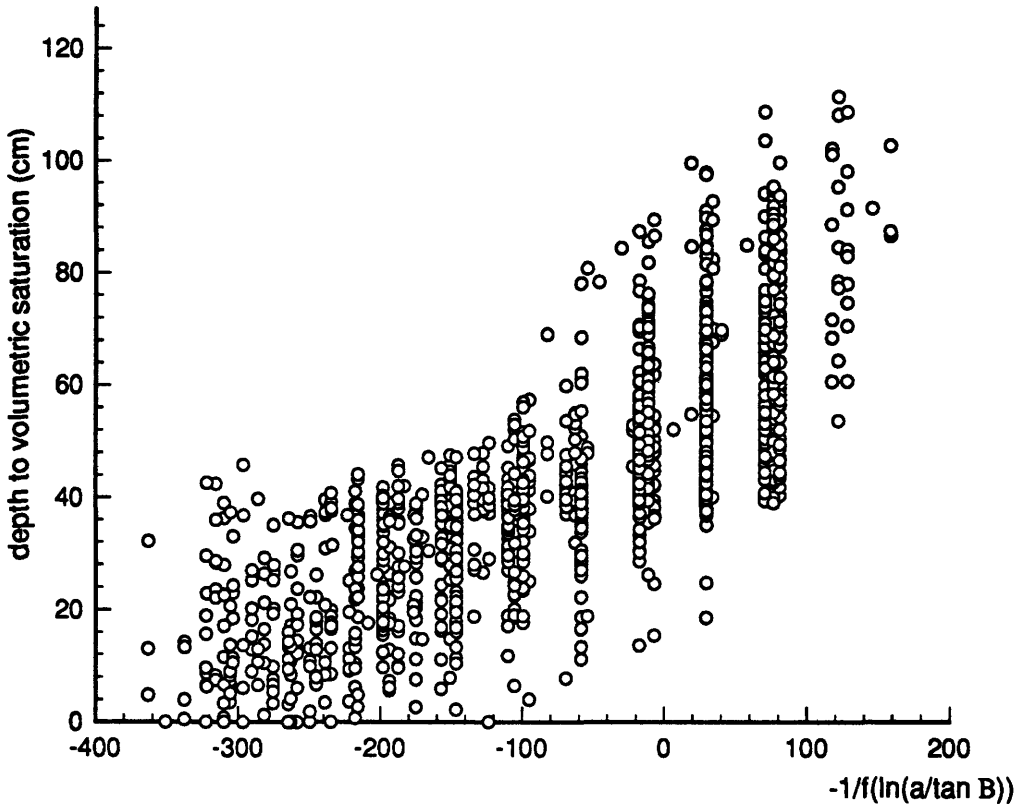

Figure 6-10: Depth to volumetric saturation versus $-\frac{1}{f}\ln(a/\tan\beta)$ for pixels with cumulative drainage areas of 11 or fewer pixels.

6.5 Comparison of model with the topographical index

Figure 6-9 plots the mean-removed depth to the water table from the equilibrium model against the mean-removed value of $-\frac{1}{f}\ln(a/\tan\beta)$ for the sub-basin discretized at a resolution of 30m. Approximately 9% of the pixels on the sub-basin are not represented here because they have zero slope. The missing points show wide spread in the equilibrium model-based estimates of water table depth, similar to the spread among other points in Figure 6-9 with strongly negative $-\frac{1}{f}(\ln(a/\tan\beta) - \lambda)$.

The positive correlation between depth and the negative topographical index is clear; however, the spread of the data is considerable and there are a number of outlying points with strongly negative $-\frac{1}{f}(\ln(a/\tan\beta) - \lambda)$ which have equilibrium model water table positions only slightly below the mean.

The correlation is much stronger if we ignore points with large contributing areas which are probably seepage faces and contributing areas. Figure 6-10 plots depth to volumetric saturation against $-\frac{1}{f}\ln(a/\tan\beta)$ for points with contributing areas of eleven pixels or fewer. Eleven pixels is the same criterion used in Figure 6-2 above to highlight the drainage pattern of the sub-basin. No attempt has been made to remove the means in this figure because the inclusion criterion was somewhat arbitrary. By comparing Figures 6-9 and 6-10, we can see that the two models are much more consistent in low and medium drainage pixels.

Deferring a physical explanation for the discrepancies between the models until the next section, we now point out two shortcomings in our method of comparison which could cause outliers in Figure 6-9 for points with large drainage. First, we have neglected the existence of a threshold in $-\frac{1}{f}(\ln(a/\tan\beta) - \lambda)$ above which every cell is a seepage face and depth to the water table cannot get any smaller. In Figure 6-9, the points which lie at the bottom along the horizontal axis are seepage faces according to the equilibrium model; inasmuch as these points also lie to the left of the (undetermined) seepage face threshold in the topography-based model, they do not represent a practical discrepancy between the models.

A second systematic reason for disparities between the models originates from the way in which drainage directions are calculated. The Tarboton et al. (1989) method for calculating drainage direction admits diagonal flow, but allows only one drainage direction from each pixel. In contrast, MODFLOW does not allow diagonal flow, but allows flow along the principal directions to more than one cell at once (in accordance with the hydraulic gradients with neighboring cells). The effect of this dissimilarity would be most acutely felt near channels, where the topography-based model would see large, direct diagonal drainage and the equilibrium model would see smaller, indirect drainage patterns. This difference explains, in part, some of the pixels that have extremely low $-\frac{1}{f}(\ln(a/\tan\beta) - \lambda)$ but that are not seepage faces according to the steady state equilibrium model.

Figures 6-11 and 6-12 give frequency distributions of depth to the water table from the equilibrium model and $-\frac{1}{f}(\ln(a/\tan\beta) - \lambda)$, both with mean removed. Note that the area under the latter graph represents only 91% of the data points, neglecting the 9% with zero slopes.

As noted in the previous chapter, the density for depth to the water table spans three distinct regions: a large midline region surrounded by appreciable tails representing zones of shallow and deep water tables. The peak of the graph occurs just above the mean water table position, very near the equilibrium water table position with zero net recharge.

In contrast, the frequency distribution of $-\frac{1}{f}(\ln(a/\tan\beta) - \lambda)$ has a right-skewed distribution. The graph does not exhibit a right tail region analogous to the deep water table region, nor does it exhibit the same substantial, almost uniform left tail which characterizes the shallow water table region.

6.6 Analysis of discrepancies

A water table profile inferred solely from a topographical index based on $\ln(a/\tan\beta)$ will not coincide well with the equilibrium model in the two areas of greatest hydrologic activity, discharge and recharge regions. In particular the two models disagree

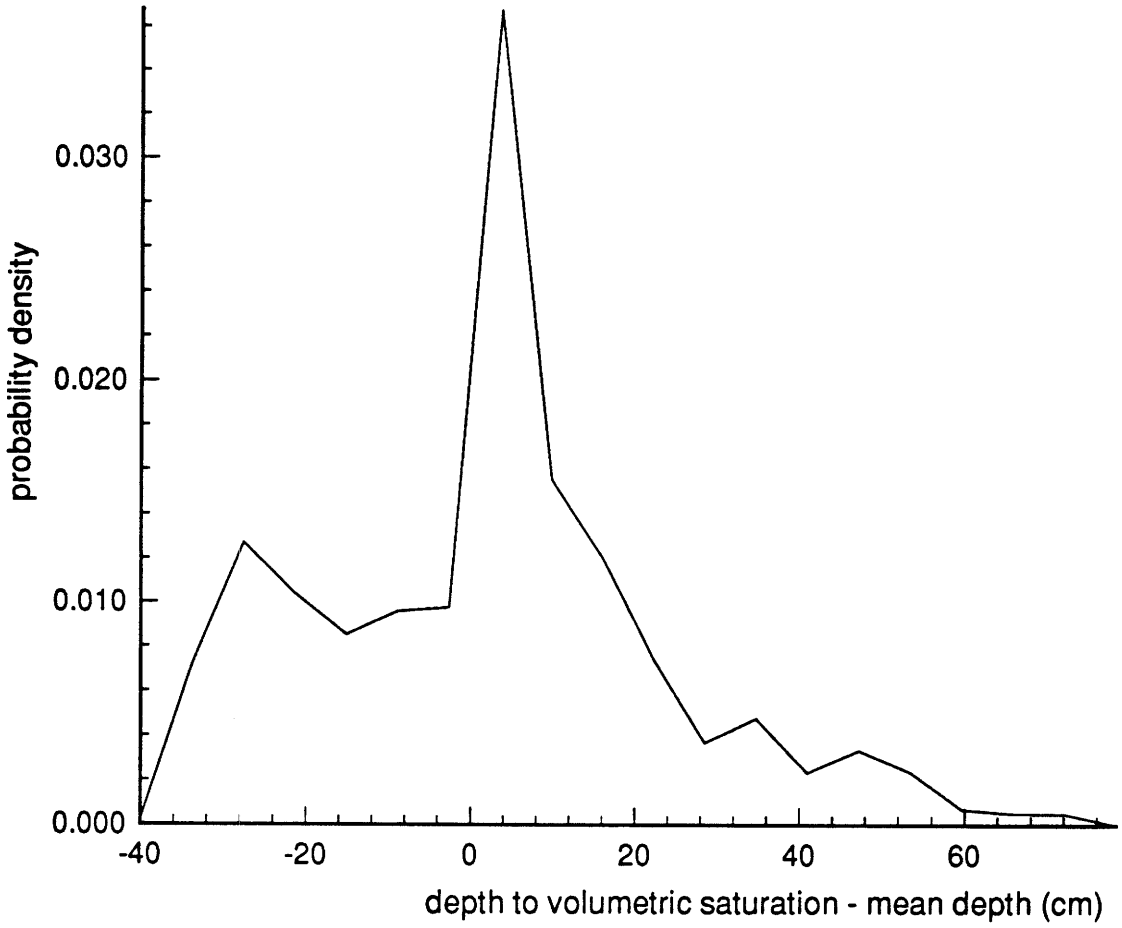

Figure 6-11: Frequency distribution of mean-removed depth to volumetric saturation.

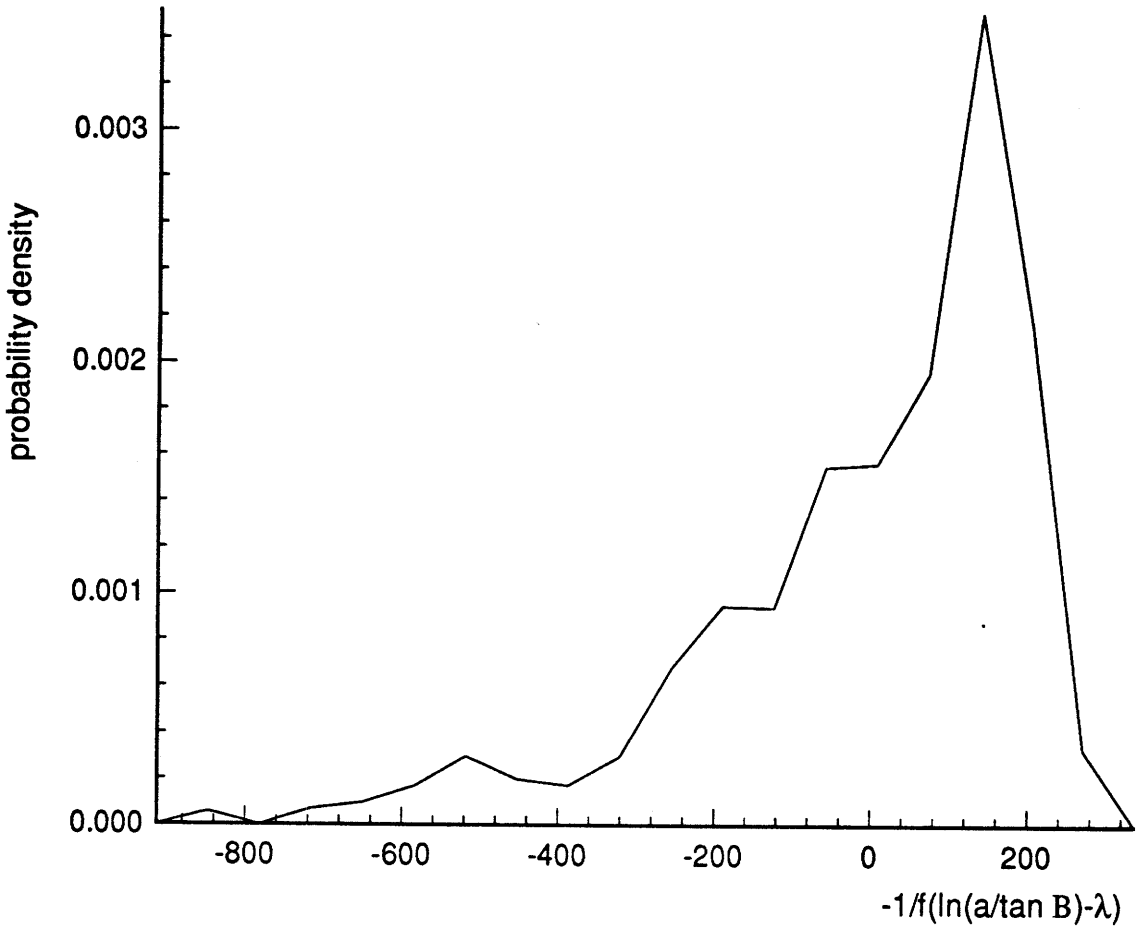

Figure 6-12: Frequency distribution of $-\frac{1}{f}\ln(a/\tan\beta)$.

on the distribution of riparian shallow water areas which contribute the most runoff.

Some of the differences between the two models may be explained in terms of assumptions used in the derivation of Equation (6.6), which contains assumptions which are not borne out by the results of the equilibrium model. First, Equation (6.1) assumes uniform recharge. In contrast, the equilibrium model couples recharge to the water table position and accounts for surface fluxes. It predicts high recharge in upslope areas and negative recharge in downslope areas.

Perhaps a more relevant measure of the spatial distribution of recharge is the average recharge draining to a pixel ("average contributing recharge"). According to the equilibrium model, upslope areas which drain small areas also have large average contributing recharge. Average contributing recharge slowly decreases over the midline where there is close to zero local recharge, and continues to decrease in the negative recharge zone in downslope regions. Only areas near major channels drain the average recharge rate of the full basin. In a topography-based model, average basin recharge may give inaccurate results in upslope areas; similarly, a recharge rate calibrated using the midline region will give poor performance in the upslope and downslope regions

A second phenomenon implied by Equation (6.4), by analogy to Darcy's Law, is that $\tan\beta$ approximates the slope of the phreatic surface. This assumption agrees with the equilibrium region in the midline region; however in the upslope and downslope areas the hydraulic slope may be considerably less steep than the surface slope. Again, this discrepancy occurs in the areas of greatest hydrologic importance, namely the discharge regions where the largest contributions to runoff and regional evaporation take place.

6.7 Conclusions

There is a correlation between surface fluxes and topographic features. This conclusion is supported both by the equilibrium model and by field experiments such as those made by Toth (1966). Shallow water tables and their related flux patterns

(high runoff, high evaporation and negative recharge) occur near high drainage areas, whereas deep water tables and their related flux patterns occur in upslope areas. In between lies a midline region of constant, near-zero net recharge.

Topography-based models produce high and low water tables in the right places. However, because they are produced from the shape of topography and not the shape of a quasi-steady state water table, and because they ignore the spatial variability of fluxes, the distribution of water table heights given by these models is not as realistic as that given by the equilibrium model.

Chapter 7

Conclusions and suggestions for future research

7.1 Summary of major findings

The major findings of this thesis are as follows:

- The seasonal model yields average annual hydrologic output which is significantly different from that of the steady state model. The position of the water table is critical in producing periods of higher hydrologic activity. In the summer rainfall climate modeled in this thesis, the water table alternates seasonally between shallow and deep positions. The shallow water table season produces high runoff, evaporation, and negative recharge. The deep water table season is hydrologically less active; there is potential for recharge, but no precipitation to drive this recharge until the spring rains.

- Cell size and DEM resolution affect the ability of the equilibrium model to accurately portray hydrologic activity over a hillslope. There is a tendency for $Z_{wt} = Z^*$ everywhere because the recharge term dominates the discretized steady state saturated flow equations. The system seeks a solution with zero q_v.

- The recharge, midline and discharge zones identified by Salvucci and Entekhabi (1995) appear in the steady state equilibrium model application to complex topography (the sub-basin case of Chapters 5 and 6). Topographically induced convergence and divergence in the saturated zone lead to recharge and discharge areas organized along the drainage network and topographic highs respectively.

- The pre-event (mean) water table predicted by the steady state model and by topography-based models such as TOPMODEL are correlated, but have different distributions. Some of the simplifying assumptions used in TOPMODEL, particularly uniform recharge, may cause these discrepancies.

7.2 Proposals for future research

There are many facets of the present research which can be refined and extended. The following topics for further investigation have been broken down into four categories: improved model efficiency, new model applications, refined study of the effect of DEM resolution, and further investigation of the aggregate behavior of hydrologic phenomena.

7.2.1 Model efficiency

The seasonal model is presently encumbered primarily by two problems: nonexistence of a solution when negative recharge approaches its limit, and slow convergence of the unsaturated water balance.

The problem of negative recharge being limited by maximum capillary rise is described in Section 2.4.2. This obstacle is conceptual, rather than algorithmic; at present the application of the seasonal model is limited to soils for which the maximum capillary rise is high enough that it never enters into calculations.

The issue of slow computation speed in the unsaturated balance may be resolved in a number of ways. The first is the use of a table-look-up format to compute equilibrium recharge. For the steady-state model, recharge can be recorded as a

function solely of water table depth. It is computationally more efficient to do this once and incorporate a table look-up scheme than it is to use bisection at every node at every time step.

A look-up table for the seasonal model, on the other hand, would have to be indexed both on water table depth and on storage changes (or water table changes, but storage changes have the advantage that they implicitly incorporate the old value of recharge). Moreover, the look-up tables must be calculated for different times of the year. Daunting though this procedure seems, the tables only need be produced once for each soil-climate system. Even though the seasonal model is presently designed to recalculate seasonal parameters every time step, interpolation between weekly values might suffice for a table look-up scheme.

A second way of increasing the speed of the model is to carry out the saturated water balance at only a fraction of the nodes in the basin, and to interpolate between these nodes to infer recharge at intermediate points. This scheme is proposed primarily as a method of installing small cell size without making the number of unsaturated water balance calculations unmanageably large.

7.2.2 Model applications

Except for the early work in Eagleson (1978a-g), soil heterogeneity and the effects of vegetation have heretofore been ignored in the equilibrium model. Horizontal soil heterogeneity could be added to the present model with relatively little effort: MODFLOW already allows for hydraulic conductivity to be entered as a matrix, and it is simple enough to enter other soil properties and even soil depth into the unsaturated code as a matrix as well.

It may also be possible to incorporate vertical heterogeneity as well. However, since the existence of soil layering affects the equilibrium soil soil moisture profile, the addition of vertical hetrogeneity involves conceptual changes in addition to data-entry modifications.

Vegetation was originally included in the Eagleson model. It is possible to incorporate vegetation into the seasonal model as well; dramatic effects may occur from

doing so, particularly in the summer runoff season.

The model can also be used to identify the effects of varying the specified depth to bedrock. Such a study will quantify the importance of hydrogeological information to the analysis of surface hydrology.

7.2.3 DEM resolution

It has already been proposed in Chapter 5 to isolate the effects of cell size from the effects of DEM resolution. In order to do this, an experiment is suggested in which horizontal cell size is left small while DEM resolution is gradually made coarser and coarser (with intermediate surface elevation values interpolated between the coarse data). The major difference between this technique and the one described under Section 7.2.1 above, is that in the present scheme unsaturated zone calculations would continue to be made at every node, including the ones with interpolated surface data.

7.2.4 Aggregation studies

It has been proposed by Wood et al. (1988) that a representative area (REA) exists over which small-scale hydrologic phenomena may be reasonably aggregated. One way of testing this theory would be to run the equilibrium model over sub-catchments within a medium-sized catchment and compare the frequency distribution of hydrologic output of the smaller and larger areas. The size of the smallest sub-catchment which preserves the flux distributions of the original catchment is the REA.

Appendix A

Components of the equilibrium model

This appendix contains expressions for the expected values of fluxes from Salvucci and Entekhabi (1995). The reader is referred to that work and to Eagleson (1978a-g) for derivations. The Salvucci and Entekhabi (1995) model predicts expected mean annual fluxes, so the units of expected evaporation, infiltration excess runoff and saturation excess runoff are in units of length per year. All other quantities either are dimensionless or may be expressed in any consistent system of units ([cm] and [days] are adopted in this thesis). A list of symbols is given in Appendix C

Several points are worth mentioning concerning notation. In the following formulas $\gamma(\cdot)$ denotes the incomplete gamma function; $\Gamma(\cdot)$ is the gamma function, but Γ also appears as a dimensionless quantity dependent on recharge and a group of parameters. $K_2(\cdot)$ represents the modified Bessel function of the second type. The quantity β from Salvucci and Entekhabi (1995) has been changed to β_{tb} in order to avoid confusion with the β appearing in $\tan\beta$ (local slope). Lastly, two changes have been made to the Salvucci and Entekhabi (1995) formulation in sign conventions: in this thesis recharge (q_v as well as q_a) is positive down and Ψ_{sat} is a positive quantity representing the magnitude of bubbling pressure head.

Equivalent steady moisture profile:

$$s_* \equiv \left(\frac{q_v}{K_{sat}} + \left(1 - \frac{q_v}{K_{sat}}\right)\left(\frac{Z_s - Z_{wt}}{\Psi_{sat}}\right)^{-mc}\right)^{1/c} \tag{A.1}$$

Maximum capillary rise:

$$w = \frac{K_{sat}\left[\frac{(Z_s - Z_{wt})}{\Psi_{sat}}\right]^{-mc}}{1 - \left[\frac{(Z_s - Z_{wt})}{\Psi_{sat}}\right]^{-mc}} \tag{A.2}$$

Bare soil evaporation:

$$\begin{aligned} E[E_s] = \frac{e_p m_\nu}{\beta_{tb}}\{1 - [1 + (2\Lambda)^{1/2}E + (2\Omega)^{-1/2}]e^{-\Lambda E} \\ + [(2\Omega)^{-1/2} + (2\Omega)^{1/2}E]e^{-\Omega E} \\ + (2E)^{1/2}[\gamma(\frac{3}{2}, \Omega E) - \gamma(\frac{3}{2}, \Lambda E)]\} \end{aligned} \tag{A.3}$$

where

$$\Lambda = \frac{\left(1 + \frac{K_{sat}s_*^c}{4e_p} - \frac{w}{2e_p}\right)}{\left(1 + \frac{K_{sat}s_*^c}{2e_p} - \frac{w}{e_p}\right)^2}$$

$$\Omega = 2\left(\frac{K_{sat}s_*^c}{e_p} - \frac{2w}{e_p}\right)^{-2}$$

$$E = \frac{\beta_{tb}S_e^2}{2e_p^2}$$

$$c = \frac{(2 + 3m)}{m}$$

$$S_e = 2s*^{1+(c+1)/4}\left[\frac{n_e K_{sat}\Psi_{sat}\phi_e}{m\pi}\right]^{1/2}$$

$$\phi_e = \frac{2m^2\pi}{3(1 + 3m)(1 + 4m)}$$

Infiltration Excess Runoff:

$$E[R_{ie}] = E[P_A]\exp\left(-\eta A_0 - [n^2\delta S_i^2]^{1/3}\right)\Gamma\left(1 + \frac{1}{2}\left[\eta^2\delta S_i^2\right]^{1/3}\right)$$

$$\cdot \left[\frac{1}{2}[\eta^2 \delta S_i^2]^{1/3}\right]^{-(1/2)[\eta^2 \delta S_i^2]^{1/3}} \cdot \left[1 - e^{(-\delta t_s^*)}(1 + \delta t_s^*)\right] \qquad \text{(A.4)}$$

where

$$t_s^* = \left[\left(\frac{S_i^2}{4A_0^2} + \frac{\forall_e}{A_0}\right)^{1/2} - \frac{S_i}{2A_0}\right]^2$$

$$A_0 = [(2 + \Gamma)/3])K_{sat}$$

$$S_i = (2\chi)^{1/2} K_{sat}$$

$$\chi \equiv \frac{-n_e(1 - s_*)\Psi_{sat}}{K_{sat}}[1 + \frac{1}{2}(c - 3)(1 - s_*)\hat{s}^{(c+1)/2}]$$

$$\Gamma \equiv \frac{\phi\Psi}{(1 - s_*)(1 + \frac{1}{2}(c - 3)(1 - s^*)\hat{s}^{(c+1)/2})}$$

$$\forall_e = n_e(1 - s_*)Z' + \frac{1}{2}n_e\phi Z'^2 - \frac{1}{2}n_e\lambda'\left((Z_s - Z_{wt}) - Z' - \Psi_{sat}\right)^2$$

$$\lambda' \equiv \frac{m}{\Psi_{sat}}\left[1 - \left(\frac{q_v}{K_{sat}}\right)\right]$$

$$\phi \equiv \frac{m\left[1 - \left(\frac{q_v}{K_{sat}}\right)\right] s_*^{(1-c)}}{\Psi_{sat}}\left(\frac{Z_s - Z_{wt}}{\Psi_{sat}}\right)^{-mc-1}$$

$$Z' \equiv \frac{(1 - s_*) + \lambda'(Z_s - Z_{wt} - \Psi_{sat})}{\lambda' + \phi}$$

$$\hat{s} = \frac{1}{2}(1 + s_*)$$

Storage excess runoff:

$$E[R_{se}] = 2m_\nu \forall_e K_2[2(\forall_e \eta\delta)^{1/2}] \qquad \text{(A.5)}$$

Appendix B

Equilibrium model assumptions

The principal assumptions and simplifications of the equilibrium models (seasonal and steady state) are as follows:

General

- All processes are stationary or periodic-stationary. No storage accumulates from year to year.
- Runoff and water emanating from seepage faces is instantly routed out of the basin. Ponding on the surface is ignored. No lateral surface inflows are considered.
- Ice, snow and vegetation are not considered. Only water movement in the liquid phase is considered.

Surface processes and unsaturated zone dynamics

- Unsaturated flow and surface processes are vertical.
- Infiltration, exfiltration, percolation and capillary rise from the water table can be formulated separately and linearly superimposed.
- Time compression methods can be applied to surface processes.

- The uniform steady moisture profile may be substituted as the initial pre-event moisture condition for the purposes of calculating surface fluxes. Carryover moisture surpluses and deficits from previous events are ignored.
- Recharge (percolation) through the unsaturated zone is uniform.
- The unsaturated moisture profile is always one of a family of equilibrium steady moisture profiles; specifically, it is the profile which transmit the current expected recharge rate through a Brooks Corey soil bounded by a water table.
- The mean storage in the unsaturated zone is approximated by the integral of the equivalent steady moisture profile.

Climate

- Storm series are represented by Poisson arrivals of independent and identically distributed rectangular pulses.
- Storm intensity and duration are statistically independent.
- Interstorm period and storm duration are statistically independent.
- Average interstorm period is much greater that average storm duration.
- Potential rate of evaporation averaged over the interstorm period has a negligible coefficient of variation. Potential evaporation may change seasonally.
- Evaporation takes place only during interstorm periods.
- Potential rate of evaporation is much greater than the rate of capillary rise from the water table.

Soil

- Soils are homogeneous in the vertical direction.
- Soils are characterized by the Brooks-Corey non-hysteretic parameterization with a tension-saturated region in the wetting curves.

- Groundwater flow is three dimensional through the depth of volumetric saturation, including the tension-saturated region.
- The water table which is at equilibrium with the mean recharge rate approximates the mean water table position.

Appendix C

List of Symbols

Dimensions are given in brackets; L is length and T is time.

a : contributing area per unit contour length $[L]$

A : contributing area $[L^2]$

A_{tot} : total area of basin $[L^2]$

A_0 : Second term of the Philip-type infiltration equation $[L/T]$

c : pore disconnectedness index of Brooks-Corey soil hydraulic model $[\cdot]$

E : parameter group appearing in the expression for mean bare soil evaporation, an index of the relative ability of the soil to evaporate at the potential rate $[L]$

E_S : period bare soil evaporation $[L]$

e_p : period potential evaporation rate $[L/T]$

f : e-folding parameter for the decrease of saturated hydraulic conductivity with depth $[1/L]$

F_a : hydrologic flux for the period $[L]$

$f_{tr}(\cdot)$: probability density function for storm duration $[1/T]$

$f_i(\cdot)$: probability density function for storm intensity $[T/L]$

h : precipitation storm depth $[L]$

H : Cartesian location of the top of the saturated and tension saturated zone $[L]$

i : rainfall intensity $[L/T]$

$K_2(\cdot)$: modified bessel function of the second type $[\cdot]$

K_{sat} : saturated hydraulic conductivity $[L/T]$

K_0 : value of the exponentially-decreasing with depth saturated hydraulic conductivity at the surface $[L/T]$

m : pore size distribution index for the Brooks-Corey soil hydraulic model $[\cdot]$

m_ν : mean number of storms $[\cdot]$

$m_\nu(t)$: mean number of storms per period $[1/T]$

n_e : effective soil porosity $[\cdot]$

P_A : period total precipitation $[L]$

q : local saturated flux in the topography-based models $[L^3/T]$

q_v : equivalent steady recharge $[L/T]$

q_a : net flux between the saturated and unsaturated zones $[L/T]$

$\mathbf{Q_g}$: vector of saturated zone flow $[L^2/T]$

R : uniform recharge rate in the topography-based models $[L/T]$

R_{ie} : period runoff by infiltration excess mechanism $[L]$

R_{se} : period runoff by storage excess mechanism $[L]$

S_e : exfiltration desorptivity $\left[L/\sqrt{T}\right]$

S_i : infiltration sorptivity $\left[L/\sqrt{T}\right]$

S_y : specific yield $[\cdot]$

s_* : value of relative soil saturation at surface for the equivalent steady profile $[\cdot]$

$\widehat{s}$: average of s_* and unity $[\cdot]$

t_b : time between storms $[T]$

t_r : storm duration $[T]$

t_s^* : time until column saturation assuming soil-controlled infiltration history $[T]$

T_0 : saturated transmissivity expressed as the ratio of the surface value of the saturated hydraulic conductivity to the e-folding parameter for its exponential decrease with depth $[L^2/T]$

T_e : basin average value of saturated transmissivity expressed as the ratio of the surface value of the saturated hydraulic conductivity to the e-folding parameter for its exponential decrease with depth $[L^2/T]$

V_{unsat} : storage in the unsaturated zone under conditions of steady equilibrium with the water table $[L]$

V_{sat} : storage in the saturated zone $[L]$

w : potential rate of capillary rise from the water table to a dry surface $[L/T]$

z_i : depth to volumetric saturation at location i $[L]$

$\bar{z}$: areal mean depth to volumetric saturation $[L]$

Z : depth to impermeable bedrock $[L]$

Z_s : surface elevation $[L]$

Z^* : depth to volumetrically saturated zone at which the net recharge is zero $[L]$

Z_{wt} : Cartesian location of the water table $[L]$

Z' : parameter group for the mean period runoff expression $[L]$

β : inverse-tangent of topographic slope $[\cdot]$

β_{tb} : inverse of mean time between storms $[1/T]$

χ : time constant appearing in the derivation of the infinite series expansion of infiltration capacity $[T]$

Ω : dimensionless parameter group appearing in the expression of mean period bare soil evaporation $[\cdot]$

Λ :dimensionless parameter group appearing in the expression of mean period bare soil evaporation $[\cdot]$

δ : inverse of mean storm duration $[1/T]$

λ : average of the logarithm of contributing area per unit contour length divided by topographic slope $[\ln L]$

λ' : parameter group for the mean period runoff expression $[1/L]$

ϕ_e : dimensionless desorption diffusivity $[\cdot]$

ϕ_i : dimensionless sorption diffusivity $[\cdot]$

$\gamma(\cdot,\cdot)$: the incomplete gamma function

Γ : time constant appearing in the derivation of the infinite series expansion of infiltration capacity $[\cdot]$

$\Gamma[\cdot]$: the complete gamma function $[\cdot]$

η : inverse of mean storm intensity $[T/L]$

σ : vector of climate parameters

Ψ_{sat} : bubbling head for the Brooks-Corey hydraulic model, the value of the capillary tension head $[L]$

$\forall_e$: storage capacity of the unsaturated zone under conditions of steady equilibrium with the water table $[L]$

$E[\cdot]$: expectation operator

$\overline{(\cdot)}$: mean value of a perturbation expansion

$(\cdot)'$: perturbation around mean value

$\Delta(\cdot)$: discrete difference in time

Bibliography

Allen, P. B. and Naney, J. W.: 1991, Hydrology of the Little Washita River watershed, Oklahoma, *Report ARS-90*, U.S. Department of Agriculture, Agriculture Research Service.

Bear, J.: 1988, *Dynamics of Fluids in Porous Media*, Dover Publications, Inc.

Beven, K. and Kirkby, M. J.: 1979, A physically based, variable contributing area model of basin hydrology, *Hydrol. Sci. Bull.* **24**, 43–69.

Bras, R. L.: 1990, *Hydrology, an introduction to hydrologic science*, Addison-Wesley.

Dawes, W. R. and Short, D.: 1994, The significance of topology for modeling the surface hydrology of fluvial landscapes, *Water Resour. Res.* **30**(4), 1045–1055.

Eagleson, P. S.: 1978a, Climate, soil and vegetation, 1, Introduction to water balance dynamics, *Water Resour. Res.* **14**(5), 705–712.

Eagleson, P. S.: 1978b, Climate, soil and vegetation, 2, The distribution of annual precipitation derived from observed storm sequences, *Water Resour. Res.* **14**(5), 713–721.

Eagleson, P. S.: 1978c, Climate, soil and vegetation, 3, A simplified model of soil moisture movement in the liquid phase, *Water Resour. Res.* **14**(5), 722–730.

Eagleson, P. S.: 1978d, Climate, soil and vegetation, 4, The expected value of annual evapotranspiration, *Water Resour. Res.* **14**(5), 731–740.

Eagleson, P. S.: 1978e, Climate, soil and vegetation, 5, A derived distribution of storm surface runoff, *Water Resour. Res.* **14**(5), 741–748.

Eagleson, P. S.: 1978f, Climate, soil and vegetation, 6, Dynamics of the annual water balance, *Water Resour. Res.* **14**(5), 749–764.

Eagleson, P. S.: 1978g, Climate, soil and vegetation, 7, A derived distribution of annual water yield, *Water Resour. Res.* **14**(5), 765–776.

Hawk, K. L. and Eagleson, P. S.: 1992, Climatology of station storm rainfall in the continental United States: parameters of the Bartlett-Lewis and Poiosson rectangular pulses models, *Report 336*, Ralph M. Parsons Laboratory, MIT, Cambridge, MA.

Kim, C. P., Entekhabi, D. and Salvucci, G. D.: 1994a, Hillslope hydrology: influence of climate, soil, geomorphology and vegetation characteristics, Unpublished manuscript (32 pages).

Kim, C. P., Entekhabi, D. and Salvucci, G. D.: 1994b, Hillslope hydrology: model development and validation, Unpublished manuscript (15 pages).

McDonald, M. and Harbaugh, A. W.: 1988, A modular three-dimensional finite-difference ground-water flow model, *Manual*, United States Geological Survey.

Mintz, Y. and Serafini, Y.: 1980-1981, Global fields of soil moisture and land-surface evapotranspiration, *Research review 83907*, NASA Goddard Flight Center technical memo.

O'Loughlin, E. M.: 1981, Saturation regions in catchments and their relations to soil and topographic properties, *J. Hydrol.* **53**, 229–246.

O'Loughlin, E. M.: 1986, Prediction of surface saturation zones in natural catchments by topographic analysis, *Water Resour. Res.* **22**(5), 794–804.

Salvucci, G. D.: 1994c, *Hillslope and Climatic Controls on Hydrologic Fluxes*, PhD dissertation, Massechucetts Institute of Technology, Department of Civil and Environmental Engineering.

Salvucci, G. D. and Entekhabi, D.: 1994a, Equivalent steady soil moisture profile and the time compression approximation in water balance modeling, *Water Resour. Res.* **30**(10), 2737–2749.

Salvucci, G. D. and Entekhabi, D.: 1994b, Comparison of the Eagleson statistical-dynamical water balance model with numerical simulations, *Water Resour. Res.* **30**(10), 2751–2757.

Salvucci, G. D. and Entekhabi, D.: 1995, Hillslope and climatic controls on hydrologic fluxes, *Water Resour. Res.* **31**(7), 1725–1739.

Satterlund, D. R.: 1987, Comment on "Prediction of surface saturation zones in natural catchments by topographic analysis" by E. M. O'Laughlin, *Water Resour. Res.* **23**(5), 1708.

Sivapalan, M., Beven, K. and Wood, E. F.: 1987, On hydrologic similarity, 2, A scaled model of storm runoff production, *Water Resour. Res.* **23**(12), 2266 – 2278.

Sivapalan, M., Beven, K. and Wood, E. F.: 1990, On hydrologic similarity, 3, A dimensionless flood frequency model using a generalized geomorphologic unit hydrograph and partial area runoff generation, *Water Resour. Res.* **26**(1), 43–58.

Tarboton, D. G., Bras, R. L. and Rodriguez-Iturbe, I.: 1989, The analysis of river basins and channel networks using digital terrain data, *Report 326*, Ralph M. Parsons Laboratory, MIT, Cambridge, MA.

Toth, J.: 1966, Mapping and interpretation of field phenomena for groundwater reconnaissance in a prairie environment, *Intern. Assoc. Sci. Hydrol. Bull.* **11**(2), 1–49.

Wolock, D. M. and Price, C. V.: 1994, Effects of digital elevation model map scale and data resolution on a topography-based watershed model, *Water Resour. Res.* **30**(11), 3041–3052.

Wood, E. F., Sivapalan, M. and Beven, K.: 1988, Effects of spatial variability and scale with implications to hydrologic modeling, *J. Hydrol.* **102**, 29–47.

Zhang, W. and Montgomery, D. R.: 1994, Digital elevation model grid size, landscape representation and hydrologic simulations, *Water Resour. Res.* **30**(4), 1019–1028.